PERIODICAL

Volume 3, No. 1
New Series

March 1957

# RECORDS
# OF
# OCEANOGRAPHIC WORKS
# IN JAPAN

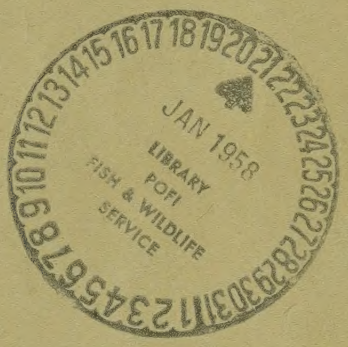


Published by
Science Council of Japan

## BOARD OF EDITORS

**Editor-in-Chief**
Shinkishi HATAI

**Editors**
Yoshio HIYAMA — Kōji HIDAKA
Yasuo MIYAKE — Hiroshi NIINO

**With**
**the Co-operation of**

**Physical Oceanography**
Kōji FUKUTOMI — Shōichirō HAYAMI
Mashito NAKANO — Tadayoshi SASAKI
Kanji SUDA — Ryūtarō TAKAHASHI
Michitaka UDA

**Chemical Oceanography**
Masayoshi ISHIBASHI — Yasuo MATSUDAIRA
Ken SUGAWARA

**Geological Oceanography**
Shōzaburō HANZAWA

**Biological Oceanography**
Denzaburō MIYADI — Yō K. OKADA
Isao TAKI — Yukio YAMADA

**Fisheries**
Hiroaki AIKAWA — Motosaku FUJINAGA
Takeo IMAI

**Secretary**
Buei ARAYA


## SUGGESTION TO AUTHORS OF PAPERS FOR THE RECORDS OF OCEANOGRAPHIC WORKS IN JAPAN

An author wishing to contribute a paper to the RECORDS OF OCEANOGRAPHIC WORKS IN JAPAN should submit in compliance with the following suggestions:

1. Manuscripts will be accepted within the scope of
   Physical Oceanography — Geological Oceanography
   Chemical Oceanography — Biological Oceanography and
   Fisheries
2. An original and a copy of his manuscript should be type-written double-spaced in 21×29.5cm paper, within 12 sheets, making 6 printed pages including plates and tables.
3. The manuscript should be addressed to the competent editor and mailed to the official in charge of the Science Council of Japan, Ueno Park, Tokyo, Japan.
4. The author is asked to follow this publication for forms of headings and references, etc.
5. The editors reserve the right to accept the manuscripts and to make minor editorial changes in them, so that all paper may conform to over-all style of this publication.

# Preface

In 1924, the National Research Council of Japan established a Sub-Committee of Pacific Science Research in order to maintain close co-operation with the Panpacific Science Congress on one hand and to promote various fields of scientific research pertaining to the Pacific on the other.

This Sub-Committee decided to publish a journal with a view to contributing to the development of oceanography in Japan, and thus the first number of the "Records of Oceanographic Works in Japan" was issued in March 1928.

This work was continued until March 1941, when it was suspended after the publication of volume XII, No. 2, due to the occurrence of the world war II.

In 1949, the National Research Council of Japan was dissolved and new organization, the Science Council of Japan, was born. At the same time the Special Committee of the Pacific Science Research changed its name to the Pacific Science Liasion Committee and continued its activities as before but continuous publication of the journal was not equally successful.

Fortunately in 1951, Japan became a member of Unesco through the resolution passed at its Sixth General Conference in Paris and this opportunity made possible the Natural Science Committee of the Japanese National Commission for Unesco in October 1952 to resolve to the effect that its activities to concentrate upon the development of marine resources. With this idea, Science Council of Japan established the Special Research Committee on Marine Resources. By close co-operation between Japanese National Commission for Unesco and the Special Research Committee on Marine Resources in the Science Council of Japan, revival of the long suspended "Record of Oceanographic Works in Japan" was planned, and the Japanese National Commission for Unesco took entire financial burden of its publication; thus Volume 1, Nos. 1 and 2 of this journal were published under compilation of the Special Committee on Marins Resources in the Science Council of Japan.

In 1954, Japan Science Council dissolved this Special Committee on Marine Resources and thus the complilation responsibility was transferred to the Pacific Science Liasion Committee of Science Council of Japan though publication of the Journal was yet carried on by the Japanese Commission Unesco and under new system Vol. 2, Nos. 1, 2, and 3, were issued.

For reviving long suspened Oceanographic Works in Japan and for publication of the Journal during those first three critical years, we wish to express our sincere appreciation to the Japanese National Commission for Unesco for

their sympathy and assistance from which the oceanographic investigators in Japan received utmost encouragement and assurance.

However, historical retrospect at once reminds us the fact that the journal ought to be published by Japan Science Council under compilation of Pacific Science Liasion Committee, instead of Japanese National Commission for Unesco. This idea was approved and agreed by both Japanese Science Council and Japanese National Commission for Unesco and both publication and compilation were ultimately transferred to the former. The Vol. II, No. 4 of the Journal was thus published by Japanese Science Council.

Taking this opportunity the editorial board wishes to express our sincere hope that this publication will serve to the development of oceanography in Japan.

Shinkishi HATAI
Editor in Chief

# CONTENTS

Preface ..... Shinkishi HATAI

An Example of Cold Eddies South of the Kuroshio ..... Jotaro MASUZAWA... 1

On the Rapid Estimation of the Dynamic Topography in the Seas Adjacent to Japan ..... Masashi YASUI... 8

A Note on the Horizontal Eddy Viscosity in the Kuroshio ... Takashi ICHIYE... 16

On the Storm Surges Caused by the Typhoon 5415 "Marie" (I) ..... Takashi ICHIYE... 26

On the Storm Surges Caused by the Typhoon 5415 "Marie" (II) ..... Takashi ICHIYE... 36

On the Tidal Mixing of Sea Water Through Narrow Channels ..... Shoitiro HAYAMI... 49

Investigation of the Sea Floor of Tsugaru Straits by Under-water Camera ... Tadayoshi SASAKI, Seiichi WATANABE, Gohachiro ŌSHIBA, Noboru, OKAMI... 56

Maximum Permissible Concentration of $Sr^{90}$ in Food and its Enviroments ..... Yoshio HIYAMA... 70

Up-take of Strontium by Marine Fish from the Enviroment (I) ..... Yoshio HIYAMA and Ryushi ICHIKAWA... 78

Mechanism of Utilization of Plankton by Some Fishes ..... Fujio YASUDA and Yoshio HIYAMA... 85

Optical Properties of the Water in the Kuroshio Current (II) ... Tadayoshi SASAKI, Noboru OKAMI, Seiichi WATANABE, Gohachiro ŌSHIBA... 92

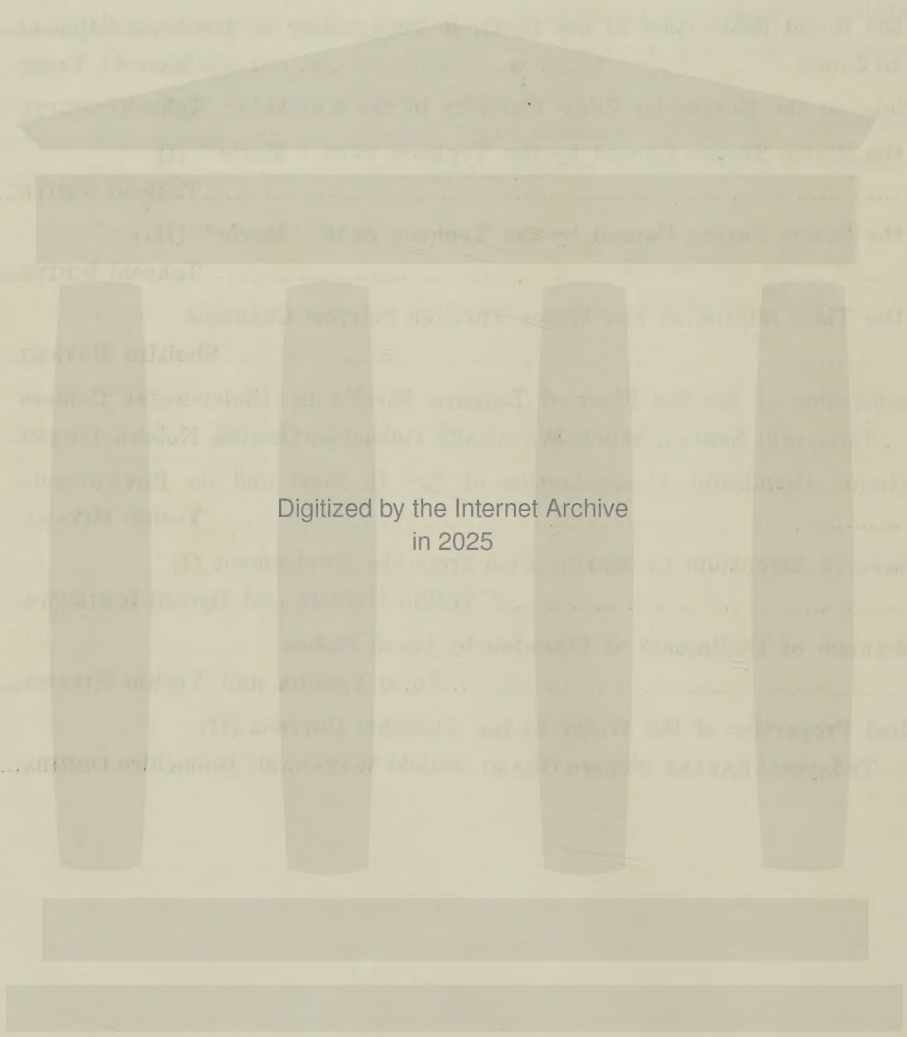

Digitized by the Internet Archive
in 2025

https://archive.org/details/records-of-oceanographic-works-in-japan-new-series_1957-03_3_1

Records of Oceanographic Works
in Japan Vol. 3, No. 1,
March 1957

# An Example of Cold Eddies South of the Kuroshio

## —Currents and Water Masses of the Kuroshio System VII—

By

Jotaro MASUZAWA

(Japan Meteorological Agency)

### 1. Introduction

The Kuroshio leaving the coast of Japan at Cape Inubo-zaki (36°N) encounters with the Oyashio flowing southwards along the coast of Japan. The boundary is correspodent to the so-called *polar frontal zone* between *the western North Pacific Central Water* and *the North Pacific Subarctic Water* named by SVERDRUP (1942). In this frontal zone, various kinds of warm and cold eddies having complicated characteristics are formed and they are everchanging within relatively a short period. However, our former observations have been unable to clarify precisely the kinematical features of the individual eddy except the large anticyclonic warm eddy north of the Kuroshio current in 1954 (MASUZAWA 1955, ICHIYE 1956).

Furthermore, simple isolated watermasses sometimes appear in the relatively homogeneous waters out of the remarkable mixing zone. That is, we can often find an isolated cold watermass to the east of Boso Peninsula in the south side of the Kuroshio main current, and a warm watermass to the southeast of Hokkaido in the Oyashio water. In his recent report, KAWAI (1955) preliminarily called the former, the cold watermass off Cape Nozimazaki ($C_N$) and the latter, the warm watermass off Hokkaido ($W_H$). For example, in May 1950 and in June 1953, an isolated cold watermass existed in the neighbourhood of 35°N, 144°E in the warmer Kuroshio water. It was an almost elliptical eddy with the long-axis about 100 M and the 100 m temperature of its center (13°C in 1950, 10°C in 1953) was about 6°C in 1950, 10°C in 1953 respectively lower than the surrounding water. Therefore, it is different from the so-called outer *cold region* which is generally observed as the slightly lower temperature zone on the south side of the *warm core* (the warmest band along the stream axis). Though it is similar to the cold eddy "Edgar" in Operation Cabot of the Gulf Strerm System (FUGLISTER and WORTHINGTON 1951), the origin, vortical strength and decay of such an isolated watermass have not yet been observed in the Kuroshio System. During the period from the spring of 1955 to the early summer of 1956, we got a chance to observe an example of the life history of a cyclonic cold eddy south of the Kuroshio current.

## 2. Cutting-off of a cold isolated watermass south of the Kuroshio

The course of the Kuroshio main current to the west of 145°E has shifted to the north since the summer of 1954. In February 1955, it arrived at 38°N, where the boundary between the Kuroshio warm and haline water and the Oyashio cold and fresh water was very sharp. The Oyashio cold water was transported southeastwards along the north side of the Kuroshio stream axis (Fig. 1). In May, the meandering of the Kuroshio current became remarkable in the entire sea from the south to the east of Japan, namely the Kuroshio east off Japan bended predominantly to the south in the vicinity of 34°N, 147°E. In general, after ICHIYE (1956), the meandering of the Kuroshio current course is to be such remarkable that the curvature of the cyclonically (convex to the south) winding course is larger than that of the anticyclonically (convex to the north) winding course.

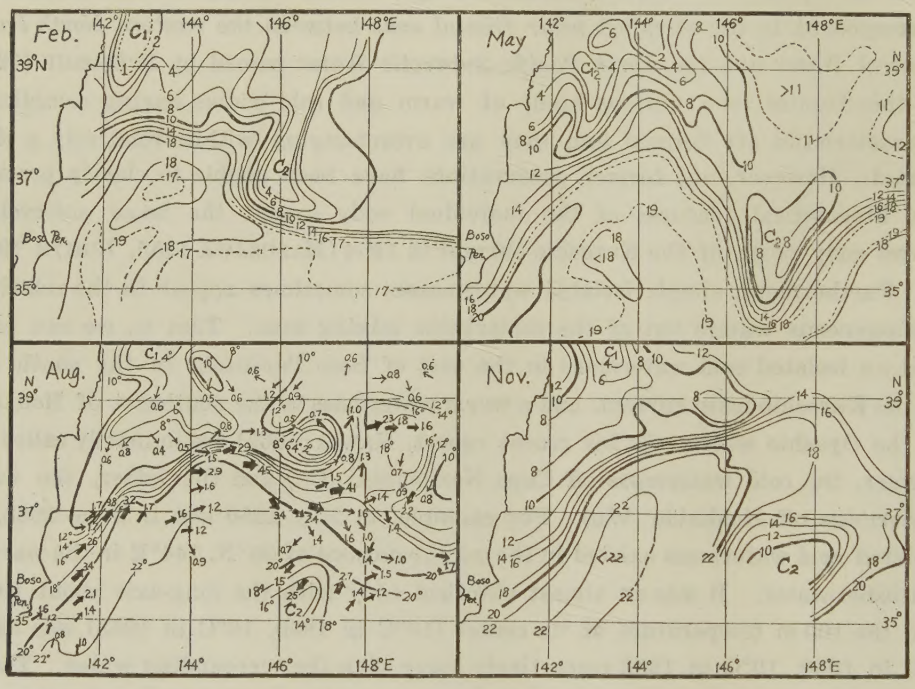


Fig. 1. Water temperature (°C) in the 100 m depth and surface current velocity (knot) with GEK in February, May, August and November, 1955.

In August, the Kuroshio forked out into three branches in the vicinity of 37°~38°N, 145°~147°E and the middle branch cut off an anticyclonic warm eddy to the north and a cyclonic cold eddy to the south. According to the observations in July southeast off Boso Peninsula, this cold water seems to have stretched southeastwards to 34°N, 144°E. Even in August, however, the cutting-off did not progress to the depths lower than 300 m and the main current in deeper layers meandered as before with a narrow trough diverting to the southwest.

In November, the cutting-off went down to deeper layers and the cyclonic cold eddy seems to have shifted northeastwards during the period from August to November, but because of the shortage of observations this is not definitely proven.

### 3. Modification of a cyclonic cold eddy

In February 1956 (Fig. 2a), an elliptical cyclonic eddy having the long-axis (NE–SE) of about 150 M and the short-axis (NE–SW) of about 70 M was clearly observed in the vicinity of 34°～35.5°N, 145°～147.5°E. The observed surface maximum velocity of the cylonic vortex amounted to 4.6 knotes which is the value comparable to the surface maximum velocity of the Kuroshio main current. Therefore, if the observation network were not quite dense, a part (especially the southern part) of the vortex would be misjudged as a part of the Kuroshio main current. The horizontal distributions of temperature and chlorinity at all depths show that the cold watermass was almost completely isolated, but that as seen in the surface currents the surface water was sppplied to the eddy at its north side and discharged from the northeast corner of the eddy.

As the cyclonic cold eddy in the vicinity of 35°～36°N, 143°～145°E in May (Fig. 2b) may be the eddy located in the vicinity of 34°～35.5°N, 145°～147.5°E once observed in February, it is estimated that the eddy shifted to the NW with the average moving-velocity of about 50 M a month. Such an upstream movement of the isolated cold watermass has already been suggested by FUGLISTER and WORTHINGTON (1951) in the Gulf Stream System. The isolated cold watermass

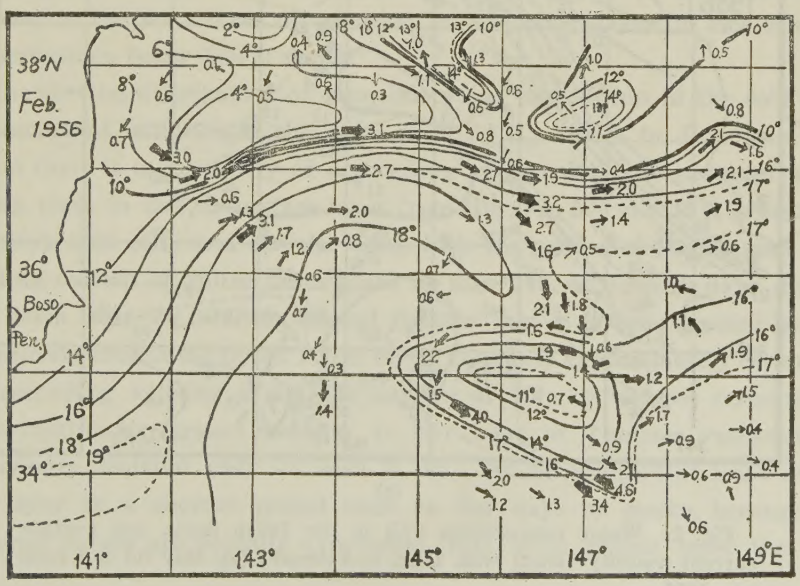


(a)

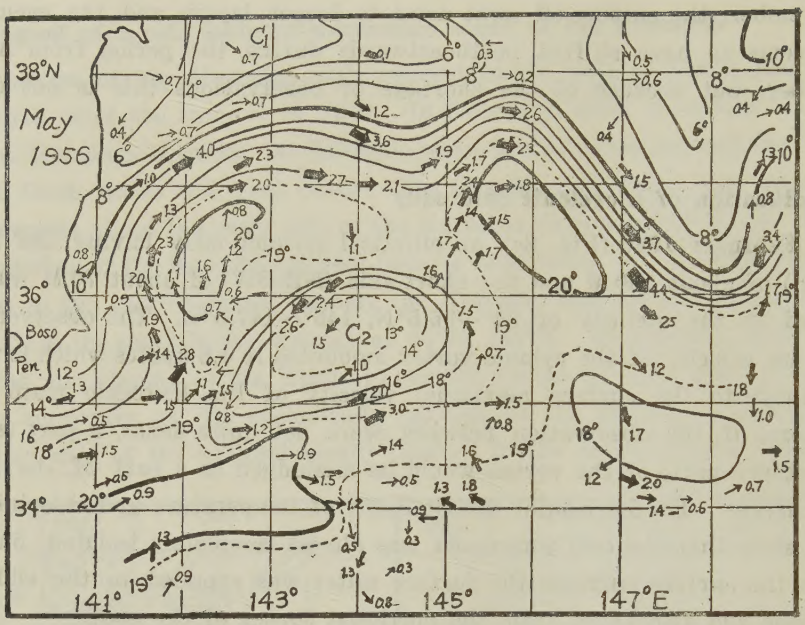


(b)

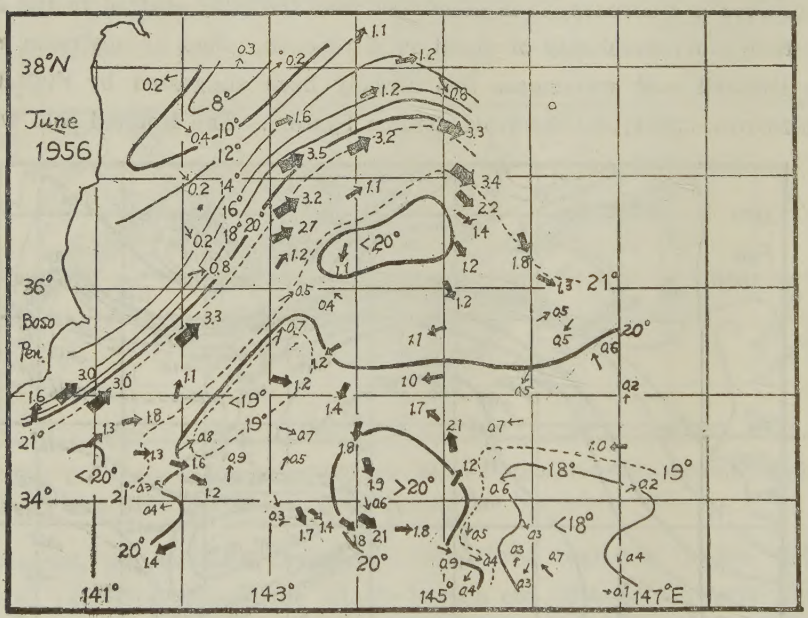


(c)

Fig. 2. Water temperature (°C) in the 100 m depth and surface current velocity (knot) with GEK in February (a), May (b) and June (c)., 1956.

($C_N$) often seen east 100～200 M off Boso Peninsula may be not discharged directly from the north to the south across the Kuroshio current, but transported from the east to the west after cutting off in the region of 34°～36°N, 146°～148°E, because we have not observed yet that the Kuroshio main current takes a southward-projecting course in the nearshore region.

Comparing the current pattern of May with that of February, the surface maximum velocity of the vortex decreased from 4.6 to 3.0 knots, while the surface maximum velocity of the Kuroshio main current was generally smaller by about one knot. And also the 100 m temperature in the cold eddy was higher by about 2°C in spite of about 1°C rising in the sourrounding warm band.

In short, if the cold eddy of May can be recognized the same one with February, then it may have been relatively stable in the period from February to May, while it has shifted westward and its vortical strength has become weak a little.

## 4. Disappearance of a cold isolated watermass

In June (Fig. 2c), detailed observations near the cyclonic eddy were carried out in succession of the May—observations, in order to see a relatively short period change of the eddy. According to these observations, in the temperature distribution of the upper layer, such a remarkably cold watermass as observed in May was not found this time, while a cyclonic vortex existed in the vicinity of 33.5°～35°N, 143°～145°E. This weak vortex is rather warmer in the upper layer and almost indifferent from the watermass distribution. But, it is impossible to see a response to the watermass distribution in the deeper layer for lack of satisfactory observations below 250 m depth.

When the vertical distribution of temperature at one station in the cold eddy of May is compared with one at the station of 34°E, 144°E in June, we may conclude that there is a possibility of descending motion with the range of 200～250 m taking place in the subsurface layer from 100 m to 500 m. If it is assumed that the cyclonic cold eddy is a circular eddy with the radius of 100 km and that the descending motion of 250 m takes place in any five or twenty days during the period from May 20 to June 20 and further that it is compensated by the horizontal convergence in the upper 100 m layer, then it is approximately estimated that the descending velocity is $5.8\times10^{-2}$ cm/sec or $1.4\times10^{-2}$ cm/sec respectively and the horizontal convergent velocity is 29 cm/sec or 7 cm/sec respectively. Such a perfectly isolated eddy as seen in May can be occluded at least in the subsurface layer in a shorter period such as few days or weeks, because the abovementioned values are actually expectable from wind effects upon the sea-surface.

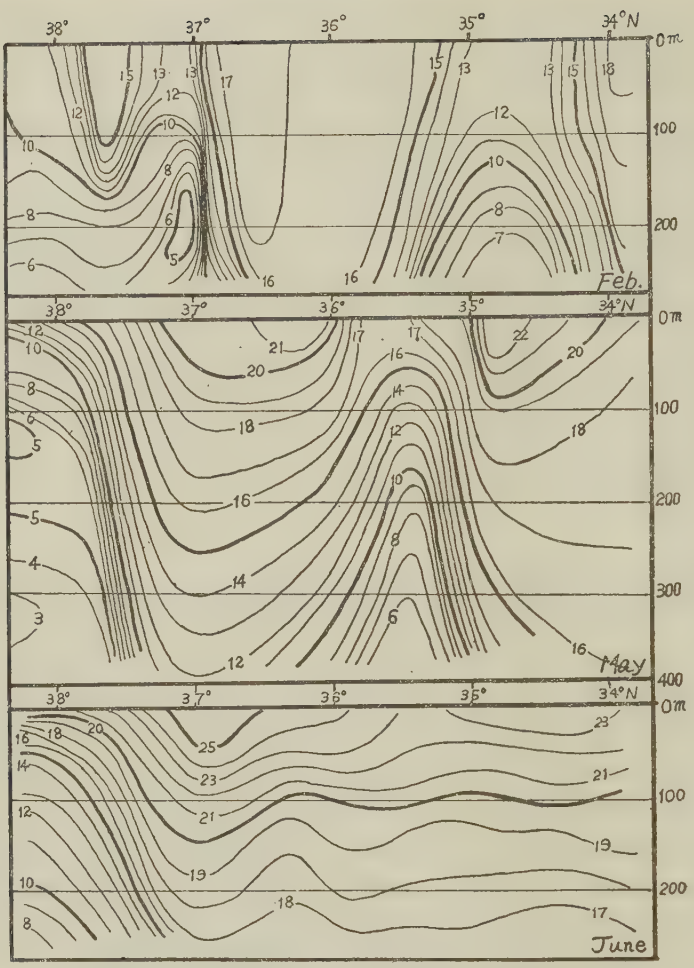


Fig. 3. Vertical distributions of temperature (°C) along 147°E in February (upper), along 144°E in May (middle) and in June (lower)., 1956.

**Acknowledgements**. The author wishes to express his hearty thanks to Dr. Y. TAKENOUTI, Dr. T. ICHIYE and Mr. M. HANZAWA, Japan Meteorological Agency and Dr. K. YOSHIDA, Tokyo University for their kind advice.

## Literatures

1) FUGLISTER, F. C. and L. V. WORTHINGTON (1951): Some results of a multiple ship survey of the Gulf Stream. *Tellus* **3** (1).
2) ICHIYE, T. (1956): On the behaviour of the vortex in the polar front region. *Oceanogr. Mag.* **7** (2).
3) KAWAI, H. (1955): On the polar frontal zone and its fluctuation in the waters to the north-east of Japan (1). (in Japanese with English abstract) *Bull. Tohoku Regional Fisheries Laboratory* No. **4**.

4) MASUZAWA, J. (1955): An outline of the Kuroshio in the eastern sea of Japan. *Oceanogr. Mag.* **7** (1).
5) MASUZAWA, J. (1956): A note on the Kuroshio farther to the east of Japan. *Oceanogr. Mag.* **7** (2).
6) SVERDRUP, H. U. *et al* (1942): *The oceans, pp.* 1060. New York

Records of Oceanographic Works
in Japan Vol. 3, No. 1,
March 1957.

# On the Rapid Estimation of the Dynamic Topography in the Seas Adjacent to Japan

By

Masashi YASUI

(Japan Meteorological Agency)

## 1. Introduction

The modern development of oceanographic instrument, especially BT and GEK, makes oceanographic observation easier and nowadays we can get the detailed characteristics of the ocean surface and subsurface very easily within a relatively short period.

However, we can obtain the dynamic topography of the sea only after having done troublesome titrations of the sea-water samples and toilsome calculations. Accordingly, it is highly desirable to get the dynamic topography immediately after the observations, even though it is a rough nature, in oder to carry out the succesive observations effectively.

Montgomery and Wooster (1954) tried to simplify the dynamic calculation procedure and Klein (1955) refined it to some extent. And yet chlorinity titration procedure is still necessary in such methods. Stommel (1947) also presented a method of dynamic computation using water temperature data only. However, his method is effective only in the area where the synthetic T–S diagrams has a simple relationship. Such as the sea off the Tohoku District of Japan, however, several watermasses are coexisting simultaneously, therefore it is almost impossible to find which type of T–S diagram should be used for to compute the dynamic height of the station.

In his previous report (1955), the author suggested a method to estimate the surface dynamic topography of the Kuroshio Area using the mean temperature. In this report the autor tries to extend this method to the seas adjacent to Japan.

## 2. Vertical distribution of $\sigma_t$

Many oceanographic stations in the seas adjacent to Japan, south and east of Honshu and north of 29°N, west of 160°E, have been occupied by Japanese oceanographers on board research vessels of the Japan Meteorolocical Agency during th last two years. We have obtained a total of 653 data with satisfactory accuracy. Plotting these data on a T–Cl diagram (Figure 1) to see the relationship between T and Cl values, we can not see any systematic relationship on this

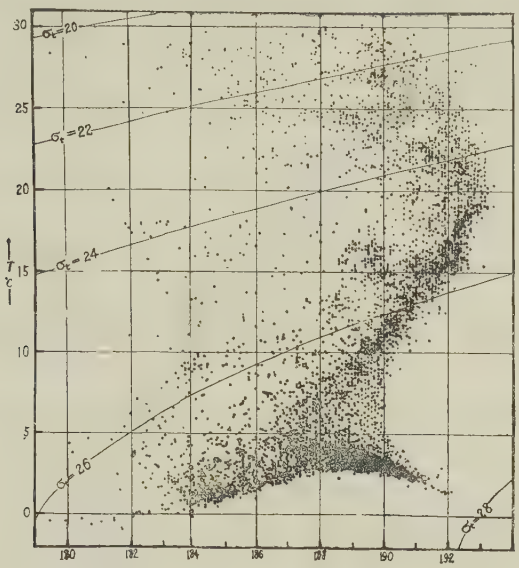


Fig. 1. The synthetic T–Cl diagram in the adjacent seas to Japan in 1954–1955.

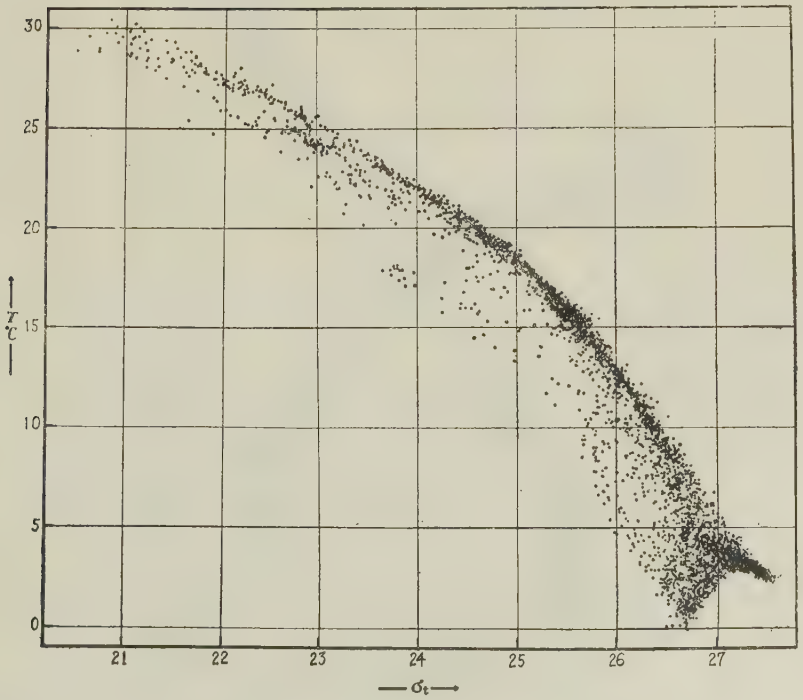


Fig. 2. The synthetic T–$\sigma_t$ diagram in the adjacent seas to Japan.

diagram. However it is seen that the equi-$\sigma_t$ curves intersect the equal temperature lines at small angeles. And we naturally expect that the T-$\sigma_t$ diagram of the same data may be more systematic, which is illustrates in the Figure 2. According to Klein, the dynamic depth anomaly could be determined only from $\sigma_t$ distribution neglecting the pressure terms. After Yoshida and Tsuchiya (1956) the corrections for the negligence of the pressure terms are given as a function of the temperature at the 500 m or 600 m layer. Therefore, we may approximately perform the dynamic computation from the vertical distribution of temperature and this diagram. Finally, after these procedures we are able to obtain the approximate values of the dynamic anomaly directly from the mean temperature.

### 3. Relationship between mean temperature and dynamic depth anomaly

In his previous paper (1955), the author has pointed out that the dynamic depth anomaly at the surface, referred to the 1000-decibar level, could be obtained from the mean temperature above 500 m subsurface layer with reasonable accuracy.

Based on this idea, we plot the dynamic depth anomaly against the mean temperature (Figures 3-7). In these figures, notations of $\Delta D_m$ and $T_n$ represent

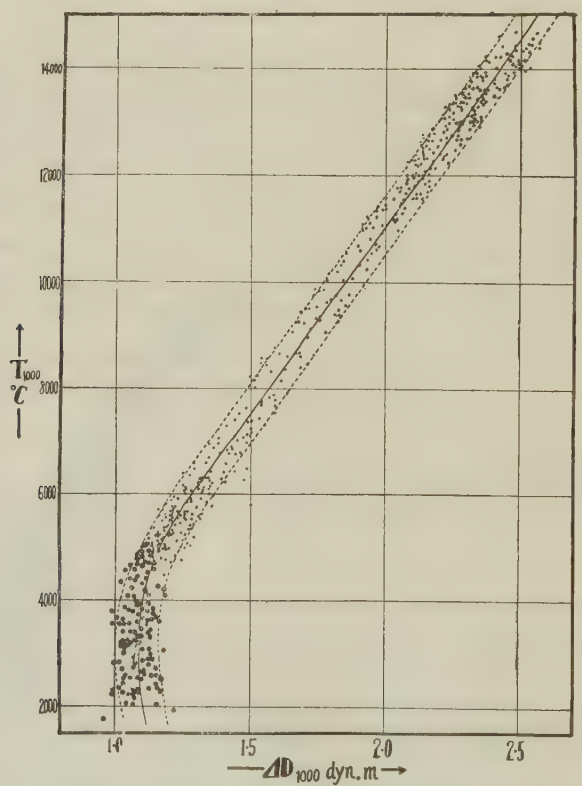


Fig. 3. $\Delta D_{1000}$ and $T_{1000}$ relationship.

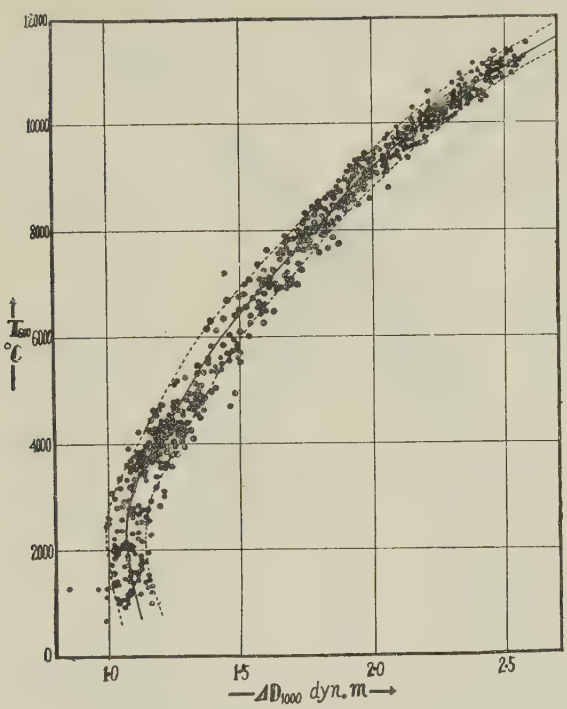


Fig. 4. $\Delta D_{1000}$ and $T_{600}$ relationship.

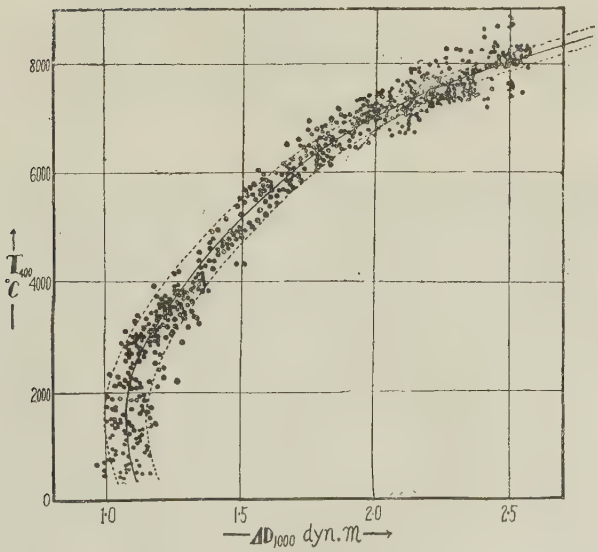


Fig. 5. $\Delta D_{1000}$ and $T_{400}$ relationship.

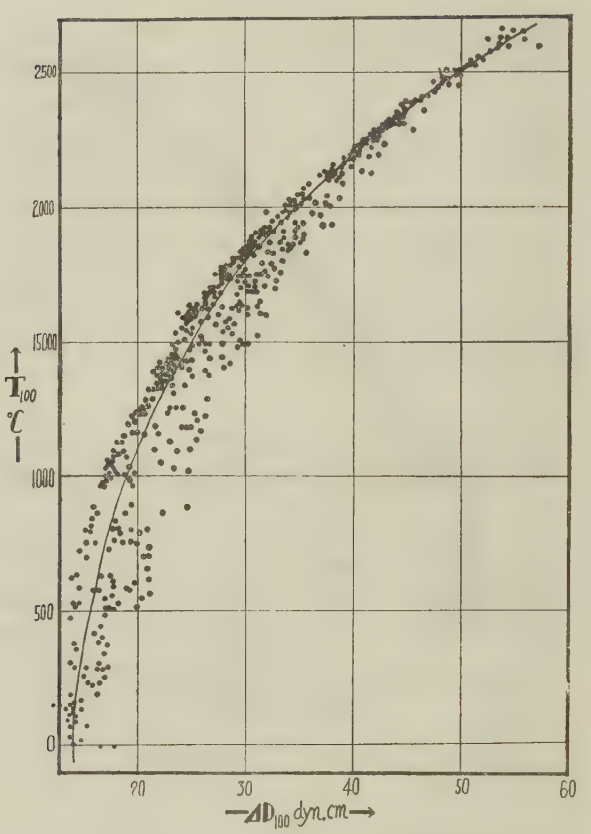


Fig. 6. $\Delta D_{100}$ and $T_{100}$ relationship.

the dynamic depth anomaly and the mean temperature respectively. The suffixes $m$ and $n$ represent the values of decibar of the layer referred to and the thickness of the upper layer in which the integration of temperature is performed respectively.

In these figures, full curves indicate the 'standard' and are drawn in sight. Dotted curves indicate the errors of ±8 cm contained in such $\Delta D$ values against the same mean temperature. Now we shall adopt this standard curve as the 'mean' and will use this as a nomograph in the following discussion.

In these figures it is immediately apparent that we can not avoid at least 8 cm error of dynamic depth anomaly estimated by the mean temperature. This error becomes larger as the thickness of the layer taken in computation becomes less, especially in the high anomaly area. Therefore, in order to estimate the surface dynamic anomaly above 1000 db levels, as noticeable from the figures, it is desirable to compute the mean temperature at least above 600 m levels.

However, it is far more accurate to use the mean temperature method than to use a single layer temperature pattern, for instance 100 or 200 m, in place of the surface topography.

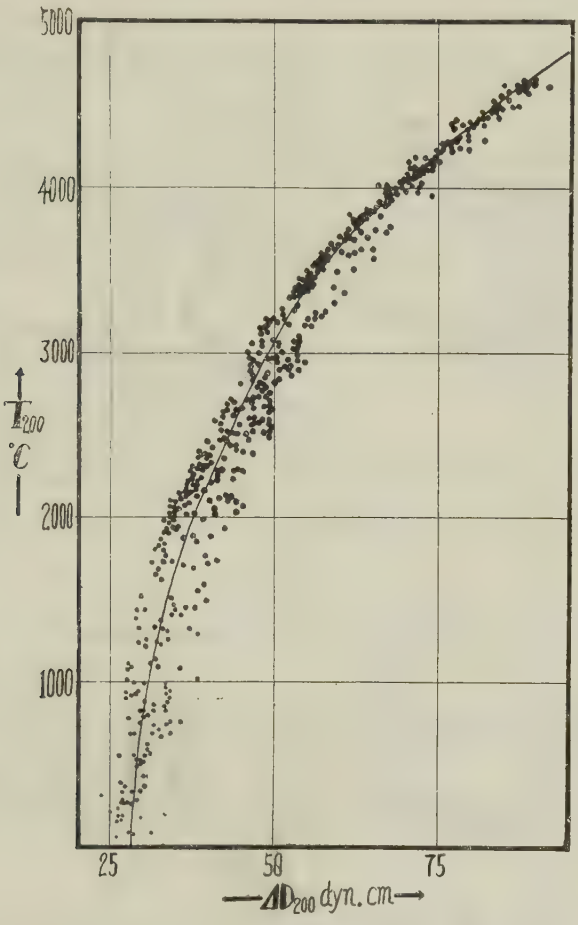


Fig. 7. $\Delta D_{200}$ and $T_{100}$ relationship.

## 4. Example

As a practical application of these diagrams, we here show the dynamic topography of several layers referred to the 1000-decibar layer, using our present method (Figure 8). Comparing these topographical charts with the charts obtained by former methods, we find a surprising agreement between them for the greater part of the reigon.

But in the region having less anomalies, the variation of anomalies is slight. In such case, agreement between the two methods is found to be poor. This is depends upon the fact that the 'standard' curves are a almost parallel to the mean temperature co-ordinate in the part of low mean temperature. Consequently, the variation of $\Delta D$ in this part is mainly due to other oceanographic elements, presumably to chlorinity distribution.

The estimation in this part can not be performed with high accuracy without

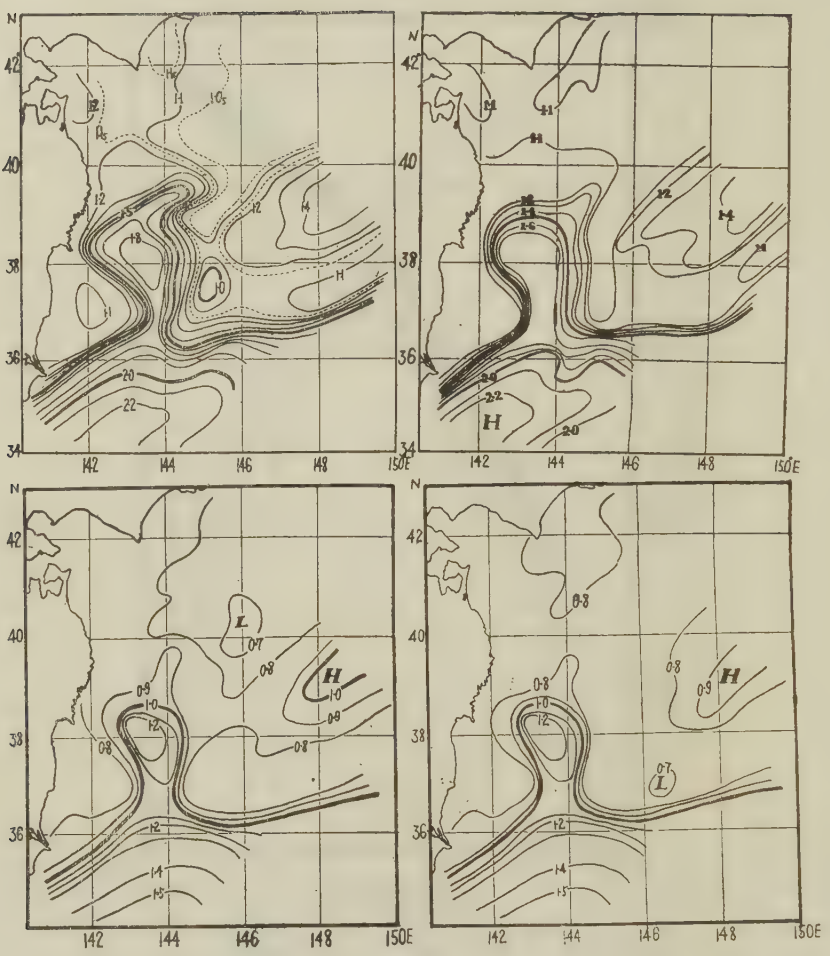


Fig. 8. Dynamic topography in dynamic meter refered to the 1000-decider layer according to observations east off Honshu in May 1954, computed by the standard technique (left) and by the mean temperature in upper 600 m and 200 m layer (right). *Upper*. At the sea surface. *Lower*. At the 200-deciber surface.

chlorinity data. Therefore the present simplified method is only applicable to the boundary area between the cold and warm water masses, such off the Tohoku District of Japan.

We examine this estimation in the North Pacific using the data of station Nos. 100–150 in the Cruise VII of the CARNEGIE. In these stations, when we adopt the mean temperature of upper 1000 m layer, the differences between two values of the dynamic depth anomaly at the surface, roughly estimated and normally computed, are within 6 cm except in the sea of the west coast of U.S.A. (Station No. 126 –No. 131) where the differences reach as far as 18 cm. But if

we adopt less thiner layer as 600 m for the mean temperature, in this case the difference increases more over 20 cm.

## 5. Acknowledgement

The author wishes to express his hearty thanks to Dr. Y. TAKENOUTI, Dr. T. ICHIYE, Dr. K. YOSHIDA, Mr. J. MASUZAWA, Mr. M. HANZAWA for their valuable advice and suggestions, and also to Mr. T. SAWARA for his assistance.

## References

KLEINE, H.T., 1955.
A new technique for processing physical oceanographic data. Preliminary Manuscript Copy (To be submitted to Journal of Marine Research).

MONTGOMERY, R.B. and W.S. WOOSTER, 1954.
Thermosteric anomaly and the analysis of serial oceanographic data. Deep-Sea Research, **2**.

STOMMEL, H., 1947.
Note on the use of *T-S* correlation for dynamic height anomaly computations. Journ. Mar. Res. **6** (2).

YASUI, M., 1955.
On the rapid determination of the dynamic depth anomaly in the Kuroshio Area. Records of Oceanographic Works in Japan **2**, (2).

YOSHIDA, K. and M. TSUCHIYA, 1956.
(to be published).

Scientific Results of Cruise VII of the CARNEGIE during 1928–1929 under Command of Captain J.P. Ault. Oceanography—1-B. Observations and Results in Physical Oceanography. Carnegie Institution of Washington Publication 545. 1945.

The results of marine meteorological and oceanographical observations. C.M.O., No, 14.—No. 18., 1954–1955.

Records of Oceanographic Works
in Japan Vol. 3, No. 1,
March 1957.

# A Note on the Horizontal Eddy Viscosity in the Kuroshio

By

Takashi ICHIYE

(Japan Meteorological Agency)

## 1. Introduction

Recently Charney (1955), Neumann (1955) and other people have entertained doubts against the large horizontal eddy viscosity introduced in the wind-driven circulation theory of Munk (1950) and have tried to explain the dynamical properties of the Gulf Stream as an inertia motion without a friction, which gives the partly successful results. On the other hand, Stommel determined the eddy viscosity in the Gulf Stream by use of the data of continuous current observation at one station, giving the value of about $10^6\,cm^2/s$ against $5\times10^8$ of Munk. It seems to be very important to determine the most reliable values of this quantity in order to develop the circulation theory, whereas the present state of oceanographic observations resticts the complete calculation of the eddy viscosity from the observed data, since this requires the continuous data both in time and space. However, the use of GEK will make it possible in the near future by taking adequate method of observation, and even in the present stage the relatively continuous records can be obtained at least concerning the space distributions of the current. Here we compute the momentum transport due to the turbulent flow near the boundaries of the Kuroshio and the results are discussed in relations with other phenomena.

## 2. The general current pattern, the data of which are used

The current observations by use of GEK were carried out extensively in the Kuroshio region by CMO and HO in March and May of 1956 (Hydrographic Office 1956, and CMO 1956) and the current pattern in the surface and the temperature distribution in the 100 m layer of these two observations are shown in Fig. 1 and 2, which indicate the Kuroshio in the southern sea off Honshu flowed almost eastwards in March, though with a small cyclonic vortex between 137°E and 139°E, which was gradually reducing its extent and intensity since last autum, and then it flowed to NE between 139°E to 142°E, where it changed its direction to east at the latitude of about 37°N, which is also somewhat southwards compared with the location in last autum. The main current in this region

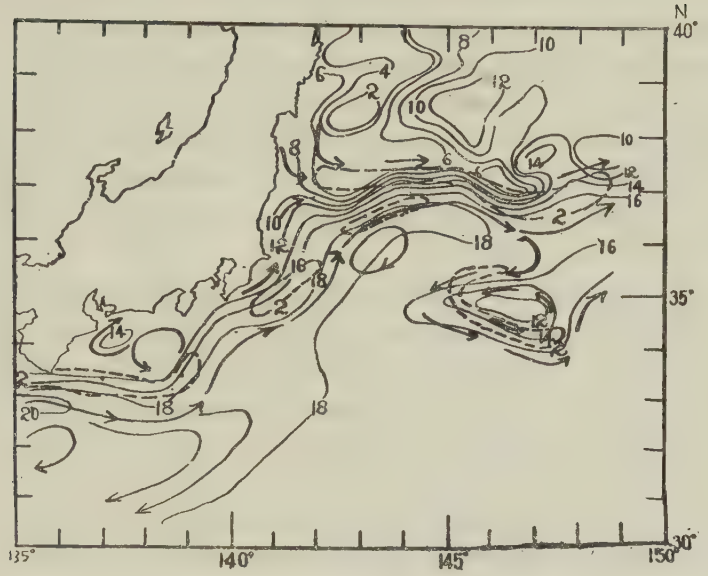


Fig. 1. Current pattern of the surface measured with GEK and water temperature (°C) in the 100 m layer in March, 1956 (Arrows indicate approximate stream lines, broken lines show the region with speed above 2 kt.)

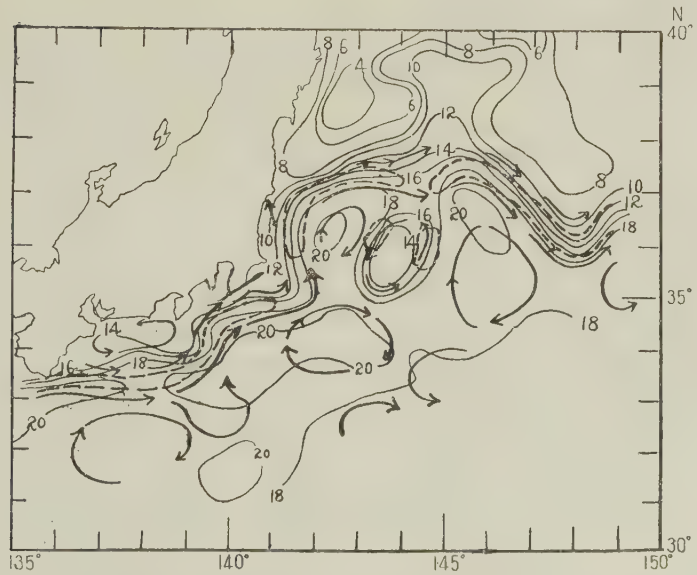


Fig. 2. Current pattern of the surface measured with GEK and water temperature (°C) in the 100 m layer in May, 1956 (See, the legend of Fig. 1)

flowed relatively straight without meandering as in all periods of 1954 and 1955, which seems to have some relations with the decay of the vortex in the southern sea, as proved with the theory of constant absolute vorticity, since the detour of the Kuroshio around this vortex forms the trough of the meandering, the first ridge of which is usually located between 142°E and 145°E (ICHIYE, 1956 b). The vortex with its center at 35°N, 145.5°E was the continuation of the one which was produced in last summer due to the southwards extension of the trough of the meandering of the Kuroshio.

In May, the condition in the southern sea was almost similar to the previous period, though to the south of the main current the weak vortices became more clearly distinguished. In the northern sea cyclonic and anti-cyclonic vortices are arranged by turns to the south of the Kuroshio, with the meandering of the main current increasing somewhat to the east of 145°E, and the cyclonic one with a center at 36°N, 144°E, which is probably the same vortex at 35°N, 145.5°E in the previous season, is distinguished with the conspicuous temperature gradient on the boundary from other two anti-cyclonic vortices, though it seems also to be seperated from the Kuroshio.

### 3. The momentum transport across the Kuroshio

In order to compute the momentum transport, we divide the region in the southern and northern part with the latitude of about 35°N, and in each region we compute it by the formula such as $u'v'=(u-\bar{u})(v-\bar{v})$ and $\bar{u}\cdot\bar{v}$ where $u$ and $v$ are the component parallel to the maximum current of the Kuroshio and that transversal to it, and $u'v'$, $\bar{u}\cdot\bar{v}$ mean the transport due to the turbulent flow and mean flow, respectively, and the averages are taken along the lines almost parrallel to the Kuroshio. Further, in May the intermediate region between 35°N and 37°N is defined, since the main current of the Kuroshio there has northerly component instead of the easterly one in other regions. The computed values of $u'v'$, $\bar{u}\cdot\bar{v}$ and mean flow $(\bar{u}, \bar{v})$ are shown in Fig. 3 and Table 1 against the mean distance $y$ of all GEK stations from the maximum current zone of the Kuroshio, the data of which are included

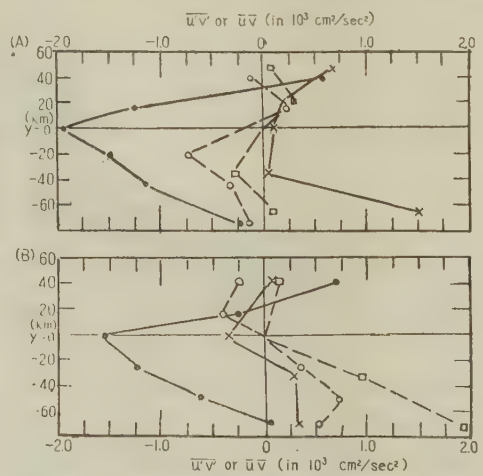


Fig. 3. Distribution of $\overline{u'v'}$ and $\bar{u}\bar{v}$ (A in March, B in May)

● $u'v'$ ○ $\bar{u}\cdot\bar{v}$ in the southern sea

× $\overline{u'v'}$ □ $\bar{u}\cdot\bar{v}$ in the northern sea

Table 1

| | $y$ (km) | $\overline{u'v'}$ $\times 10^3$(cm$^2$/sec$^2$) | $\bar{u}\cdot\bar{v}$ $\times 10^3$(cm$^2$/sec$^2$) | U (cm/sec) | $\varphi$ (deg.) | $\overline{u'^2}$ $\times 10^3$(cm$^2$/sec$^2$) | $\overline{v'^2}$ $\times 10^3$(cm$^2$/sec$^2$) |
|---|---|---|---|---|---|---|---|
| March | | | | | | | |
| Southern Sea | 38 | 0.57 | −0.12 | 15 | 137 | 1.23 | 0.76 |
| | 16 | −1.25 | 0.21 | 79 | 75 | 1.78 | 4.16 |
| | 0 | −1.93 | 0 | 155 | 77 | 7.58 | 0.61 |
| | −19 | −1.48 | −0.73 | 114 | 81 | 3.65 | 1.31 |
| | −43 | −1.17 | −0.31 | 54 | 83 | 1.83 | 1.87 |
| | −74 | −0.23 | −0.28 | 41 | 87 | 1.75 | 0.72 |
| Northern Sea | 46 | 0.63 | 0.05 | 13 | 78 | 0.72 | 1.11 |
| | 22 | 0.21 | 0.29 | 24 | 59 | 1.02 | 2.43 |
| | 0 | 0.12 | 0 | 177 | 96 | 6.57 | 0.56 |
| | −34 | 0.08 | −0.23 | 67 | 98 | 3.53 | 1.80 |
| | −65 | 1.49 | 0.03 | 41 | 92 | 0.65 | 1.20 |
| May | | | | | | | |
| Southern Sea | 42 | 0.69 | −0.23 | 35 | 94 | 1.13 | 0.68 |
| | 17 | −0.26 | −0.36 | 28 | 112 | 0.98 | 3.19 |
| | 0 | −1.56 | 0 | 140 | 84 | 3.24 | 0.97 |
| | −24 | −1.23 | 0.34 | 70 | 81 | 2.74 | 0.94 |
| | −51 | −0.63 | 0.73 | 54 | 68 | 1.71 | 0.84 |
| | −68 | 0.04 | 0.27 | 34 | 70 | 0.32 | 0.43 |
| Sea bet. 35° and 37°N | 38 | 0.47 | −0.10 | 17 | 46 | 0.63 | 1.25 |
| | 0 | 0.20 | 0 | 93 | 2 | 2.86 | 0.97 |
| Northern Sea | 43 | 0.03 | 0.08 | 34 | 91 | 1.04 | 1.75 |
| | 0 | −0.34 | 0 | 116 | 95 | 3.50 | 1.12 |
| | −32 | 0.31 | 0.98 | 81 | 86 | 0.92 | 0.74 |
| | −64 | 0.36 | 1.94 | 62 | 55 | 1.27 | 0.98 |

$y$: the mean distance from the maximum current zone ($y=o$) to the GEK stations. Positive values mean the left hand side to the Kuroshio.
$u, u'$: velocity components parallel to the mean velocity at $y=o$
$v, v'$: those transversal to the mean velocity at $y=o$
U, $\varphi$: the mean velocity and its direction. (North in taken 0°)

into the sum in the mean values of $\overline{u'v'}$ and $\bar{u}\cdot\bar{v}$. The figure and table indicate the remarkable features, which is common in both observations, such as

(1) In the southern sea, the values of $\overline{u'v'}$ are generally negative, or they give southward transport, the maximum of which occurs at the zone of maximum velocity of the Kuroshio, with contrast to the condition of the westerly, where the greatest northward transport is obtained. (STARR and WHITE, 1952)

(2) In the northern sea, $\overline{u'v'}$ is as a whole, positive and less than in the southern sea numerically, with the (algebraic), minimum value near the maximum velocity zone, which corresponds to the condition in the southern sea.

(3) The transport due to the mean motion $\bar{u}\cdot\bar{v}$ are generally much less than those of turbulent motion numerically except of the northern sea in May, and also they seem to have (algebraically) larger values in the northern sea than in the southern sea, corresponding to the values of $\overline{u'v'}$.

The eddy viscosity $K$ can be obtained from such momentum transport due to the turbulent motion and the mean velocity with the formula.

$$K\, d\bar{u}/dy = -\overline{u'v'} \qquad (1)$$

and the results of the computation are also shown in Table 2, where only in a few cases the eddy viscosity can be determined, owing to its negative values in some cases. This table indicates that $K$ is of the order of $10^6 \sim 10^8$ cm$^2$/sec and it is of $10^6 \sim 10^7$ cm$^2$/sec in the main current of the Kuroshio, where the estimated values are relatively reliable owing to the good accuracy of $d\bar{u}/dy$. The negative values of $K$ at the left hand side of the Kuroshio ($y>0$) in the southern sea are apparently due to the negative $\overline{u'v'}$. This seems to be caused by the condition that the eddy flux there is produced not with the free turbulence within the current, but with the forced one due to the friction at the coast or to the cyclonic vortex observed in the considered region, where the energy exchange between such vortex and the Kuroshio is determined by the author (ICHIYE 1954). Phenomenologically, the difference in signs of $u'v'$ in the northern and the southern sea seems to be due to the inclination of the trough lines to the mean current, where the negatiue inclination (from the left upper to the right lower for the current flowing to the right) is expected in the southern sea and the positive one in the northern sea, as seen in Fig. 2, though in the pattern of March it is not clear (MACHTA, 1949 ; ICHIYE, 1956 a).

Table 2

| | $y$ (km) | $K$ $\times 10^7$ (cm$^2$/sec) |
|---|---|---|
| March | | |
| | −10 | 7.7 |
| S | −31 | 3.2 |
| | −58 | 16.6 |
| | 11 | 0.24 |
| N | 34 | 11.2 |
| May | | |
| | −12 | 4.7 |
| S | −38 | 13.7 |
| | −60 | 3.3 |
| M | 19 | 0.78 |
| N | −16 | 0.27 |

S = Southern Sea
N = Northern Sea
M = Sea betw. 35° and 37°N

## 4. The relations between the mean flow and turbulent motion

Other quantities giving the energy of turbulent flow such as $\overline{u'u'}$ $\overline{v'v'}$ are also computed from the same data as above, which are shown in Table 1. This table indicates that the values of $u'u'$ are usually larger than $v'v'$ and the former has its maximum at $y=0$ or at the maximum current zone of the Kuroshio, whereas the latter has a peak to the immediate left of it. In May, these values seem to be rather reduced from the previous period.

The relation of the energy of the mean motion and the turbulent motion is given by

$$dE/dt=\iint\left\{u'u'\frac{\partial\bar{u}}{\partial x}+v'v'\frac{\partial\bar{v}}{\partial y}+u'v'\left(\frac{\partial\bar{v}}{\partial x}+\frac{\partial\bar{u}}{\partial y}\right)\right\}dx\,dy \qquad (2)$$

for two-dimensional motion, where $E$ is the energy of the mean motion and $d/dt=\partial/\partial t+\bar{u}\partial/\partial x+v\partial/\partial y$.

In the present case, the average process is taken along the lines almost parallel to the main current of the Kuroshio, and when we take $x$ axis as such lines, then (2) may be written as

$$d\overline{E}/dt=\int\left\{\overline{v'v'}\frac{\partial\bar{v}}{\partial y}+\overline{u'v'}\frac{\partial\bar{u}}{\partial y}\right\} \qquad (2')$$

where $\overline{E}$ means the average energy of the mean motion on $x$-axis. From the data given in Table 1, the 1st and 2nd integral of the equation (2′) can be computed, which are shown in Table 3. The 1st integral is not negligible compared

Table 3

| | Range of $y$ (km) | | $\int\overline{u'v'}\frac{\partial\bar{u}}{\partial y}dy$ $\times10^3$ (cm³/sec⁻³) | $\int\overline{v'^2}\frac{\partial\bar{v}}{\partial y}dy$ $\times10^3$ (cm³/sec⁻³) | $\int(\bar{u}^2+\bar{v}^2)dy$ $\times10^9$ (cm³/sec⁻²) |
|---|---|---|---|---|---|
| March | | | | | |
| S | 27 | −58.5 | 23.1 (0.20) | − 5.4 (−0.06) | 70.8 (0.83) |
| N | 34 | −50 | 6.3 (0.07) | 20.0 ( 0.24) | 78.2 (0.93) |
| May | | | | | |
| S | 30 | −60 | 11.2 (0.12) | −38.8 (−0.43) | 65.4 (0.73) |
| N | 21.5 | −49 | 14.6 (0.21) | −21.5 (−0.31) | 46.5 (0.66) |

"Range of $y$": from $y=27$ km to $y=-58.5$ km
Values in ( ) : Values per 1 km breadth of the current.

with the 2nd term, as seen in the table, and the latter has always positive values, whereas the former is negative except in the northern sea of March. The values of $\overline{E}$, corresponding to the computation of the right hand side (2′), are also determined, and shown in Table 3, but the decrease of $\overline{E}$ from March to May is contradictory to the positive values of the right hand side both in the southern and northern sea. However, in each period, the qualitative agreement is obtained by assuming the stationary case and taking $d\overline{E}/dt=\bar{u}\partial\overline{E}/\partial x$, since the positive value of the right hand side of (2′) corresponds to the increase of $\overline{E}$ from the southern sea to the northern sea (March) aud *vice versa* (May), though the accuracy of the data seems to be too insufficient to prove it definitely. In other words, the equilibrium state concerning the exchange between the mean flow and turbulent motion should be attained in relatively short period, thus the knowledge about the supply of the energy from the latter to the former seems to be insufficient for the forecasting of the change in the energy of the mean flow during

a long interval of several months, though the exchange of the mean current and the cyclonic vortex in the southern sea may be an useful tool for this purpose (ICHIYE, 1954).

Another relation between the mean flow and turbulent motion is given by

$$d\bar{u}/dt = -\partial\overline{u'v'}/\partial y \quad \text{or} \quad \partial\bar{u}/\partial t = -\partial\overline{u'v'}/\partial y - \partial\bar{u}\cdot\bar{v}/\partial y \qquad (3)$$

which indicates that the velocity $\bar{u}$ increases or $d\bar{u}/dt>0$, and $\partial\bar{u}/\partial t>0$ in the right hand side of the maximum current zone, and it decreases in the left hand side or in the northern zone of the Kuroshio both in the southern sea and northern sea, as shown from the values in Table 1. However, the change in $\bar{u}$ or $d\bar{u}/dt$, $\partial\bar{u}/\partial t$ does not correspond to such conditions, except the fact that in the northern sea the increasing meandering of the Kuroshio in May made its mean location shift southwards from the previous period. Therefore, it seems that the relation (3) also should be applied to shorter period fluctuations of the mean flow, though the definite conclusion may be obtained after carrying out more adequate observations.

## 5. Application to the plankton distributions in the southern sea

It was reported by Kitou (1956) that the plankton larvae of littoral benthos were collected abundantly at the stations on the northern boundary of the Kuroshio in 1955, The plankton samplings in 1956 also indicate similar result, and the large population was observed at a station which is also located on the northern boundary, though it is nearer to the coast than in the last year owing to the shrinkage of the cold water vortex, as stated before.

In Fig. 4, the distributions of total numbers of such larvae (*Ophioplutens, Echinoplutens, Cypris, Cyphonautens* etc.) and the corresponding oceanographical condition are shown for the observation of May and July in 1956. It is noted that these two distributions have common features such as the second maximum population at St. 3. In both observations, St. 1 is clearly located at the coastal water region, thus it has the maximum population, whereas the second maximum is not observed at St. 2, but at St. 3. This is due to the condition that the values of $u'v'$ are negative near the maximum current zone or St. 3 as stated in § 3 and the coastal water is transported southwards into the Kuroshio on the northern boundary by the turbulent motion, then it is advected speedily eastwards with the strong current, without loss owing to diffusion. Therefore, the stations to the south of St. 3 have much less population than St. 3, because of the small velocity there resulting in the loss with the diffusion, on one hand, and of the effect of St. 3 as a barrior to further southwards transport.

When we assume that $s'v' \propto \bar{s}\,u'v'$, where $s$ means the population of larvae, with bar and dash as defined as § 3, then we have

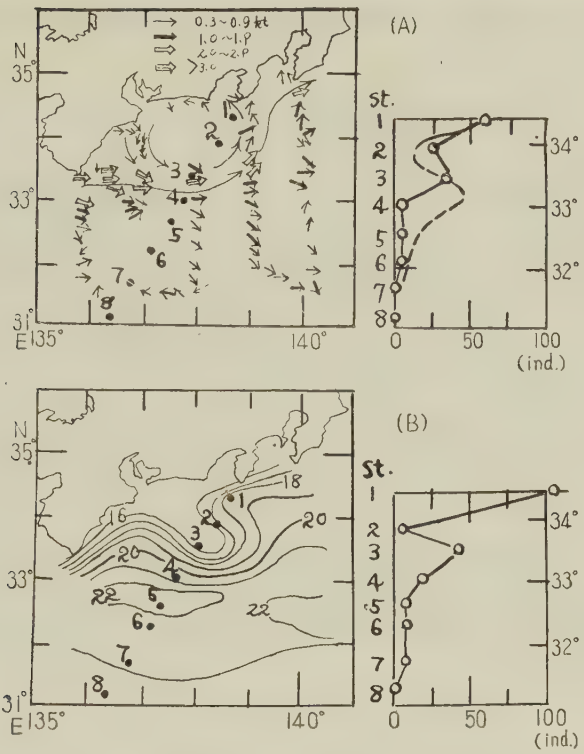


Fig. 4. Distributions of larvae of littoral benthos and oceanographical conditions.

(A) May, 1956. (Left: surface current measured with GEK)
Broken line shows the computed distribution.

(B) July, 1956. (Left: temperature in the 100m layer)

$$d\bar{s}/dt = -\frac{\partial \bar{s}\overline{v'}}{\partial y} = -\frac{\partial \bar{s}\,\overline{u'v'}}{\partial y}$$

or when we put [ ] the average between $y=y_1$ and $y=y_2$ $(y_2>y_1)$, then

$$d[\bar{s}]/dt = \{(\bar{s}\,u\,\overline{v})_1 - (\bar{s}\,\overline{u'v'})_2\}/(y_2-y_1) \qquad (4)$$

where suffices 1 and 2 mean the value at $y=y_1$ and $y=y_2$. Qualitative applications of (4) suggest that the right hand side of (4) becomes negative near St. 2, where $(u'v')_1<0$, $(u'v')_2>0$ as shown in Table 1 and further $(\bar{s})_2$ may be large, since $y_2$ is near the coast, thus it gives the decrease of $[\bar{s}]$. Near St. 3, $(u'v')_2$ has a large negative value when we take $y_2 \fallingdotseq 0$ or near the maximum current zone, and $(\bar{s})_1$ may be reduced conspicuously due to the intense eastwards transport of $\bar{s}$ near $y=y_2$, the result of which gives the large positive value for $d[\bar{s}]/dt$. To the south of this, both $[s]_1$ and $[s]_2$ are near zero, giving a very small value of $d[\bar{s}]/dt$.

More simple and formal explanation for the observed distributions as given from the relation

$$-\frac{\partial}{\partial y}\left(A\frac{\partial s}{\partial y}\right)=\frac{\partial}{\partial y}(sv) \tag{5}$$

where $S$ in this equation means $\bar{s}$, and $A$, $v$ are a mixing coefficient and velocity component transversal to the main current. In practice, $v$ should not be interpreted as the mean velocity, but considered to include the effect of $u'v'$, since the latter cannot be expressed with the term such $K\,\partial\bar{u}/\partial y$ for $y>0$, as stated in § 4. Further we assume $A$ is proportional to the energy of turbulent motion $u'u'+v'v'$, and integrating (5) formally, we have

$$S=\left\{S_a+P\int_a^y \exp\left[-\int_a^m V dn\right]dm\right\}\exp\left[\int_a^y V dn\right] \tag{6}$$

where $S_a$ and $P$ mean the value of $S$ and $dS/dy$ at $y=a$, and $V=v/A=\text{const.}\times u'v'/(u'v'+v'v')$. We make use of the values of Table 1 and take $S_a$ and $P$ from the observed value of May shown in Fig. 4, then the computed curve for adequate constants is shown in Fig. 4 with a broken line, which gives the good agreement with the observed data.

## 6. Conclusion

The present estimation of eddy viscosity is not so satisfactory, since the data used for the calculation of $u'v'$ etc. are not of the continuous record but of the discrete values given only at each siation, and further, we cannot take the average about the time to the present stage. However, the order of it seems to be not so unreasonable, and the conditions that the southern region the maximum current zone has the largest peak of negative transport $u'v'$ corresponds to the observed facts about the plankton of littoral benthos larvae. Therefore, we can conclude at least qualitatively that the eddy viscosity in the Kuroshio is of the order of $10^6\sim10^7$ which is intermediate between Stommel's and Munk's value.

In another point of view, the eddy viscosity determined by Stommel is only of the limited period for the small scale domain, whereas Munk's value is concerned with the large scale circulation under the assumption of stationary condition, thus they are quite different in scale both of time and space. It seems to be important to obtain the relation of the time scale to the eddy viscosity such as the Batchlor and Heisenberg's 4/3 power law with the scale of the space, though in a common sense it has been accepted better to take the less value of the eddy viscosity for the shorter period motion. (ICHIYE 1951).

## Literatures

CHARNEY. J.G. (1955): The Gulf Stream as an internal boundary layer. *Proc. Nat. Acad. Sci.* U.S.A., **41**.

CMO, Oceanographic Section (1956): Report of the oceanogrcphic observations in the sea east of Honshū in February~March, 1955. That of May~June, 1956. (To be published) *Oceanographical Rep.* (In Japanese) Vol. **5**, No. 2 and No. 3.

Hydrographical Office (1956): State of the sea adjacent to Japan. Feb.~Mar. and May~June (Charts)

ICHIYE, T. (1951): On the variation of oceanic circulation (1) *Oceano. Mag.* (Tokyo) **3** (2).

ICHIYE, T. (1954): On the variation of oceanic circulation (IV) *Geophys. Mag.* (Tokyo) **2**.

ICHIYE, T. (1956 a): On the properties of the isolated cold and fresh water along the edge of the Kuroshio (Hydrography of the polar front region IV). *Oceano. Mag.* (Tokyo) 8 (1).

ICHIYE, T. (1956 b): On the variation of oceanic circulation in the adjacent sea of Japan. *UNESCO Symposium Report.* (To be published)

KITOU, M. (1956): The correlation of the oceanographical conditions to the distributions of plankton larvae of littoral benthos in Enshu-nada. (in Japanese) *Journ. Oceano. Soc. Japan,* **12** (3).

MACHTA, L. (1949): Dynamic characteristic of a tilting trough model. *Journ. Met.* **6** (4).

MUNK, W.H. (1950): On the wind driven ocean circulation. *Journ. Met.*

NEUMANN, G. (1955): On the dynamics of wind-driven ocean currents. *Meteorol. Pap.* New York Univ. **2** (4).

STARR, V.P. and WHITE, R.M. (1952): *QJRMS* **78**.

STOMMEL, H. (1955): On the horizontal eddy viscosity determined from the serial current observation. *Deep Sea Res.* **2** (3).

Records of Oceanographic Works
in Japan Vol. 3, No. 1,
March 1957.

# On the Storm Surges caused by the Typhoon 5415 "Marie" (I)

By

Takashi ICHIYE

(Japan Meteorological Agency, Oceanographical Section

## 1. Introduction

The Typhon 5415 "Marie" attacked Japan on September 26 in 1954, and caused many damages at various places, including the disastrous wreckages of Toya-maru and other ferry-steamers in Hakodate Harbour. This typhoon landed at the Kagoshima Bay at 2 h of 26, with the minimum pressure of 965 mb and the maximum wind speed of 40 m/s, then it passed through the eastern part of Kyūshū northeastwards with the speed of 75 km/h. After attacking the western Honshū, it advanced into the Japan Sea at 8 h, and proceeded over the Japan Sea, as developing further. At 21 h, it passed off the western coast of Hokkaido, with the minimum pressure of 956 mb, which is also the lowest pressure of this typhoon near Japan. Then it advanced furthur northeastwards, entering into the Okhotsk Sea. (Geophysical Review, 1955)

This typhoon caused strong storm surges at various ports and bays on the coast of Japan, and they were especially conspicuous within the right half of the storm area. Further it is noted that the storm surges at the coast where the typhoon center passed near by have the features of the progressing wave accompanying with the typhoon, and that those in the shallow bays on the Pacific coast of Honshū were also severe even in the distant regions from the typhoon, owing to the set up of the sea level by the southerly wind of long duration.

## 2. General features of the storm surges

In Fig. 1 the course of the typhoon and the tidal stations, of which the data are available here are shown. The hourly deviations of tidal heights at each station are computed with the observed heights minus predicted ones, where the latter is obtained from the resultant curves of harmonic predictor for the stations with exact harmonic components and it is taken as the running averages of the observed heights after and before the date of the attack of the typhoon with the similar method for filling up the gap of tidal heights in case of harmonic analysis for the stations without them. (DOODSON, 1928)

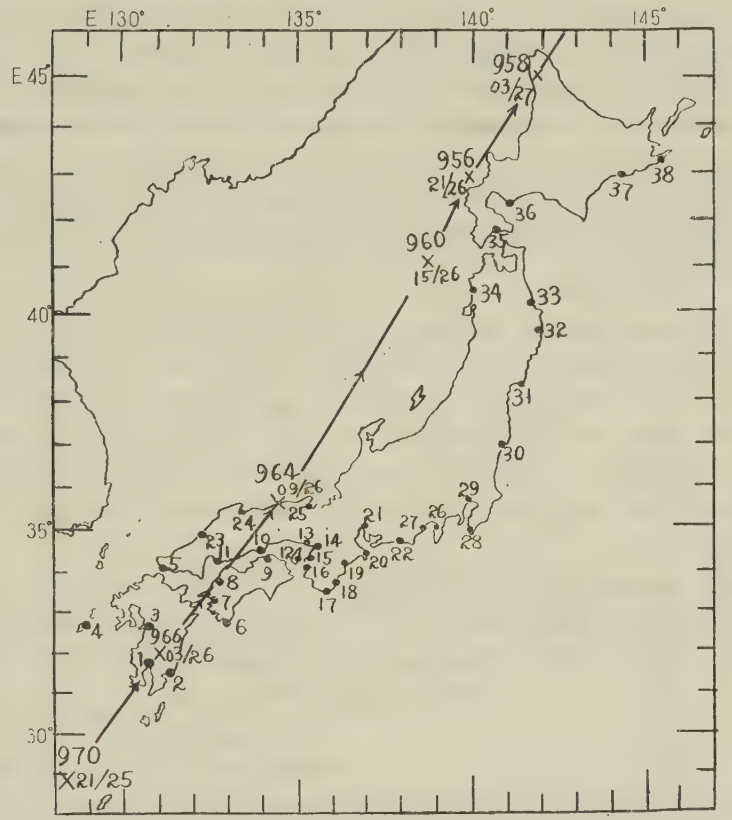


Fig. 1. Tidal stations and the course of the Typhoon 5415.
(● Tidal stations; × 964 09/26 center of the typhoon at 9 h of 26th with the minimum pressure of 964 mb)

Name of the statioes

| | | | |
|---|---|---|---|
| 1 | Kagoshima | 20 | Toba |
| 2 | Aburatsu (Data incomplete) | 21 | Nagoya |
| 3 | Misumi* | 22 | Maisaka* |
| 4 | Tomie* | 23 | Tonoura |
| 5 | Shimonoseki | 24 | Sakai |
| 6 | Shimizu | 25 | Miyazu* |
| 7 | Uwajima | 26 | Uchiura |
| 8 | Matsuyama | 27 | Shimizukō |
| 9 | Takamatsu | 28 | Mera |
| 10 | Uno* | 29 | Tokyo |
| 11 | Kure* | 30 | Onahama* |
| 12 | Sumoto | 31 | Ayukawa |
| 13 | Kobe | 32 | Miyako |
| 14 | Osaka | 33 | Hachinoe* |
| 15 | Tannowa* | 34 | Iwasaki |
| 16 | Wakayama* | 35 | Hakodate* |
| 17 | Kushimoto | 36 | Muroran* |
| 18 | Urakami* | 37 | Kushiro |
| 19 | Owase* | 38 | Hanasaki* |

For the stations with the asteric, the predicted tides are obtained by taking the average of the observed values at 25 hours later and earlier than the considered time. For other stations, they are obtained from the predicted curve drawn with the harmonic components.

In Fig. 2, the maximum deviations $D_m$ for each station are plotted against the minimum pressure $p_m$ observed there. Further, the stations are classified in the figure into four classes, that is, the stations in the right half of the storm area and those in the left half, which are further divided in the groups of those on the coast of the bays with the mean depth of less than 100 m and those on the open coast or in the bays deeper than 100 m. The points of Fig. 2 are rather scattered, but when we examine their distributions carefully, the following characteristic features are seen.

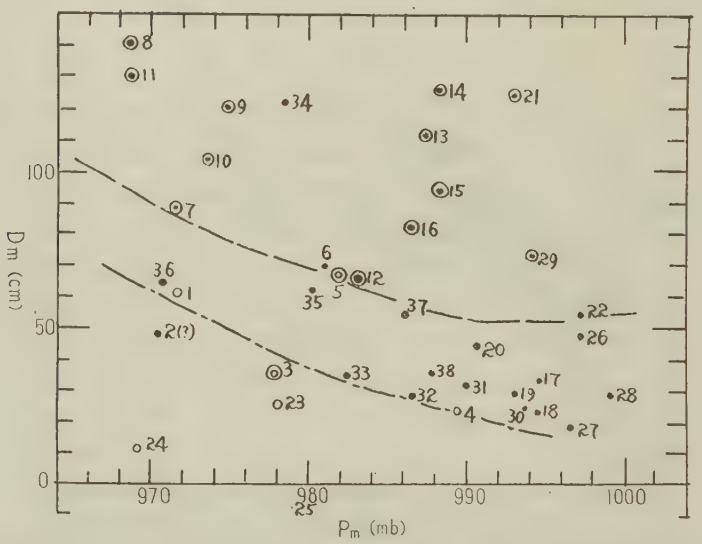


Fig. 2. The relation between the maximum tidal deviation ($D_m$) and the minimum pressure ($P_m$) at each station.

○ ◎: Stations in the right half of the storm area
● ⊙: Stations in the left half of the storm area
◎ ⊙: Stations on the coast of a bay with the mean depth less than 100 m
○ ●: Stations on the coast of the open sea or of a bay with the mean depth more than 100 m

(1) Generally, the maximum deviations decreases with the increasing minimum pressure, especially for the stations which are on the open coast, the ranges of which are indicated with the broken lines in the figure, and this is reasonable, since the minimum pressure is, as a whole, proportional to the distance of the station from the typhoon center.

(2) The storm surges at the stations in the right half of the storm area are generally smaller in their maximum deviations, compared with those in the left half, which is also expected, since the wind are usually stronger in the latter.

(3) Among the stations within the left half, those of 13, 14 and 15 (the

Osaka Bay) 21 (the Ise Bay) and 29 (the Tokyo Bay) show larger deviations than expected from the minimum pressure or the distance from the typhoon, and this is due to the effect of the set up of the water by the strong southerly wind in shallow bays.

(4) The deviations of St. 8, 9, 10 and 11 are also especially high, and these stations are on the coast of the Seto Inland Sea. Further, they are located near the path of the typhoon, therefore they are affected both with the effect of the set up and that of the wave accompanying with the typhoon.

(5) The stations 23, 24 and 25 are on the coast of the Japan Sea, and the storm surges at these stations are exceptionally small, compared with other stations with similar distance from the typhoon, which is probably due to the condition that they are on the open coast, and the southerly wind was more predominant in the present case, adding to the condition that the wave or sea level elevation proceeding with the typhoon from the southern sea could not enter into the Japan Sea.

However, the storm surge at St. 34, which is also on the coast of the Japan Sea, is so conspicuous that its point in Fig. 2 seems to suggest similar conditions to those in the shallow bays. In fact, this station has a peculiar feature, as stated after.

### 3. The durability of the storm surges

As a rule, the storm surges at some bays indicated conspicuous peak-like forms in the mareograms in the past, especially when the typhoon passed through the bays. (ICHIYE, 1951) Therefore, the durability of the storm surges defined with the value such as $(D_2+D_1+D_0+D_{-1}+D_{-2})/5D_0$ seems to have some relationships to the conditions of the sea near the stations and the distance from the typhoon, where $D_0$ means the maximum of the hourly deviations and $D_n$ or $D_{-n}$ means the deviation at $n$ hours later or earlier than the time when $D_0$ was observed.

Further, the distance of the each station from the typhoon may be represented more adequately by the difference between the minimum pressure $p_m$ and that of the typhoon center $p_0$ at the time when $p_m$ was observed, than the value $p_m$ itself. Therefore, the durability defined as above for each station are plotted in Fig. 3a against $p_m-p_0$, and the relations between the distance from the path of the typhoon and the values $p_m-p_0$ are also shown in Fig. 3b. The distribution of the points in Fig. 3a seems to be more regular than that of Fig. 2, showing the general increase of durability as the values of $p_m-p_0$ increasing, which in turn are roughly proportional to the distance from the typhoon. Further, the durablity at the stations in shallow bays is somewhat less than that of other stations, except the stations of the Inland Sea stated in (4) of the previous section, and this suggests that the storm surges in the shallow bays had the peaklike forms

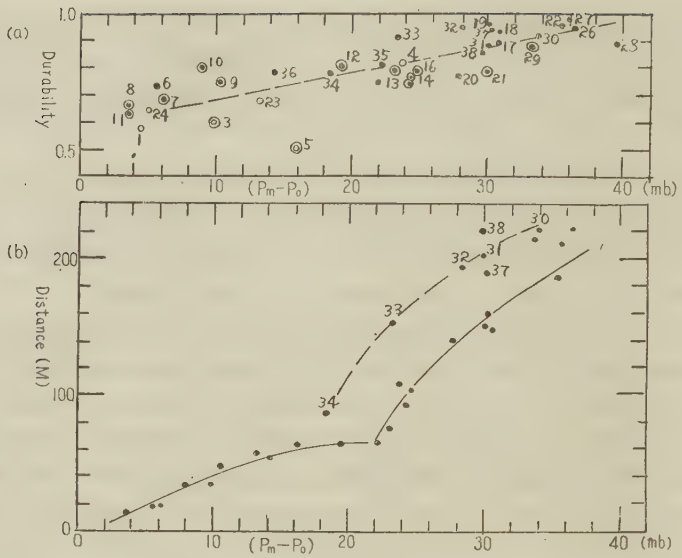


Fig. 3. The relation between the durability of the storm surge and $P_m - P_0$, and the relation between the distance from the course of the typhoon and $P_m - P_0$, for each station.
($P_0$ means the pressure at the typhoon center when $P_m$ was observed at each station. Refer to Fig. 2 as for the symbol for each station.)

also in the present case. However, such difference in durability of the bays is not so remarkable as expected from the past records, which is perhaps due to the condition that the bays which had been affected with the peak-like storm surges in the past are distant from the typhoon in this case. Fig. 3b indicates clearly the clearly the relationships between the distance from the typhoon center and the pressure, especially suggesting the existence of the inner and outer zone of the typhoon (DUNN, 1951). On the other hand, the relations in the outer zone seems to be different for the northern stations where the minimum pressure were observed after 15 h of 26th when the typhoon entered into the Japan Sea, and this seems to be due to the change of the structure of the typhoon, though the detailed discussion is unnecessary here. In the present paper, Fig. 3b may be referred only to compare the distance from the center and the durability.

## 4. Relations between the wind stress and the storm surges

Since the orographic conditions of each tidal station are different and so complicated, it is difficult to obtain the general relations between the wind conditions and storm surge being valid for all stations. However, the effects of shallow bays making the relations more complicated are, in some cases, not so conspicuous as shown in Fig. 3, that we may expect to get some simple rules about them, even though they are valid exactly not for all stations.

The storm surges on the open coast are relatively simple in their mechanism, and thus we may apply the results for such case to all the stations considered. For this purpose, we take two simple cases of the stationary wind stress and of the infinite fetch.

4. 1 Relations under the stationary assumption of the wind stress. In this case, the elevation of the sea level can be given by the equation

$$\zeta=\int_0^f \frac{(T-B)dx}{gh}=\frac{m}{g}\int_0^f\left(\frac{T}{h}\right)dx \qquad (1)$$

which is obtained immediately from the equation of motion $g\partial\zeta/\partial x=\nu\partial^2 u/\partial z^2$ and the condition that the current flux $\int_0^h u\,dz$ should vanish due to the coast, where $T$ and $B$ are the wind stress and bottom stress perpendicular to the coast, $f$ and $m$ mean the fetch and the constant, $h$ the depth of the sea, $\nu$ the eddy viscosity. The constant $m=1$ for the case of no bottom friction ($B=0$) and $m=3/2$ for the case of no bottom current ($B=-T/2$), though it has values dependent on $K=\frac{3\nu}{h}\left(\frac{T}{k}\right)^{\frac{1}{2}}$ for the general conditions at the bottom such as $|B|=k u_0^2$, where $u_0$ and $k$ mean the bottom current and frictional constant, respectively. (ICHIYE, 1952)

In order to apply the relation (1) to the present case, we compute the values of $\int_0^f (T/h)dx$ from the wind data and the depth distribution obtained from the charts for each station at 3 h, 9 h, 15 h and 21 h of 26th, and plot these values against the observed deviations of tidal heights corrected for the pressure effect, which is done by substracting the values $1.02(\bar{p}-p_n)$, where $\bar{p}$ is the monthly mean pressure in September of 1955 and $p_n$ is the pressure at the considered time for each station. For the practical computation of $\int_0^f\left(\frac{T}{h}\right)dx$ the following processes are taken.

(1) From the wind data at a weather station near a tidal station, we compute the wind stress $T$ by use of the Rossby's formula. (SVERDRUP, 1945)

(2) The component of $T$ perpendicular to the coast is obtained, where the direction of the wind is determined referring to the isobars in the weather charts.

(3) The value of $\int_0^f\left(\frac{T}{h}\right)dx$ is computed by the simplified formula $Tf/\bar{h}$, where the mean $\bar{h}$ is taken along the perpendicular to the coast.

(4) At the stations in a bay we take $f$ as the fetch of the ordinary sense, and for the stations on the open coast $f$ is taken as the distance from the coast the isobath of 200 m, since this is the boundary of the continental shelf around Japan, and in practice, the depth $h$ increases abruptly above this limit, with slight contributions to the integral.

(5) For some stations on the open sea, where the above boundary is ambiguous,

we estimate the range of the constant $T$ from the isobars in the weather charts, which is taken as $f$.

(6) We express $T$ in $cm^2/s^2$, $f$ in km and $\bar{h}$ in m.

The results of these computations are shown in Fig. 4, where only the values of the stations affected conspicuously by the typhoon at each time are plotted, since it seems to be useless to plot many points clustered near the origin. This figure indicates the following features about the relations of the observed wind effect ($O_w$), $D_n-1.02(\bar{p}-p_n)$, and the computed one ($C_w$), $T_n f/\bar{h}$.

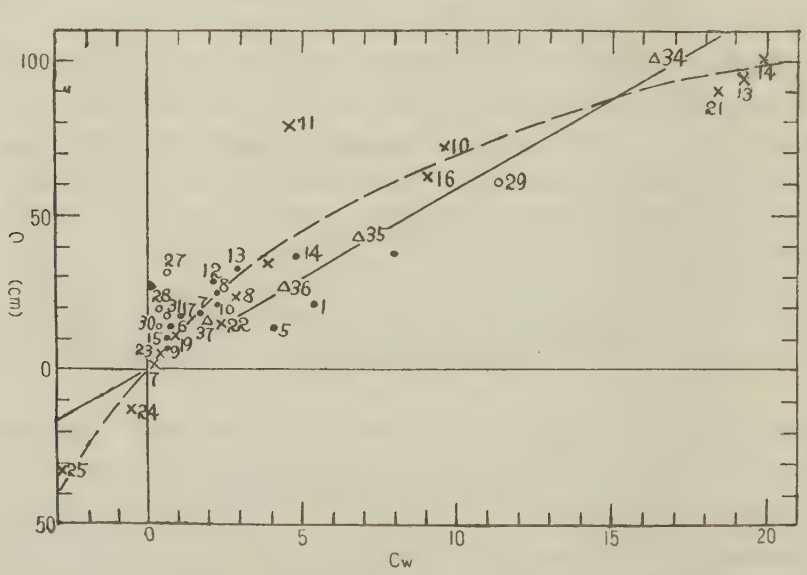


Fig. 4. The relation between the $O_w$ (observed tidal deviations corrected for pressure effect) and the $C_w$ ($Tf/\bar{h}$, where $T$ wind stress in $cm^2/s^2$, $f$ fetch in km, $\bar{h}$ mean depth of the sea in m)

● at 3 h of 26th × at 9 h
○ at 15 h △ at 21 h

Full line $O_w=5.8\,C_w$
Broken line $O_w=15.5\ (C_w)^{0.63}$

(1) The points at 3 h are scattered only in the neighbourhood of the origin, especially suggesting that the Owe at St. 1 and 5 was small compared with the value of Cwe owing to the predominance of the pressure effect.

(2) Most stations were affected by the storm surges at 9 h and at the stations in the shallow bays (13, 14 and 21) the Cwe gives the largest values, indicating the general proportionality between the Owe and the Cwe, except some stations.

(2-1) The point of St. 11 is quite apart from other points, indicating the Owe is far greater than the Cwe, which is reduced owing to the small fetch and to northerly wind, notwithstanding the shallowness of the sea and the strong wind. Such disagreement seems to be due to the effect of the wave advancing

with the typhoon (ARAKAWA and YOSHITAKE, 1936) which transported the water from the sea south to the bay of the station, thus making the effective fetch far longer than geographically determined.

(2-2) It is noted also that the sea level of St. 24 and 25 on the coast of the Japan Sea was rather depressed by the off-shore wind, which is reflected in the Cwe of the negative values.

(3) As a time proceeded, the storm surges at the more northern stations became conspicuous, as expected. The points of St. 29 and 34 show the similar relation of the Owe and Cwe as those at 9 h. Those of stations on the Pacific coast of the northern Honshū at 15 h indicate the smaller values of Cwe as compard with the Owe, though the absolute values of both are small, and this seems to be due to the underestimation of the fetches.

(4) We can see the remarkable proportionality between the Owe and Cwe even among the points at different time, except those near the origin.

(5) When this proportional constant is determined by the method of least squares, we have

$$O_w=(5.8\pm1.1)C_w \quad \text{(with 90\% confidence limits)} \qquad (2)$$

whereas the theoretical relation gives the value such as $\zeta=\frac{fT}{gh}=1.02fT/\bar{h}$ in case of no bottom friction for the present unit system of $f$, $T$ and $\bar{h}$. In other words, the constant of (2) corresponds to take $m=5.7$ instead of 1 or 3/2, which suggests that Cwe in the examples is underestimated. The reasons may be due to the overestimation of $\bar{h}$ in taking $f/\bar{h}$ instead of $\int_0^f \frac{dx}{h}$, because the set up of the sea is caused mainly by the accumulation of the water near the coast, thus the depth there being most effective, and also due to the rise of sea level by the travelling wave, which is not taken into account of the present computation under the stationary assumption.

(6) The distribution of the points suggests the better fit to the power law. Thus, determing the constants by the method of least squares as before, we have

$$O_w=15.5\,(C_w)^{0.63}$$

This power law indicates that the coefficient $m$ decreases with increasing values of Cwe, which corresponds to the case of the reverse bottom current and bottom stress to the wind (ICHIYE, 1952), since the theoretical value $m$ is given by

$$m=\frac{1}{2}(K+3-K\sqrt{K^2+2})$$

which decreases also with increasing values of $K$, where the latter is proportional to the Cwe here defined.

(7) As a conclusion, the possibility of forecasting the storm surges by use of the predicted weather charts is verified, because the relatively regular pro-

portionality is valid between the Owe and Cwe for all stations even at the different stages of the typhoon.

4 2 Non-stationary wind stress with the infinite fetch.

We have the equation of the elevation of the sea level in the sea extending infinitely to one direction as

$$\partial^2\zeta/\partial t^2 = \frac{\partial}{\partial x}\left(gh\frac{\partial\zeta}{\partial x}\right) - \frac{\partial T}{\partial x}$$

from the equation of motion $\partial u/\partial t = -g\partial\zeta/\partial x + \nu\partial^2 u/\partial z^2$ and that of continuity $\partial\zeta/\partial t = -\int_0^h u\,dz$ under the assumption of no bottom friction. This equation can be applied to the storm surge on the open coast, and especially for $\partial T/\partial x = 0$, $h = \text{const.}$, the solution is given by $\zeta = F(x-ct) - F(x+ct)$ for the condition that $\zeta = 0$ at $x = \infty$. Further, from the boundary condition at the coast $x = 0$, $\int_0^h u\,dz = 0$ or $\partial\zeta/\partial x = T/gh$, we obtain the elevation at $x = 0$ as $\zeta = \frac{1}{c}\int_0^t T\,dt$, with $c = \sqrt{gh}$

This equation is valid only on the open coast, but we apply it to all the stations considered, from the analogy in the previous sub-section.

We compute the values of $(T_{-1}+T_{-2}+T_{-3}+T_{-4}+T_{-5})/C$ instead of $\frac{1}{c}\int_0^t T\,dt$, where $T_{-n}$ means the component of the wind stress perpendicular to the coast at the time $n$ hours earlier than the hourly maximum deviations determined in § 3. We plot the hourly mamimum deviations corrected for the pressure effect (Omw) $D_0 - 1.02(p-p_0)$ against the computed one (Cmw) $\sum T_{-n}/C$ in fig. 5.

For the computation of Cmw, the depth in the speed of the long wave $C$ is

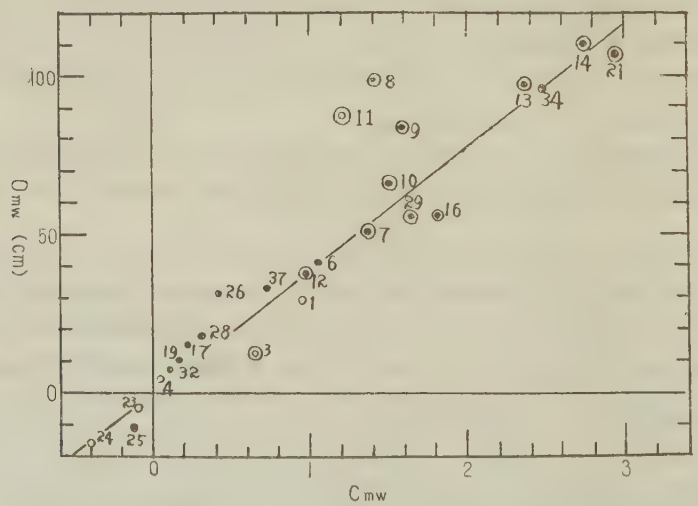


Fig. 5. The relation between the Omw (observed maximum deviation corrected for pressure effect) and the Cmw ($\sum T_{-n}/C$; $c$ means the speed of the long wave $\sqrt{gh}$ in m/s) (Refer to fig. 2, as for the symbol of each station.)

taken as the mean depth of the bays, for the stations in them and as the one computed in the Cwe for the stations on the open coast.

The distribution of the points indicates the following features. (The unit of $T$ is $cm^2/s^2$ and that of $C$ is $m$.)

(1) General proportionality is seen between the Omw and Cmw, except some points of the stations near the path of the typhoon.

(2) The points deviated much from such regularity are for St. 8, 9 and 11, which are all in the Seto Inland Sea and near the typhoon center, thus the effect of advancing wave causing such disagreement, in addition to the complicated orographic cohditions making the estimation of $\bar{h}$ uncertain, as stated before.

(3) The proportional constant determined by the method of least squares (omitting the points stated in the above item) is 38, which remakably corresponds to the theoretical value of 36, for

$$\zeta=\frac{1}{c}\int_0^t T\,dt=\left[\frac{1}{2}(T_{-1}+T_{-5})+T_{-2}+T_{-3}+T_{-4}\right]\times 1\text{ hour}/C\fallingdotseq 36\sum T_{-n}/C$$

in the present unit system, with contrast to the relation between the Cwe and the Owe in 4-1.

(4) This result can be also applied to the forecasting of the storm surges, when we can verify the proportionality between Cmw and Omw for more examples and obtain the constant almost common to any typhoon.

## Literatures


Arakawa, H. and Yoshitake, M. (1936): On the elevation of the surface of the sea under the influence of a travelling low pressure. *Proc. Phys.—Math. Soc. Japan.* **3** Series, Vol. 18.

Doodson, A. T., (1928): On the analysis of tidal observations. *Phil. Trans. A.* Vol. **227**.

Dunn, G. E., (1950): Tropical cyclones. *Compendium of Meteorology*, pp 887~901. Geophysical Review (1955): No. **661** September 1954.

Ichiye, T. (1951): On the abnormal high water caused by the Typhoon "Jane" (In Japanese) *Oceanog. Report.* Vol. **2**, No. 2.

Ichiye, T. (1952): A short note on the wind factor determined by the slope of sea surface. *Mem. Kobe Mar. Obs.* Vol. **10**.

Records of Oceanographic Works
in Japan Vol. 3, No. 1.
March 1937.

# On the Storm Surges caused by the Typhoon 5415 "Marie" (II)

By

Takashi ICHIYE
(CMO, Oceanographical Section)

## 5. Storm surges at the stations near the path of the typhoon.

The stations 6, 7, 8 and 11 are located in the course of the typhoon, thus they have commonly large values of maximum deviation and also the small durability. In fig. 6, hourly deviations at each station are plotted with the air pressure and wind data at St. 8, and the mareogram of the last two stations is shown in fig. 7.

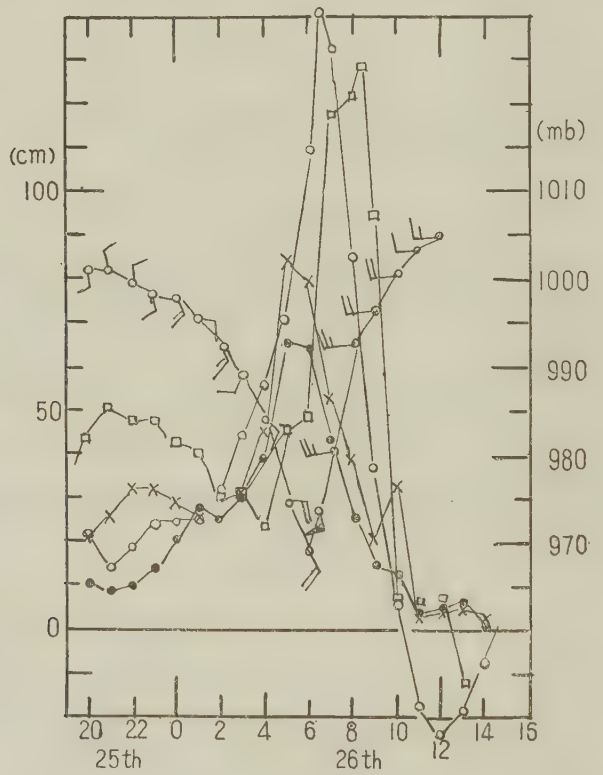


Fig. 6. Tidal deviations at St. 6 (● Shimizu) 7(× Uwajima) 8 (○ Matsuyama) and 11 (□ Kure), and the corresponding meteorological data at St. 8.

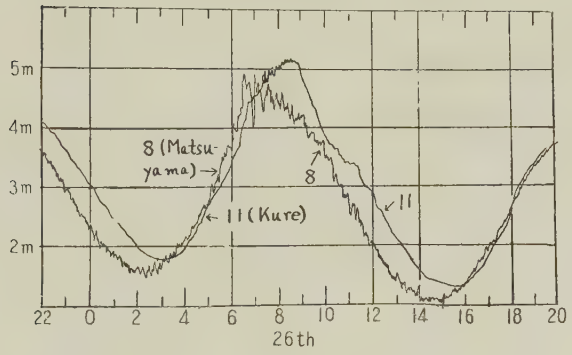


Fig. 7. Mareograma at St. 8 and 11

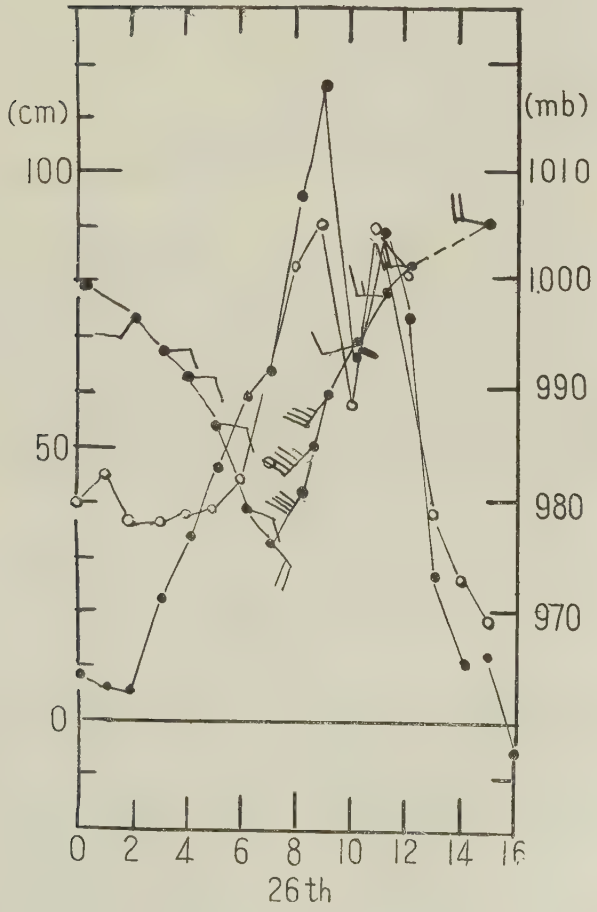


Fig. 8. Tidal deviations at St. 9 (● Takamatsu) and 11 (× Uno) and the corresponding meteorological data at St. 8.

As often stated in Part I, the stations 8 and 11 indicate the peculiar features, which are mainly due to the wave advancing with the typhoon. As shown in fig., the deviations increase abruptly for 8 and 11 from those at 6 and 7, and this is not only due to the difference in the meteorological conditions at these stations, but also due to the effect of such wave which increased its amplitude at the former stations located at the end of the shallow sea and also owing to the condition that the propagating velocity of such wave in the channel connecting these stations agrees well to the advancing speed of the typhoon. (WADATI, 1938). In fact, the latter was 85 km/h or 24 m/s for the considered region, and the velocity of the long wave near St. 6 and 7 (the Bungo Channel) is about 27 m/s, that near St. 8 (the Iyo-Nada) is 23.5 m/s, and that near St. 11 (the Hiroshima Bay) is 15 m/s. Therefore, theoretical increase of the amplitude computed by WADATI's theory reached to 5.6 times from St. 7 to St. 8.

Such consideration may be supported further from the fact that the wind effective for the set up of the sea level was much weaker at St. 8 and 11 than at 7.

The station 9 is in the right half of the storm area but it showed the conspicuous storm surge, whereas the abrupt decrease of the deviation after the maximum one seems to be due to the effect of the northerly wind of long duration.

## 6. The peculiar features of the storm surges at St. 9 and 10.

These stations are also located in the straits of the Inland sea with the complicated orographic condition and conspicuous values of tidal height were observed. The mareograms and the deviations at each station are shown in fig. 8 and 9, respectively, which indicate the remarkable double peaks for each station. The exact heights and the time of these double peaks are as follows, according to the report of Kobe Marine Observatory.

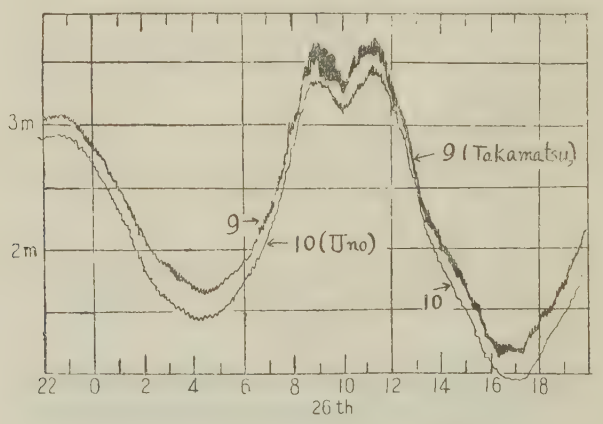


Fig. 9. Mareograms at St. 8 and 11.

| | the 1st. | peak | the 2nd | peak |
|---|---|---|---|---|
| at St. 9, | 9 h 00 m | 355 cm | 11 h 17 m | 367 cm |
| at St. 10, | 9 h 10 m | 335 cm | 11 h 15 m | 344 cm |

Since they occurred almost coincidently at two stations, located on both sides of the straits, they seem to have relation with the wave propagating through the Seto Inland Sea as one channel. In fact, the propagation diagram of the long wave show in fig. indicates the travel time from the region of St. 8 and 11 is about 3 h 20 m and that from the Osaka Bay (St. 13 and 14) is 1 h 50 m, whereas the maximum tidal height at the former occurred from 7 h 12 m to 8 h 26 m, as indicated in the figure and that of the latter occurred at about 9 h 10 m. Therefore, we can estimate that the two waves propagating from both sides of the channel met with each other in the considered region at about 10 h 30 m to 11 h 40 m, which seems to be the cause of the occurence of the double peaks at

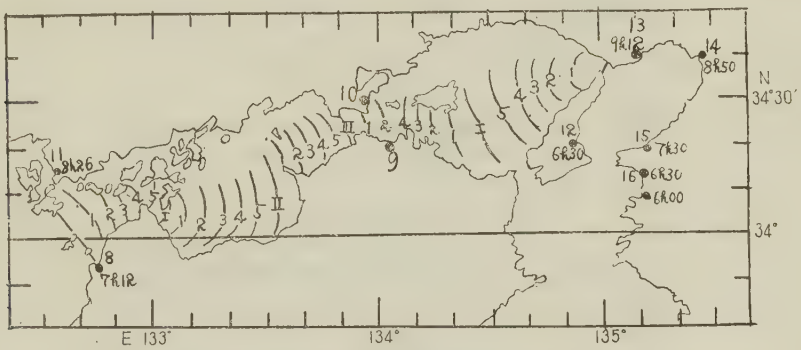


Fig. 10. Propagation diagram of the long wave in the Seto Inland Sea. (The curves indicate the wave front at an interval of ten min. The time near each station means that of occurrence of the maximum tidal height there.)

these stations, because we cannot find any cause in the meteorological conditions at the time of the second peak, since the wind became weak, and pressure also rose, as shown in fig. 10.

## 7. Storm surges at the stations on the coast of shallow bays.

These stations are common in the conditions that they have larger values of the storm surge, compared with those on the open coast having similar meteorological conditions and locations relative to the typhoon. Station 34 is included in this group, since it showed the same characteristic features as others of the group, as stated below.

7-1. St. 13 and 14 (the Osaka Bay). (Fig. 11 and 12 for St, 13, and 13 and 14 for St. 14)

The station 14 was affected with most conspicuous storm surge, owing to the

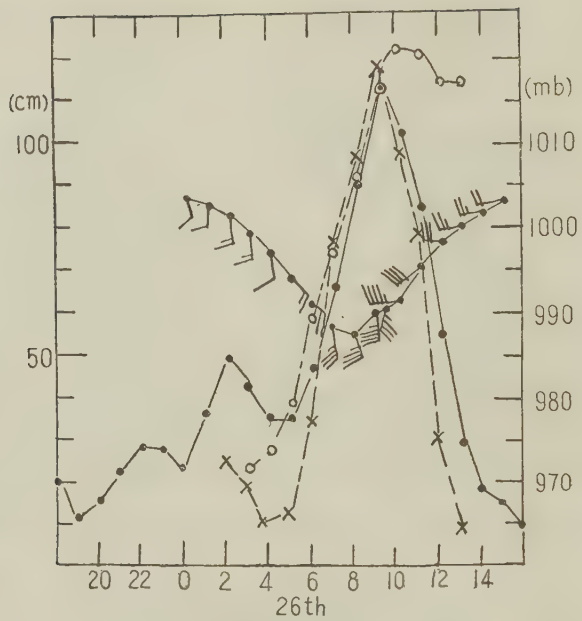


Fig. 11. Observed and computed tidal deviations and the corresponding meteorological data at St. 13 (Kobe)

● Observed deviations
○ Computed deviations with $k\sum T_{-n}$
× Computed deviations with (3–1)

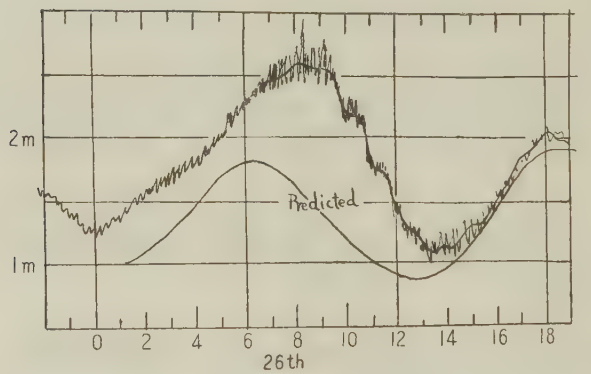


Fig. 12. Mareogram at St. 13.

strong SW wind, which caused the set up at this station located in the northeastern end of the bay. Further, the oscillations of the period of about 4 hours were observed both at St. 13 and 14 from 25th to 27th, which are due to the longitudinal secondary undulations of the Osaka Bay, and it is noted that the period was shorter than those observed in the Typhoon "Jane" of 1950 (ICHIYE, 1951). The mareograms of two stations are similar to each other, except the oscillations of the period of about two hours are predominant at St. 14, whereas

those of one hour's period were conspicuous at St. 13 from 7 h to 17 h of 26th, and the former is due to the longitudinal seiche of the bay, where the node passes near St. 13 and the latter seems to be due to the transversal seiche with

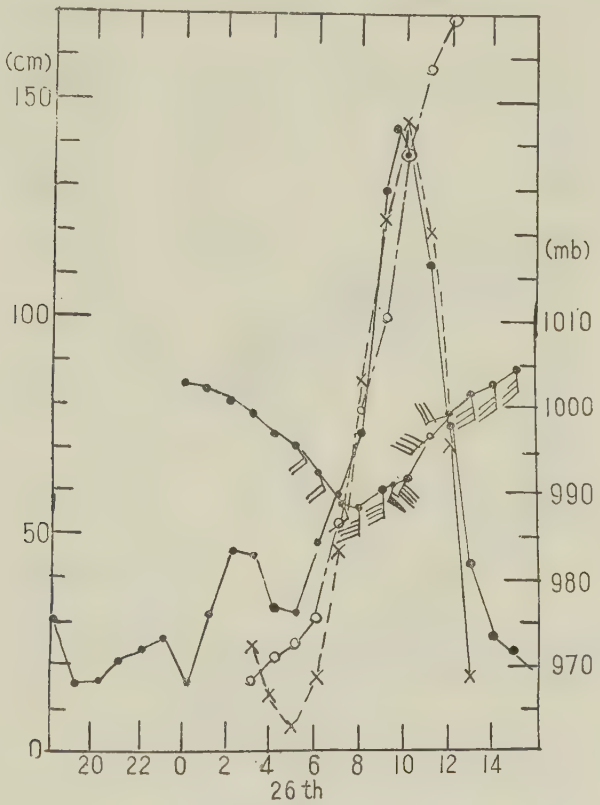


Fig. 13. Observed and computed tidal deviations and the corresponding meteorological data at St. 14 (Osaka)

● Observed deviations
○ computed with $k\sum T_{-n}$
○ computed with (3–1)

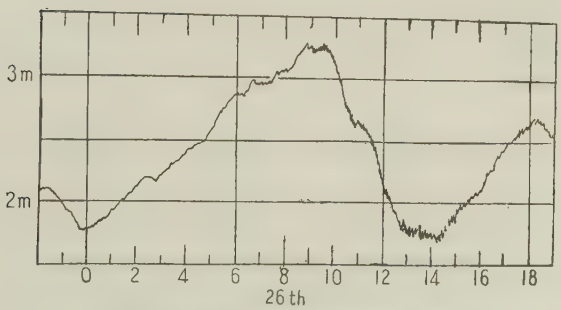


Fig. 14. Mareogram at St. 14.

the node passing through St. 14. (HIDAKA, 1931)

7-2. St. 21. (the Ise Bay). (Fig. 15 and 16)

The maximum deviation of 125 cm was observed almost at the same time as

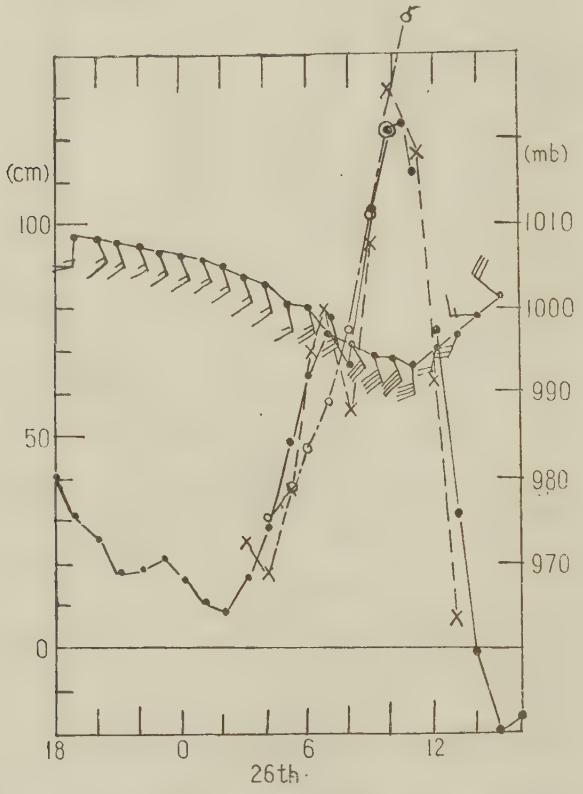


Fig. 15. Observed and computed tidal deviations and the corresponding meteorological data at St. 21 (Nagoya)

● Observed deviations
○ Computed with $k\Sigma T_{-n}$
× Computed with (3-3)

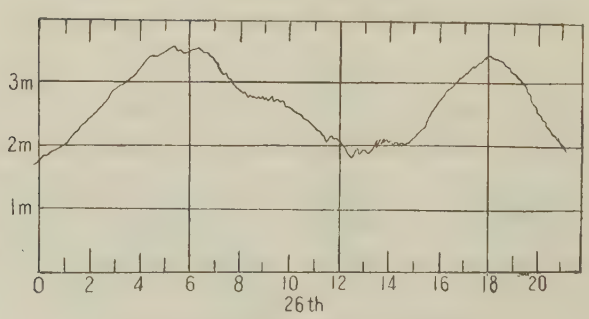


Fig. 16. Mareogram at St. 21

the maximum wind (10 h 20 m, S 22.2 m/s), and the decrease of the deviation after then was quite abrupt. The oscillations of about one hour's period were observed from 2h to 18h of 26th, which are somewhat shorter in their period, compared with the secondary undulations of the Ise Bay observed in other cases. (TERADA *et al*, 1908)

7-3 St. 29 (the Tokyo Bay) (Fig. 17)

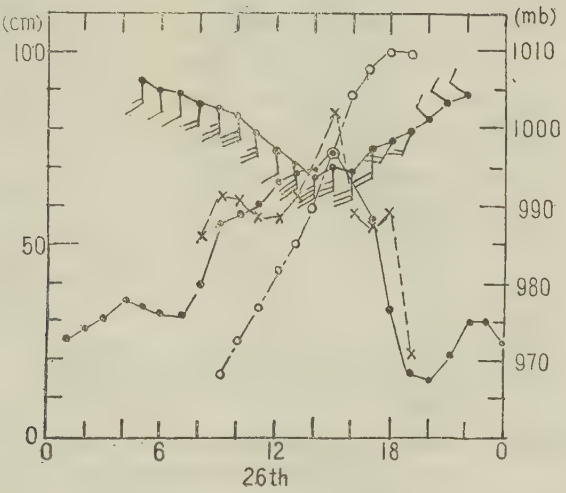


Fig. 17. Observed and computed tidal deviations and the corresponding meteorological data at St. 29 (Tokyo)

● Observed deviations
○ Computed with $k\sum T_{-n}$
× computed with (3-2)

The maximum deviation occurred from 13 h to 16 h, corresponding to the minimum pressure and maximum wind. It showed rather large values, considering the relatively weak wind of 12~18 m/s, and this is perhaps due to the condition that the wind duration was long, with the constant southerly direction which is most effective for the elevation of the sea level at this station. The mareograms also indicates no conspicuous secondary undulations, suggesting that the impulsive force was not so intense on the bay.

7-4 St. 34 (Fig. 18 and 19)

This station is located on the open coast of the Japan Sea, but the storm surge here shows the similar tendency to other stations in the shallow bays. The tidal deviations were rather small even to the period 15 h~17 h after the passage of the minimum pressure, but they increased abruptly after the increase of the wind velocity to about 25 m/s at about 18 h with the abrupt change in the wind direction from S to SW, the increase reaching about 43 cm from 19 h

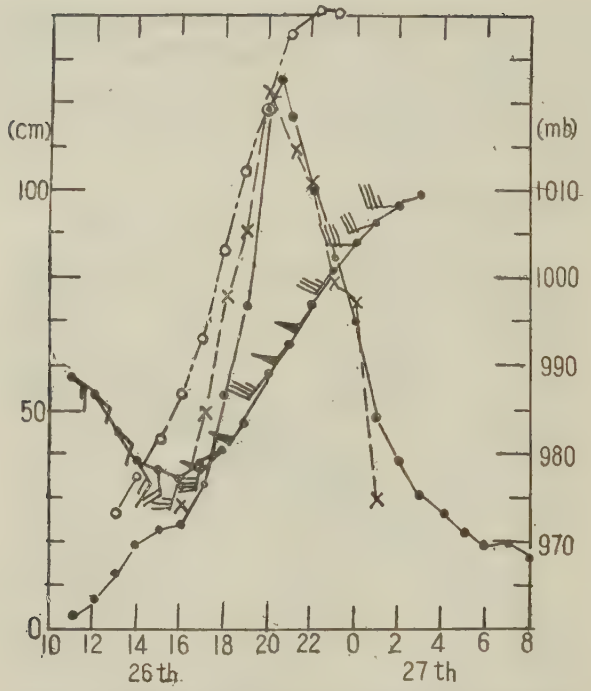


Fig. 18. Observed and computed tidal deviations and the corresponding meteorological data at St. 34 (Iwasaki)

● Observed deviations
○ Computed with $k\sum T_{-n}$
× Computed with (3–3)

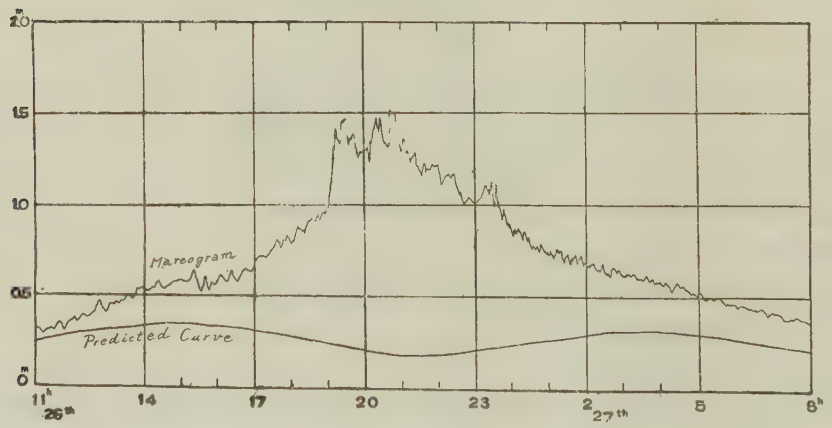


Fig. 19.

to 19 h 15 m. The maximum deviation of 133 cm occurred at 20 h 42 m, and after 22 h the deviations decreased abruptly. Such large deviations and their peak-like form seem to be due to the conditions that the typhoon in the Japan

Sea had the strong fronts accompanied, thus the water was accumulated in the region with the abrupt change of the wind stress, and the elevated sea level propagating with the typhoon caused the serious storm surges on the coast (ICHIYE, 1950 a and b). Such conditions are further strengthened to increase the storm surge by the topographic effect of the sea around the station, the bathymetric chart of which is shown in fig. 20, indicating that the station is located on the coast of something like a bay bounded by two capes and the continental slope. Therefore, the travelling long wave may increase its amplitude near the station, as if it enters into a shallow bay. As an example we compute the period of the secondary undulations or shelf seiche in the regions A and B indicated in fig. 20, the result of which is as follows:

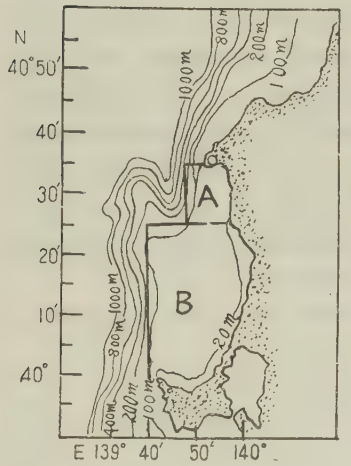


Fig. 20. Bathymetric chart near St. 34.

(A and B indicate the regions where the periods of the proper oscillations are computed.)

| | Shelf seiche (transversal) | | | Longitudinal seiche |
|---|---|---|---|---|
| | A | B | A+B | A+B |
| $L$(km) | 12 | 23 | 20 | 69 |
| h(m) | 69 | 66 | 67 | 87 |
| $T$(min) | 31 | 62 | 52($T=4L/\sqrt{gh}$) | 89($T=2L/\sqrt{gh}$) |

The shelf seiches seem to correspond to the oscillations with the period of about 30 min.~50 min. observed from 19 h to Oh of 27th.

## 8. The relations of the wind stress and the storm surges at the stations in the bays.

It is generally shown that these stations are influenced with the proper oscillation of the bay not only in the free oscillations but also in the storm surge, which corresponds to the forced oscillations (WADATI, 1938; ICHIYE, 1951). Therefore, they show the peak-like storm surges at some cases, and it is necessary to take into account of this effect in order to obtain the relations between the meteorological conditions and the elevation of the sea level at these stations.

In section 4-2, we compare $\int T\,dt/C$ with the maximum deviation, and obtain the relatively reasonable relation, but such method is inapplicable to the relation between the hourly values of deviation and the wind stress. For example, we compute the sum of $T_{-n}$ from $n=9$, where $T_{-n}$ means the wind stress perpendicular to the coast at $n$ hours earlier than the time of the maximum deviation, assuming

that the relation $D_m = k\sum_{n=9}^{m} T_{-n}$ is valid for every $m$ values, in which $D_m$ means the tidal deviation corrected for the pressure effect at $m$ hours later or earlier than the time of the maximum deviation. The constant $k$ is determined by the relation $k = \sum_{n=9}^{0} T_{-n}/D_0$, so as to give the agreement with the observed value for the maximum deviation $D_0$. Then we compute hourly deviations by use of $k$ determined as above, the results of which are plotted in fig. 11, 13, 15, 17 and 18. These computed $D_m$ indicate a large disagreement with the observed deviations at each station, especially after the time of $D_0$, since the computed values of $\sum T_{-n}$ do not decrease generally so rapidly after $n=0$, but rather increase.

Such disagreement of the estimated and observed deviations may be corrected by taking into account of the proper oscillations of each bay.

The equation of the forced motion about the elevation of the sea level for any sea is given by

$$\partial^2\zeta/\partial t^2 = g\left\{\frac{\partial}{\partial x}\left(h\frac{\partial\zeta}{\partial x}\right)+\frac{\partial}{\partial y}\left(h\frac{\partial\zeta}{\partial y}\right)\right\}-\frac{\partial T_x}{\partial x}-\frac{\partial T_y}{\partial y}+\frac{\partial}{\partial x}\left(h\frac{\partial p}{\partial x}\right) \qquad (1)$$

where the term $-\frac{\partial}{\partial x}\left(h\frac{\partial p}{\partial x}\right)+\frac{\partial}{\partial y}\left(h\frac{\partial p}{\partial y}\right)$ expresses the effect due to the variable pressure distribution of the typhoon. When we put $\zeta_m$ as the series of normal functions corresponding to the adequate boundary conditions, the solution of the equation (1) is expressed by

$$\zeta = \sum A_m\zeta_m,\ A_m(t) = \frac{1}{\lambda_m}\int_0^t \sin\lambda_m(t-\tau)d\tau\int F(x, y, \tau)\zeta_m dxdy \qquad (2)$$

where $F$ represents the forced terms. and $\lambda_m$ means the eigenvalue corresponding to $\zeta_m$. (ICHIYE, 1951)

This solution is mathematically exact but it is very difficult to compute practically, first due to the complicated forms of the normal functions $\zeta_m$ and secondly to the uncertainity of the forced term $F$ determined from the observed values of wind and pressure, since this contains the first and second derivatives of the observed data. Therefore, we should take the simplified relation, in order to apply to the forecasting of the storm surges.

For this purpose, we assume the next relation between the wind stress and the elevation

$$\zeta-\zeta_p = j\int_0^t \sin\lambda(t-\tau)T(\tau)d\tau \qquad (3)$$

where $j$ is the constant to be determined for each station, $\lambda$ is the eigenvalue of the first mode normal function, and $\zeta_p$ is the elevation due to the static pressure effect.

The basic assumptions of this equation are that the effect of the pressure acts only statically, as in the case of simple pressure distribution such as $\partial p/\partial x$

$=\partial p/\partial y=0$, and that the contributions from the higher modes of proper oscillation are neglected, which seems to be reasonable, since for the constant forced term the contributions from the first, second, third and higher modes are proportional to $\frac{1}{\pi}$, $o$, $\frac{1}{3\pi}$, $o$, $\frac{1}{5\pi}\cdots$, when we take the eigenfunctions of the seiche in a closed, rectangular bay such as $\zeta_m=\frac{2}{L}\cos\frac{m\pi x}{L}$.

For the practical computations we should take more simple formula, and we replace the integral (3) with the following summations, by computing the interpolated values of the wind stress from the hourly ones. For St. 13 and 14, the longest period of the second undulations of the bay is about 5 hours, thus for the value of $\zeta$ at time $t$ hours we compute the summation such as

$$\begin{aligned}\zeta-\zeta_p=j\sin 36^\circ\Big\{&T\Big(t-\frac{1}{2}\Big)+T(t-2)-T(t-3)\\&-T\Big(t-4\frac{1}{2}\Big)+T\Big(t-5\frac{1}{2}\Big)+T(t-7)-\cdots\cdots\Big\}\\&+j\sin 72^\circ\Big\{T(t-1)+T\Big(t-1\frac{1}{2}\Big)-T\Big(t-3\frac{1}{2}\Big)-T(t-4)+\cdots\cdots\Big\}\end{aligned}\qquad(3\text{—}1)$$

For St. 29, the period is about 150 min. in the first mode of the longitudinal seiche of the Tokyo Bay (WADATI, 1939), thus we take it as three hours for the computation and the next summation is computed

$$\zeta-\zeta_p=j\Big\{T\Big(t-\frac{1}{2}\Big)+T(t-1)-T(t-2)-T\Big(t-2\frac{1}{2}\Big)+\cdots\cdots\Big\}\qquad(3\text{—}2)$$

For St. 21 and 34, the longest mode has the period of about 2 hours, thus the next form is taken

$$\zeta-\zeta_p=j\Big\{T\Big(t-\frac{1}{3}\Big)+T\Big(t-\frac{2}{3}\Big)-T\Big(t-1\frac{1}{3}\Big)-T\Big(t-1\frac{2}{3}\Big)+T\Big(t-2\frac{1}{3}\Big)+\cdots\cdots\Big\}\qquad(3\text{—}3)$$

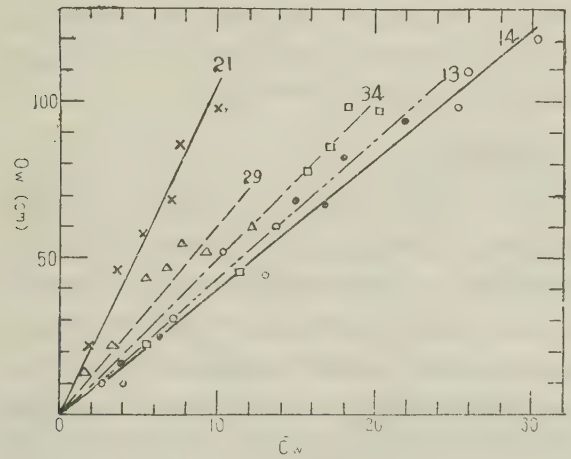


Fig. 21.

The relation between the tidal deviations corrected for pressure effect (Ow) and the computed wind effect modified by the proper oscillation ($\overline{\text{Cw}}$) for each station in a shallow bay.

- ● St. 13 (Kobe)
- ○ St. 14 (Osaka)
- × St. 21 (Nagoya)
- △ St. 29 (Tokyo)
- □ St. 34 (Iwasaki)

The relations between these computed values of $\sum T(C_w)$ and the observed hourly deviations corrected for the pressure effect (Ow) are plotted in fig. 21 for each station, which suggests the remarkable proportionality between them. Therefore, we can determine the constant $j$ for each station from these correlations, and in turn we compute the hourly deviations by use of these constants $j$ the results of which are plotted in each figure of deviations. We can see the better agreement with the observed deviations, especially after the occurrence of the maximum deviation.

In fact, we can apply this method to the forecasting of the storm surges in the bays, with an good accuracy. When we take into account of the contributions from higher modes we can increase the accuracy of the forecasting.

## 9. Conclusion.

In the present paper, the general tendency of the storm surges at the various stations on the coast of Japan caused by the Typhoon 5415 is described, by taking the relations between the maximum deviations and the minimum pressure observed at each station. Further, the durability of the storm surges seems to increase as the increasing distance to the typhoon path. The relations between the wind stress and the heights of the storm surges at each station are obtained, which suggest the method of forcasting in two ways, that is, the forecasting of the storm surges at every station at each map time by use of the predicted weather charts, and that of each station by use of the successive wind data there. (Part I)

Next, the characteristic features of the storm surges at several stations are described in details, where the stations are devided into three groups, the first consisted of the stations located near the typhoon course, and the second giving the interesting double peak storm surges, and the third consisted of the stations in the shallow bays. In the last the method of forecasting the storm tide even in the shallow bays, where the effect of the proper oscillation is important, is also suggested, which is very simple in practical computation, but gives the better agreement with the observed data than other methods.

## Literatures

HIDAKA, K. (1931): On the longitudinal seiche of the Osaka Bay. (In Japanese) *Bull. Kobe Mar. Obs.* Vol. **41**.

ICHIYE, T. (1950a): On the meteorological tide. (In Japanese) *Journ. Meteoro. Res.* Vol. 1, No. 13.

ICHIYE, T. (1950b): On the long wave caused by the wind discontinuities. *Mem. Kobe Mar. Obs.* Vol. 8.

ICHIYE, T. (1951): On the abnormal high water caused by the Typhoon "Jane" (In Japanese) *Oceanog. Report.* Vol. **2**, No. 2.

TERADA, T. *et al.* (1908): An investigation on the secondary undulations of oceanic tides. *Journ. Coll. Sci. Tokyo*, Vol. **24**.

WADATI, K. (1938): On the storm surge of the Osaka Bay caused by a typhoon. (InJapanese) *Umi to Sora* (*Sea and Sky*) Vol. **18**, No. 21.

WADATI, K. (1939): On the storm surge of the Tokyo Bay caused by a typhoon. (In Japanese) *ibid.* Vol. **19**, No. 3.

Records of Oceanographic Works
in Japan Vol. 3, No. 1,
March 1957.

# On the Tidal Mixing of Sea Water Through Narrow Channels

By

Shoitiro HAYAMI, Yoshiaki FUKUO and Daisuke YODA
(Geophysical Institute, Kyoto University)

**Abstract**

Surface waters were sampled in Naruto and Akashi Straits which communicate Seto Inland Sea—Japanese Mediterranean—with open sea. Their chrolinity and specific gravity at 0°C were determined. The difference between the specific gravity calculated from observed chrolinity by Kundsen table and a directly measured one, which was called provisionally as excess specific gravity, was also calculated; and correlation diagrams of the excess specific gravity and chrolinity were constructed. These diagrams were applied for the first time to water type analysis with a satisfactory result. It was disccussed to what extent the horizontal mixing of waters in the straits by tidal currents might be explained as a diffusion phenomenon caused by a large scale horizontal turbulence made up of tidal currents as suggested by H. Stommel.

**1.** The water of Seto Inland Sea—Japanese Mediterranean—communicates with open seas through narrow straits such as Hayasui, Shimonoseki, Naruto and Akashi. As no steady current is perceptible in this sea[1], the exchanges of its water with outer seas are believed to be mainly effected through tidal currents, though slow convection currents due to density defference may play some part in the water exchange. The exchange and mixing of sea water by tidal currents gradually have attracted attension of the oceanographers these years, but the observational materials are still lacking to derive a general conclusion. In view of such a situation, the present authors made some observations and analysis of tidal mixing through the straits of Naruto and Akashi which connect Harimanada, a large basin of Seto Inland Sea, with Kii Channel and Osaka Bay respectively as shown in Fig. 1 (A).

Surface waters were taken on board the ferry boats along their courses between Akashi and Iwaya in Akashi Strait and between Fukura and Muya in Naruto Strait, the lengths of the courses being 12 km and 6 km for Naruto and Akashi Straits respectively. The courses of ferry boats are shown in Fig. 1 (B).

The water was sampled at the depth of about 50 cm below sea surface by metalic bucket sampler and the sampling was made ten times at equal intervals along the courses AB in Fig. 1 (B). At each sampling 180 cc of sea water was taken and poured into a bottle of 1800 cc in capacity, hence we got one bottle full of water for each sailing which represented an average surface water along the course at the central epoch of the respective sailing. The samplings were made as far as possible at every sailing of the ferry boats, but they were stopped at night, because the ferry boats operated only in day time. The samplings were made every day from May 30 to April 12, 1955, for Naruto Strait and from August 2 to 16, 1955, for Akashi Strait.

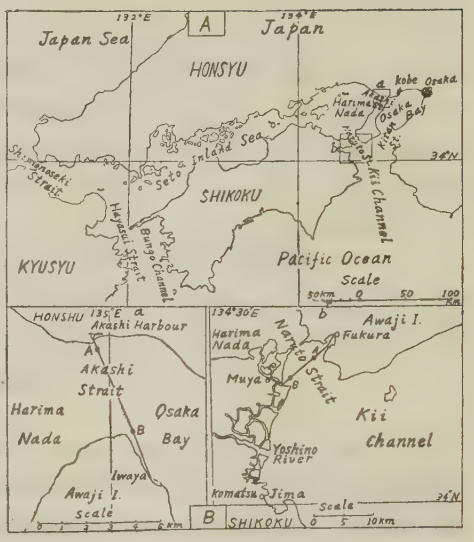


Fig. 1.

**2.** For a study of water exchange and mixing, it is most convenient to use the method of water type analysis. In this method, it is customary to use chrolinity and temperature as representatives of the conservative quantities of water samples. In the present case where the surface water was sampled, the water temperature will be affected by meteorological conditions and is not suitable for water type analysis. Considering the accuracy and readiness of measurements, chrolinity and density, instead of chrolinity and temperature, were determined for each sample. The omission of temperature measurement made the field work very easy. The chrolinity was determined by Fajans' method with normal sea water and Knudsen burette and pipette. The accuracy was $\pm 0.01‰$. The density was measured by an apparatus specially designed and constructed by the senior author[2]. The accuracy of the measurement was of the order of $2\times10^{-6}$ g/cm$^3$.

The density of water was reduced to the value exactly at 0°C. From the density at 0°C, specific gravity ($\rho_0'$) at 0°C referred to the standard temperature 4°C, was calculated and further $\sigma_0'$, which is given by $\sigma_0'=(\rho_0'-1)\times1000$, was derived. The corresponding specific gravity ($\sigma_0$) was also calculated from the observed chrolinity by Knudsen table. Both values $\sigma_0$ and $\sigma_0'$ do not generally agree and we shall provisionally call the difference $(\sigma_0-\sigma_0')$ as excess specific gravity. It is denoted by $\Delta\sigma_0$. The Knudsen table was originally prepared under an assumption that the relative composition of the salts in sea water is always the same throughout the entire oceans. In actual seas, especially in coastal waters,

however, this assumption does not obtain, and the relative composition of sea salts varies with location and time. The excess specific gravity $\Delta\sigma_0$ may, then, be regarded to represent a deviation of the relative composition of sea salts of the actual sea from Knudsen's normal sea and may be used as an effective indicator representing the quality of sea salts, while the chrolinity indicates the quantity of sea salts. An excess specific gravity-chrolinity correlation diagram may, therefore, be used for water type analysis. It was applied for the first time to the present case with a satisfactory result. In the following, chrolinity is denoted by *Cl*.

**3.** The basic observational materials obtained for the present investigation are all graphically shown in the following: In Fig. 2, the time variations in *Cl* and $\Delta\sigma_0$ in Akashi Strait, predicted tidal current at the central portion of the same strait and tidal curves at Kobe and Akashi harbours, are shown. In Fig.

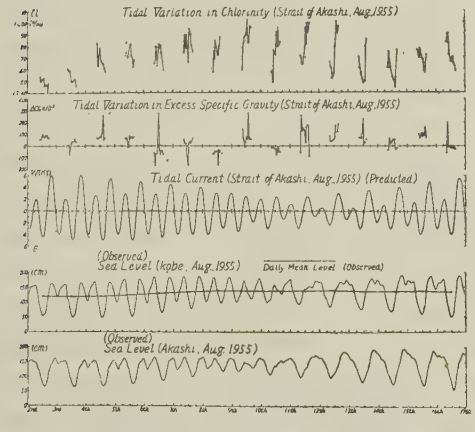
Tidal Variation in Chlorinity (Strait of Akashi, Aug. 1955)
Tidal Variation in Excess Specific Gravity (Strait of Akashi, Aug. 1955)
Tidal Current (Strait of Akashi, Aug. 1955) (Predicted)
(Observed) Sea Level (Kobe, Aug. 1955)
Daily Mean Level (Observed)
(Observed) Sea Level (Akashi, Aug. 1955)

Fig. 2.

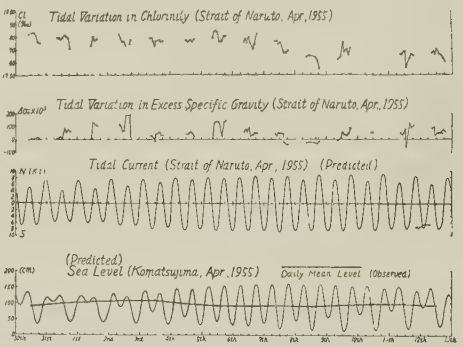
Tidal Variation in Chlorinity (Strait of Naruto, Apr. 1955)
Tidal Variation in Excess Specific Gravity (Strait of Naruto, Apr. 1955)
Tidal Current (Strait of Naruto, Apr. 1955) (Predicted)
(Predicted) Sea Level (Komatsujima, Apr. 1955)
Daily Mean Level (Observed)

Fig. 3.

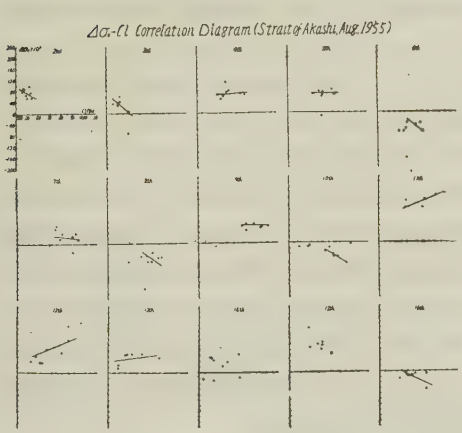


Fig. 4.

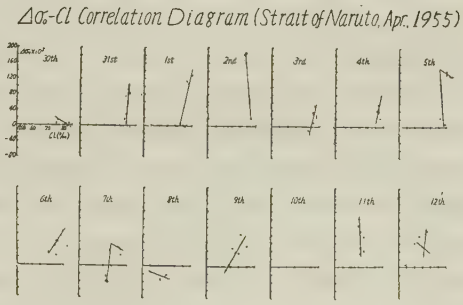


Fig. 5.

3, similar curves are given for Naruto Strait. In Figs. 4 and 5 correlation diagrams are shown day by day for Akashi and Naruto Straits respectively, where full lines indicate regression lines. A ($\Delta\sigma_0 - Cl$) synthetic correlation diagram in Akashi Strait for fifteen days is shown in Fig. 6, while the same diagram in Naruto Strait is given in Fig. 7. Day by day regression lines are also shown in full lines in these figures and white circles in Fig. 6 represent the values near the time of slack water.

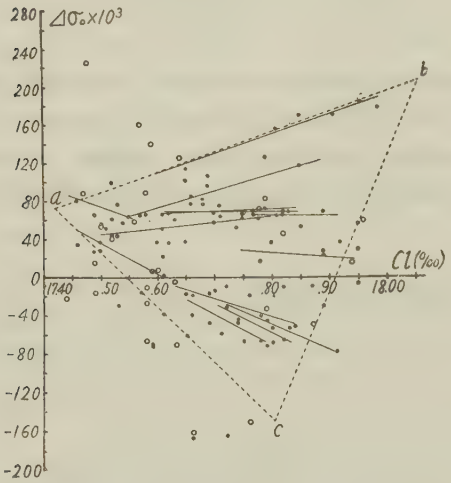


Fig. 6.

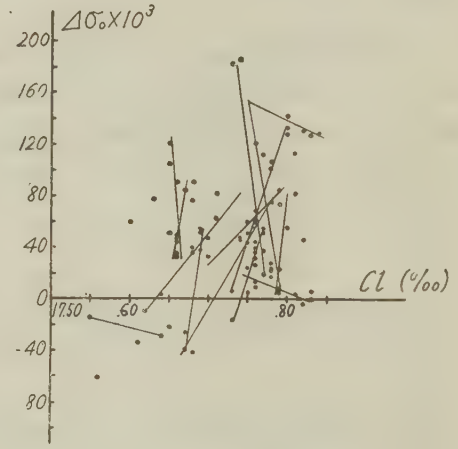


Fig. 7.

4. The tidal variation in $Cl$ and $\Delta\sigma_0$ which are shown in Figs. 2 and 3 indicate clearly that the exchanges of water through the straits are governed by tidal currents. In Akashi Strait, it will be noticed that full lines, representing regression lines in the synthetic correlation diagram (Fig. 6), converge to one point denoted by $a$. This point represents the water of Harimanada. On the other hand, these lines diverge in the reverse direction and their envelope forms a triangle, in which nearly all points are contained. It will deserve special attension that among the points which scatter outside the triangle, many points occur at or near the time of slack water. Regarding other two vertices of the triangle, the point $b$ represents the coastal water of the northern portion of Osaka Bay, while the point $c$ is the water of the northern part of Kii Channel flowing into Osaka Bay through Kitan Strait[3]. The water of Osaka Bay which appears in the eastern part of Akashi Strait and mixes with the water of Harimanada represented by the point $a$, falls on the straight line connecting the points $b$ and $c$, that is, it is mixing of two water types represented by the points $b$ and $c$, but the relative amount of their mixing is incessantly changing.

The water appearing in Akashi Strait is mixing of two types of water, one

being represented by the point $a$, the other by the points on $bc$-line, and the relative amount of mixing is determined by the tidal conditions in Harimanada and Osaka Bay as is suggested in Figs. 2 and 6. The water exchange through Naruto Strait is different from Akashi Strait. The day by day regression lines in the ($\Delta\sigma_0-Cl$) synthetic correlation diagram (Fig. 7), do not converge to any point and many of them run nearly parallel to $\Delta\sigma_0$ axis. The orientation of regression lines, however, suggests that three main types of water appear in this strait. Among them, one of high chrolinity (type I) corresponds to points on $bc$-line in Fig. 6, the type of low chrolinity rnd positive $\Delta\sigma_0$ (type II) represents the water of Harimanada origin, while the type of low chrolinity and negative $\Delta\sigma_0$ (type III) is the coastal water around the estuary of Yoshino River—a river of large discharge emptying into Kii Channel near Naruto Strait. Inferring from Fig. 3, the waters of these three types are supposed to be arranged in Naruto Strait from north to south in the order of succession II, III and I, and, repeating the tidal mixing, they fluctuate north and south according to the difference of daily mean sea levels between Harimanada and Kii Channel.

**5.** As was noticed above, the exchanges of water through Naruto and Akashi Straits are governed by tidal currents in the straits. Some years ago, H. Stommel[4] proposed a model of a large scale horizontal turbulence made up of tidal currents and, applying the concept of mixing length, discussed the horizontal mixing by tidal currents as a sort of diffusion phenomenon. Though his idea is very ingeneous, the observational evidence seems to be still lacking. The evidence obtained above will contribute something to this important problem.

As is seen in Figs, 4, 5, 6 and 7, the points ($\Delta\sigma_0$, $Cl$) are nearly arranged on a straight line from slack to slack and they have a tendency to scatter at and near the time of slack. This fact sugests that the length $l$ travelled by a tidal current from slack to slack may be assumed to represent mixing length. Then, the mixing coefficient $A$ will be given by a formula

$$A=\alpha\bar{u}l, \qquad l=uT \tag{1},$$

where $u$ is the mean velocity of a tidal current, $\alpha$ is a proportional factor representing the degree of mixing and $T$ is the half period of a tidal current. Now we shall imagine a working model such that two semi-infinite water bodies of chrolinity $Cl_1$ and $Cl_0$ are initially ($t\leq 0$) separated by a vertical boundary plane ($x=0$) and then suddenly mixed by tidal currents in the direction of $x$, positive eastward, then the distribution of chrolinity along $x$-direction at any moment $t>0$ will be given by

$$Cl=\frac{Cl_1+Cl_0}{2}+\frac{Cl_1-Cl_0}{2}\,erf\left(\frac{x}{2\sqrt{At}}\right) \tag{2}.$$

The expression (2) may be transformed into a dimensionless form

$$f\left(\frac{x}{l}\right)=erf\left(\frac{x/l}{2\sqrt{At/l}}\right), \quad \text{where} \quad f\left(\frac{x}{l}\right)\equiv\frac{2Cl-Cl_1-Cl_0}{Cl_1-Cl_0} \tag{3}.$$

In the present observation $t$ is given by $T$ in the sense of average. The observed variations in chrolinity are time distributions, but on the concept of mixing length, they may be transformed into space distributions by a substitution

$$x=x_0-\int_{t_0}^{t} u_0 \sin\pi\left(\frac{t-t_0}{T}\right)dt \tag{4},$$

where $u_0$ is the maximum velocity of a tidal current, $x$ is the position where a volume of water observed at $(x_0, t)$ is expected to appear at the time $t_0$ of the preceding slack.

This model was applied to the variation in chrolinity in Akashi Strait. The chrolinities at the point $a$ and points of intersection of daily regression lines and $bc$-line in Fig. 6 were assigned to the values of $Cl_0$ and $Cl_1$ respectively. The values of $l$ and $u_0$ were calculated from the predicted tidal current in Fig. 2. The formula (4) only gives the relative value of $x$. Its absolute value must be estimated from the origin of the $x$-axis, that is, the point where error function in (3) vanishes. In the actual state, the position of this point is not stationary, but fluctuates east and west according to the advective current caused by the long period fluctuations of the daily mean sea level. It will be difficult to determine such a position. Nevertheless, if the present model is applicable, it will be approximately determined for each half period from slack to slack by interpolating or extrapolating the graph of an error function which fits best to the relative distribution of the points observed during the same period.

The values of the function $f(x/l)$ in (3) were, then, plotted against $x/l$, the result of which was shown in Fig. 8. In this figure white circles represent average values of $f(x/l)$ for every interval of $x/l$ equal to 0.1. The full line in Fig. 8 is the graph of an error function which fits best to the white circles. The fitness is moderate, but will be sufficient to suggest that the relation (3) may be valid in the average of large number. From Fig. 8 we get

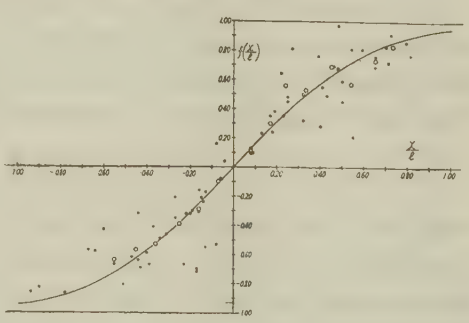

Fig. 8

$$erf\left(\frac{x/l}{2\sqrt{At/l}}\right)=0.95 \quad \text{for} \quad \frac{x}{l}=1 \tag{5}.$$

Hence by a table of error function, we get

$$\frac{l}{2\sqrt{At}}=1.4 \quad \text{or} \quad At=\frac{1}{7.8}l^2 \tag{6}.$$

In our case $t$ is equal to $T$, so that

$$A=\frac{1}{7.8}ul \tag{7},$$

which is the same with the formula (1) and we get

$$\alpha=0.13 \tag{8},$$

in other words, about 10% of the water mixes every half period of a tidal current.

**6.** The present work was carried out under a financial support of the Marine Resources Exploration Research Committee, Japan Committee of Unesco and of the Akashi Strait Research Committee, Kobe Municipal Office. The authors should like to express their cordial thanks to the officers of these organizations for their invaluable assistance and encouragement.

## References

1) Hidaka, K.: On the Eastward Current in Seto Inland Sea. Umi to Sora, Vol. 17, 1937.
2) Hayami, S.: Water Mass Analysis Applied to River Outflows. Pub. n° 37 de l'Assoc. Int. d'Hydrologie (Assem. gén. de Rome, Tome II), 1954.
3) Hidaka, K., and Yasui, J.: Measurements of Sea Water Density by Nansen's Submerged Hydrometer. Umi to Sora, Vol. 18, 1938.
4) Stommel, H., and Arons, A.B.: A Mixing Length Theory of Tidal Flushing. Trans. Amer. Geophys. Union, Vol. 32, 1951.

Records of Oceanographic Works
in Japan Vol. 3, No. 1,
March 1957.

# Investigation of the Sea Floor of Tsugaru Straits by Underwater Camera

By

Tadayoshi SASAKI*, Seiichi WATANABE**, Gohachiro ŌSHIBA**
and Noboru OKAMI**

* Tokyo University of Fisheries and Scientific Research Institute.
** Scientific Research Institute, Tokyo.

**Abstract**

As a part of the cooperative investigation with the National Railway Corporation on the construction of the submarine tunnel at Tsugaru straits a total number of more than 1,500 photographs of the sea floor were taken by "Kaken" underwater camera.

Outline of the improvements made on the camera used in the operations, the areas and spots photographed, and a comparison of the dredge samples and sea floor photographs are described.

## 1. Introduction

The National Railway Corporation has been planning a submarine tunnel between Tappi-Zaki in Aomori Prefecture and Shirakami-Saki in Hokkaido. The investigation in connection with this project will be concerned mainly with making an accurate bathymetric-line chart on the basis of echo sounder reading, dredging, elastic wave tests, boring, and a study of ocean bottom formations through the use of underwater photographs.

Fig. 1. Photographing operation on board a ship.

The Scientific Research Institute was asked by the National Railway Corporation to make underwater photographs for the above project. Our research team thus spent a total of 17 days in August 1955 making a total of approximately 1,500 shots on the spot. The following account deals briefly with the results of our investigation.

## 2. Type of Underwater Camera Used

The underwater camera used in the present investigation was an improved type of the "Kaken" underwater camera. The specifications of the original type have been reported previously.[1] The improvements were made in the following points.

(1) A water-tight camera case made of mild steel was covered with zinc metallizing to prevent corrosion and finished with lacquer.

A rubber cord having a round cross-section was fixed in a groove on the flange of the case as shown in Fig. 3.

(2) The frame of the camera and automatic winder was made of gun metal to increase its working accuracy.

(3) The camera holder has been reformed to facilitate attachment and removal of the camera and to facilitate insertion of the film. This camera may also be used in the same way as any ordinary camera. In the case of color films, all necessary adjustments for underwater photography can be made on the basis of a study of pictures made on board a ship.

(4) The shape of the flash lamp case has been made a diamond-shape as shown in Fig. 2 to insure smooth movement along the ocean floor.

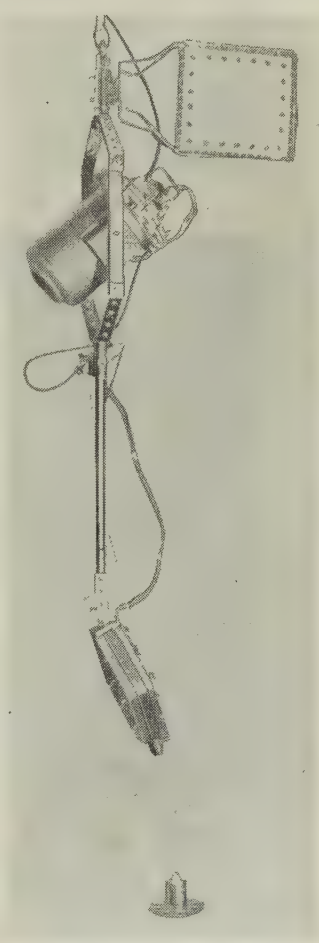

Fig. 2. General view of the "Kaken" underwater camera.

## 3. Camera lens, Illumination, and Films

The "Olympus 35" (F3.5; $f=40$mm) was used with the camera holder. F stop 11 was used for black and white pictures, while F stop 3.5 was used for color films. In all cases, the shutter speed was 1/50 sec. For illumination, a "west"

1) T. Sasaki, S. Watanabe, G. Ōshiba, and N. Okami: J. Sci. Res. Inst., 49 (1955), 107.

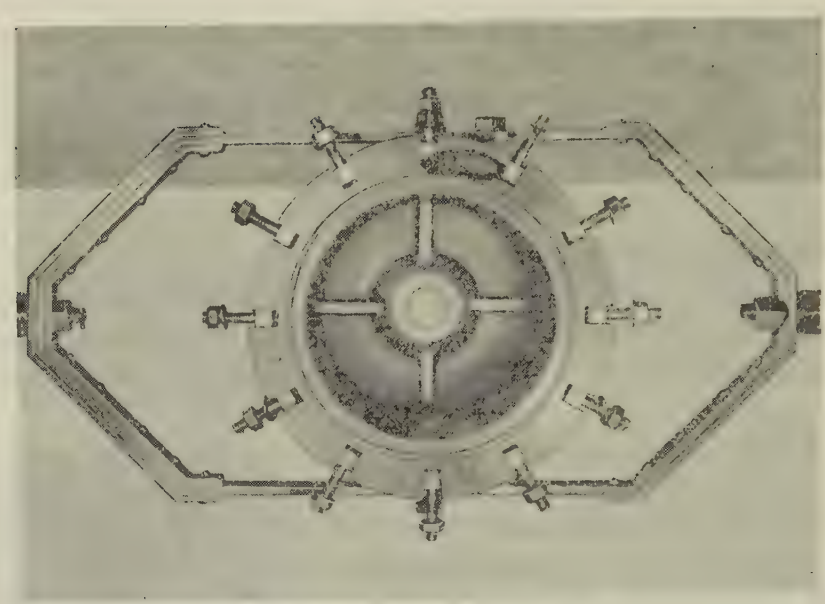

Fig. 3. Water-tight camera case.

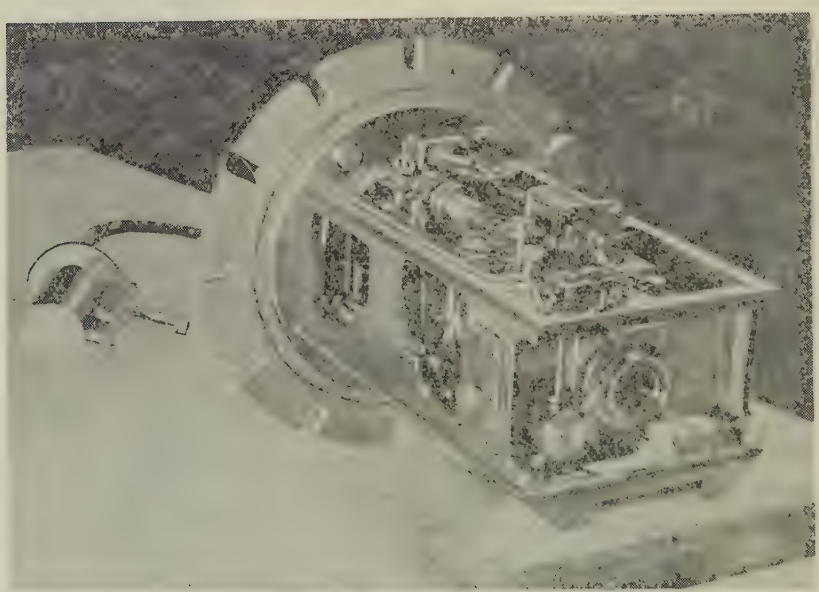

Fig. 4. Inner part of the camera.

synchro No. 5 flash bulb was used. "Fuji" X-ray films (for fluorography) were used for black and white pictures, and "Fujicolor" films for color photographs.

## 4. Notation for Dredging Samples

Special efforts were made to take photographs only at the actual spot of dredging operations. Dredging samples have been indicated by symbols in the

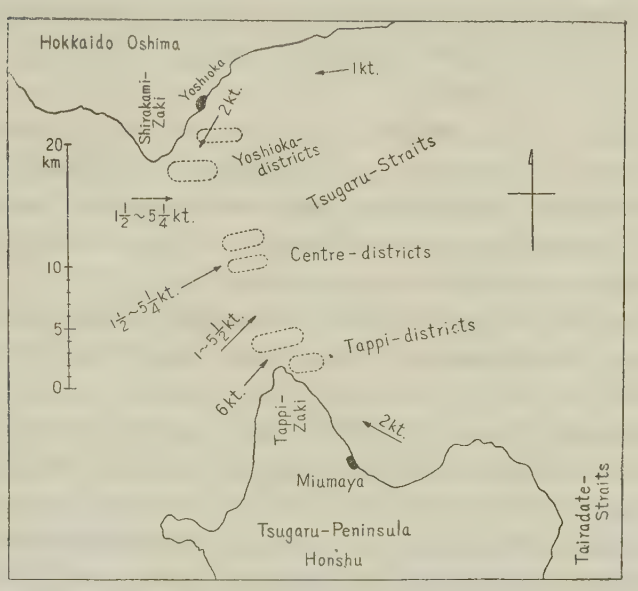


Fig. 5. An outline-map of the west part of Tsugaru Straits.

brief notes under the photographs. Table 1 lists the symbols and nomenclature used in connection with dredging samples.

Table 1

| Tertiary formation | | Palaeozoic formation | | Igneous rocks | |
|---|---|---|---|---|---|
| slsh | siliceous shale | clsl | clayslate | bst | basalt |
| hdsh | hard shale | qt | quartzite | ad | andesite |
| ms | mudstone | ch | chert | lp | liparcite |
| sts | siltstone | gw | graywacke | gb | gabbro |
| ss | sandstone | | | dr | diorite |
| cg | conglomerate | | | gr | granite |
| (g) tf | (green) tuff | | | | |

## 5. Ocean area investigated and spots photographed

In accordance with a decision of the Geological Department of the National Railway Corporation, the following three areas situated along the projected tunnel were selected as investigation areas: Tappi-Zaki, the middle of the straits, and Yoshioka. A total of 182 stations were selected at these areas.

Although a strong current which at times was as much as six knots made operations extremely difficult, all possible steps were taken to make all shots at the actual dredging spot.

The transparency of the water was more than 20 meters and color of the sea was a clear blue. This greatly facilitated our work.

## 6. Samples of Sea Floor Photographs taken at the Three Investigation Areas, "Tappi-Zaki," the Middle of the Straits, and "Yoshioka."

(1) Vicinity of "Tappi-Zaki"

Fig. 6 shows a bathymetric-line chart of the "Tappi-Zaki" area. The pictures were taken in two sub-areas, the east side of "Tappi-Zaki" and off the point. The white circles in the figure indicate the initial take spot and the black circles refer to intermediate and final take spots. These circles thus indicate the course of the ship as it drifted along the current.

The sea floor of the east side of "Tappi-Zaki" is covered with sand flat rock formations. The photographs were taken at depth from 30 to 70 meters along the bathymetric-line. These pictures are shown in Plates 1–4.

A maximum current speed of six knots was observed off "Tappi-Zaki." In this area, the photographs were taken from west to east. At the west side of the projected tunnel, the configuration of the sea floor was extremely complicated, and floor was covered with steep rocks abundant with marine life. These steep rock formations greatly hampered our operations. On the east side of the projected tunnel, however, the ship drifted in a north-easterly direction with the

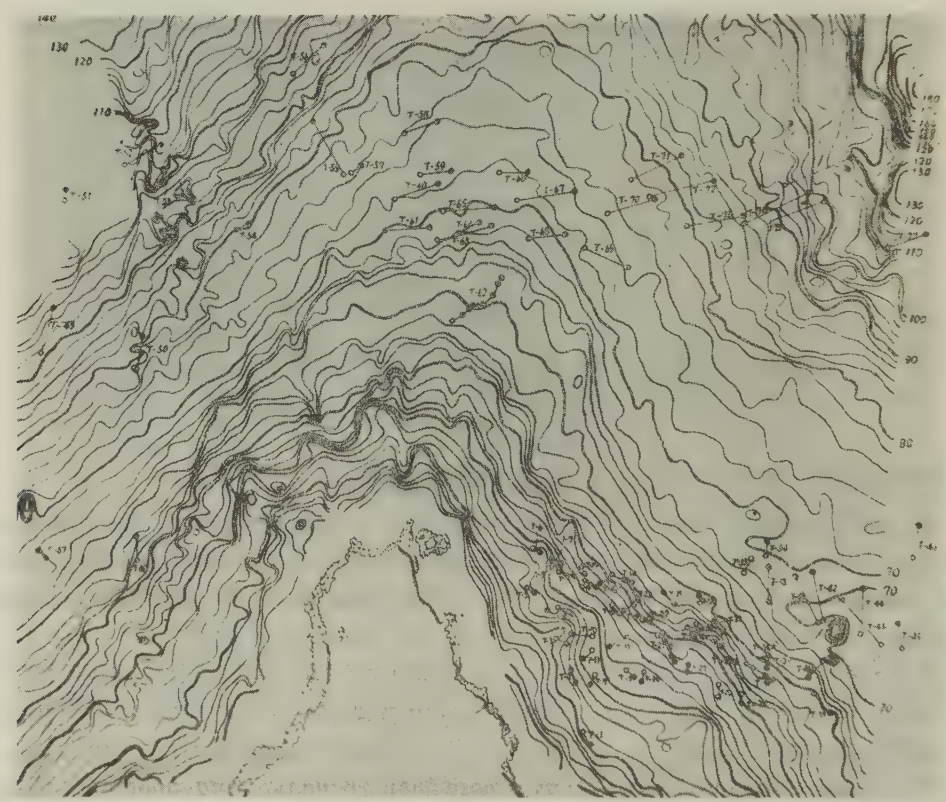

Fig. 6. Bathymetric-line chart and spots photographed near "Tappi-Zazi."

depth increasing gradually from 70 to 120 meters. There was thus no danger of getting the underwater camera caught in any obstacles. The photographs taken in this area are shown in Plates 5 and 6.

(2) The Middle Part of the Straits

Fig. 7 shows a bathymetric-line chart of the middle part of the straits. The southern part of this sea floor was almost flat except for one steep slope between 60 and 130 meters at the west end of the area. When the current speed exceeded five knots, the inclination of the cabtyre cable increased to more than 60 degrees, a condition which tended to render the action of the bottom contact indicator rather uncertain.

In the northern part of this sea floor, there was another steep slope as shown in Plate 7 and the floor was covered was sharp rocks abundant with marine life. The small number of take spots is to be attributed to the technical difficulties encountered. The major part of the dredging samples were rocks such as sandstone, siltstone, tuff etc., with gravel next in order. No samples of sand were obtained. The pictures of this area are shown in Plates 7 and 8.

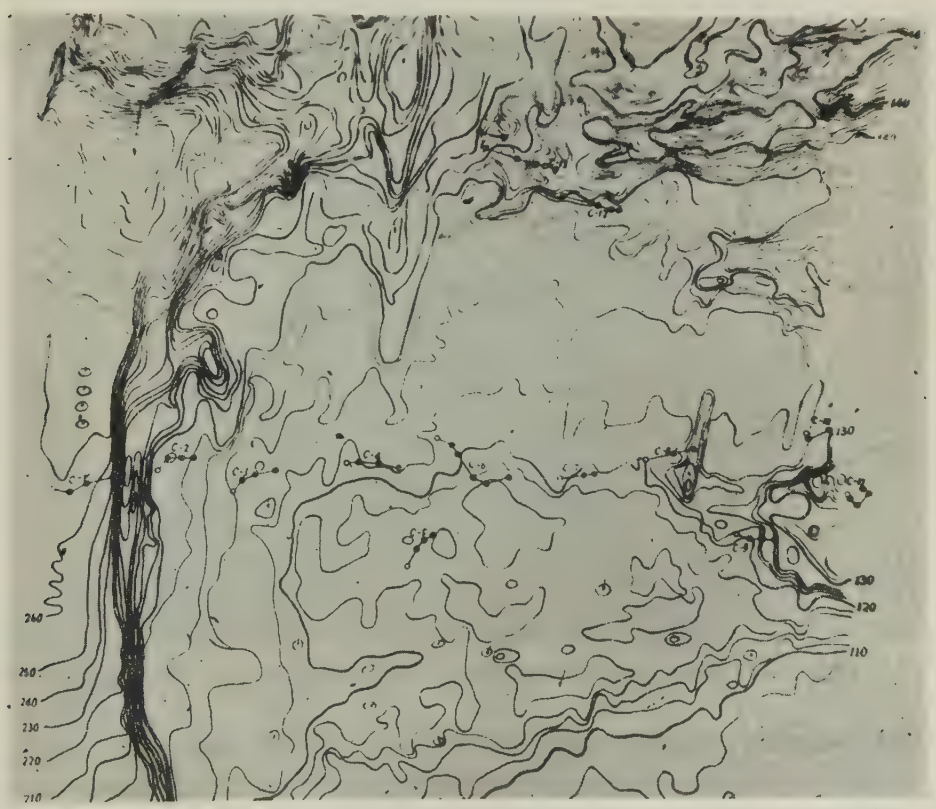


Fig. 7. Bathymetric-line chart and spots photographed in the middle of the straits.

(3) Vicinity of "Yoshioka"

Fig. 8 shows a bathymatric-line chart of the "Yoshioka" area. A steep slope of 40–70 meters is found off the point of "Shirakami." The sea floor to the south slopes off gradually to a depth of 110 meters. The sea floor of this area was covered with rough sheets with abundant marine life. Plates 9–12 show the pictures of this area. Most of the area between the coast and this steep slope is shallow water 20–50 meters in depth. The floor of this area was covered with sand, gravel, and flat sheets. The marine life in this area was characterized by a large abundance of sea-urchins and by a scarcity of seaweed growth, which greatly facilitated our work.

Fig. 8. Bathymetric-line chart and spots photographed near "Yoshioka."

## 7. Comparison of Dredge Samples and Sea Floor Photographs

Although dredge samples normally coincide with the corresponding sea floor photographs, there are cases where a discrepancy exists. Plate 16 is an example

of the former case, while Plates 17 and 18 are illustrative of the latter case. Thus, Plates 17 and 18 show rock formations covered with spots of white sand, whereas the dredge samples show only small objects such as shells and sand. It is thus apparent that any conclusion based on a study of dredge samples alone may often prove fallacious.

## 8. Conclusion

The foregoing account has dealt with the improvements made on the camera used in the operations, the areas and spots photographed, and a comparison of the dredge samples and sea floor photographs. Out of a total number of more than 1,500 photographs, only a few of the most typical have been presented.

In the light of the experience gained in the course of this operation, the following suggestions are offered in the belief that their adoption will greatly facilitate future operations of this type.

(a) Ships used should be preferably large ones of approximately 100 tons.
(b) Winches should be able to be operated both electrically and by hand to enable operation at both high and low speeds.

The authors gratefully acknowledge his appreciation of the permission granted him by the Geological Department of the National Railway Corporation to use the underwater photographs.

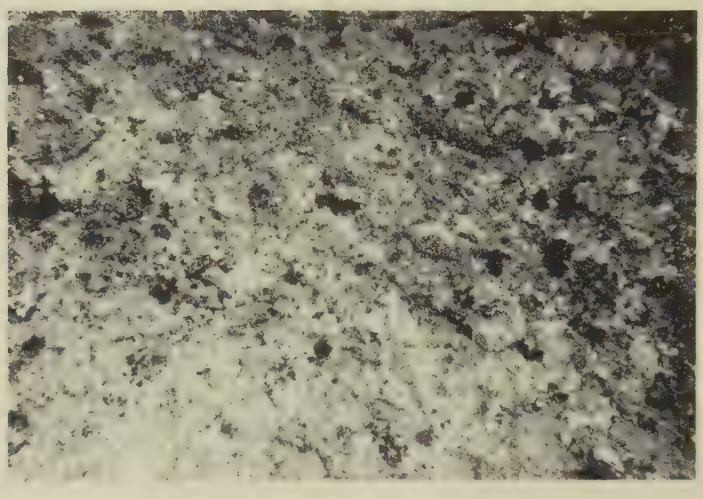

Plate 1

Photo. No.: T 3, 9
Dredge No.: T 646
Depth: 27 m
Dredge sample:
rock–ad, gravel–ad

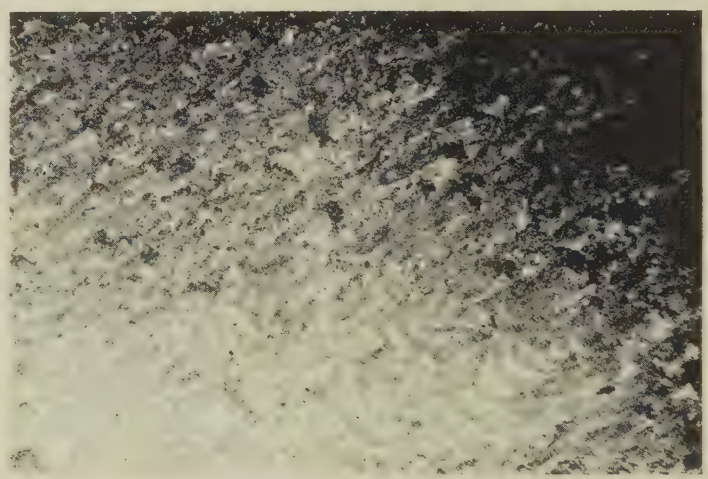

Plate 2

Photo. No.: T 32, 2
Dredge No.: T 139
Depth: 60 m
Dredge sample:
rock–ms, gravel–ms, ad, lp
Marine life: Thuiaria

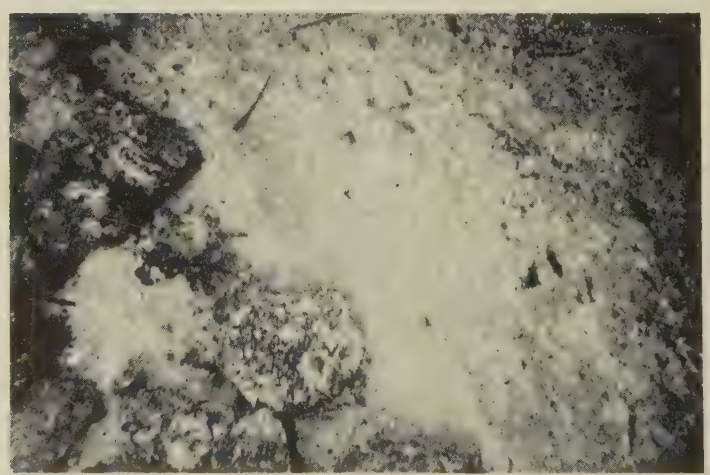

Plate 3

Photo, No.: T 1
Dredge No.: T 599
Depth: 30 m
Dredge sample:
rock–ad, gravel–ad

Plate 4

Photo. No.: T 25
Dredge No.: T 184
Depth: 60 m
Dredge sample:
Gravel–ad, tf, lp, ms
Sand–rough sand with shells.

Plate 5

Photo. No.: T 53, 6
Dredge No.: T 471
Depth: 105 m
Dredge sample:
rock–ss hdsh, (ms)
gravel–ad, hdsh
Marine life–sponge, Thuiaria

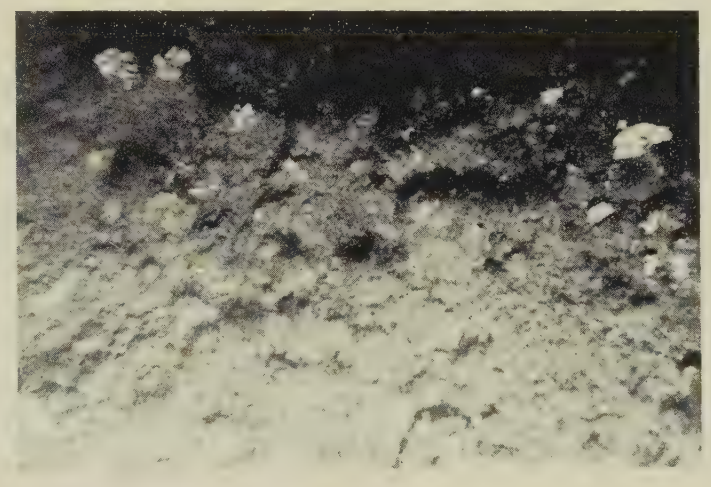

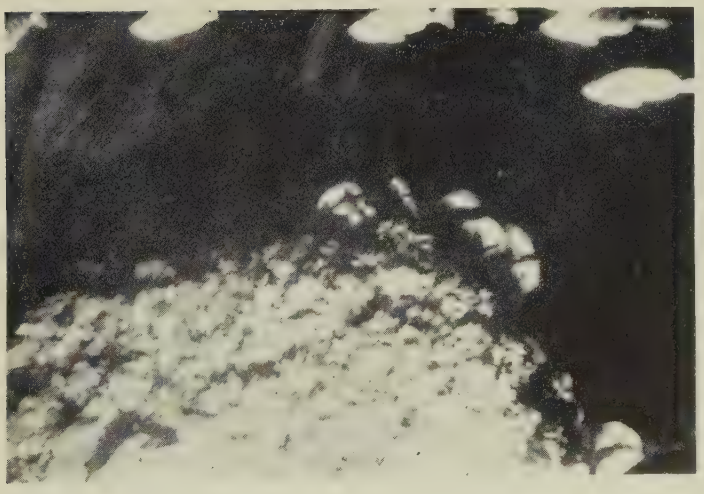

Plate 6

Photo. No.: T 54, 1
Dredge No.: T 429
Depth: 75 m
Dredge sample:
rock–tf, dr, ms
gravel–ad, slsh, gw
Marine life: acorn-shell

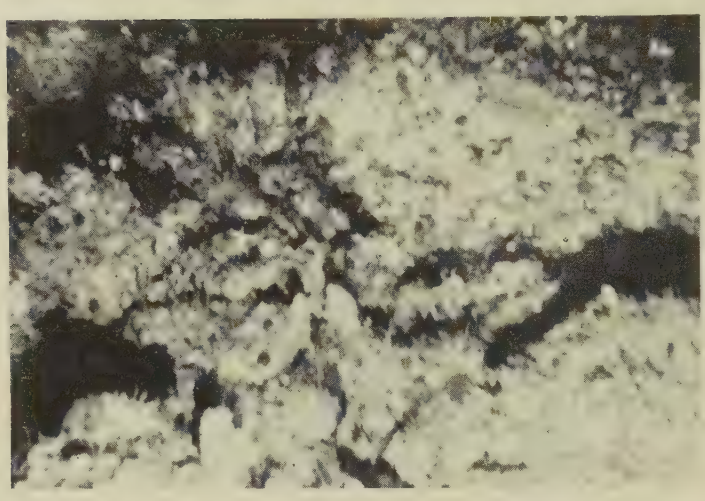

Plate 7

Photo. No.: C 7, 5
Dredge No.: C 307
Depth: 118 m
Dredge sample:
gravel–ad

Plate 8

Photo. No.: C 9, 7
Dredge No.: C 149
Depth: 121 m
Dredge sample:
rock–ss
gravel–sts, ad

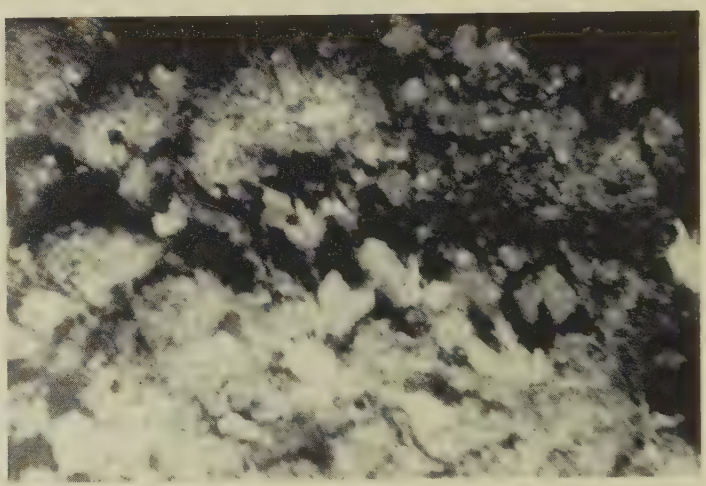

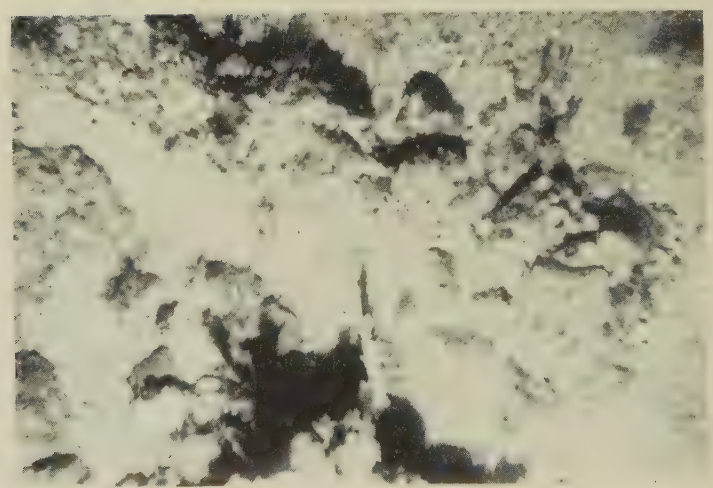

Plate 9

Photo. No.: Y 2, 2
Dredge No.: Y 703
Depth: 82 m
Dredge sample:
rock–ms, tf
gravel–ms, tbr, slsh, bst, ss

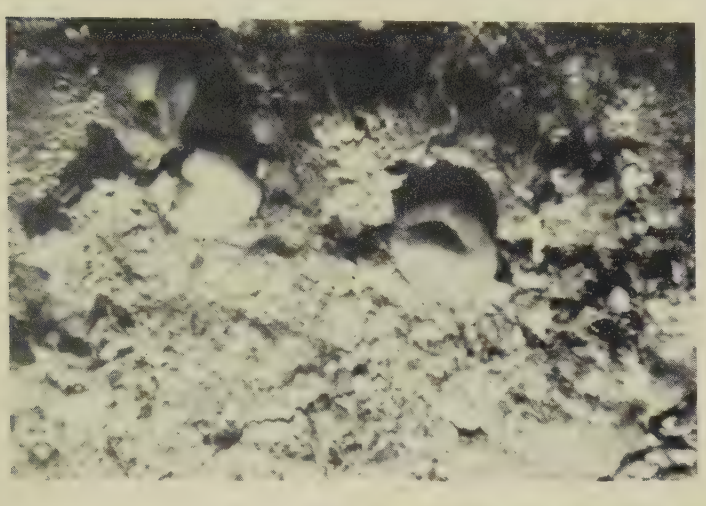

Plate 10

Photo. No.: Y 5,8
Dredge No.: Y 586
Depth: 98 m
Dredge sample:
rock–sts gravel–tf, ss, tf, ms, slsh, ch, bst
Marine life–glass sponge, Caligorgia

Plate 11

Photo. No.: Y 11, 7
Dredge No.: Y 851
Depth: 70 m
Dredge sample:
rock–hdsh, tf
gravel–tf, hdsh, clsl
Marine life–sponge, sea-urchin, Thuiaria

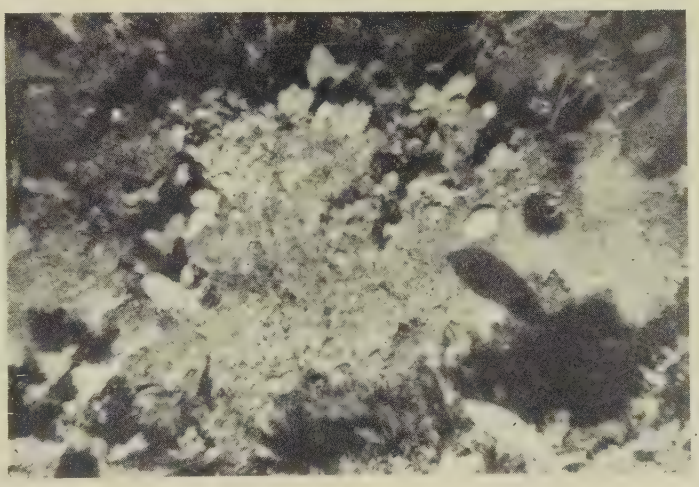

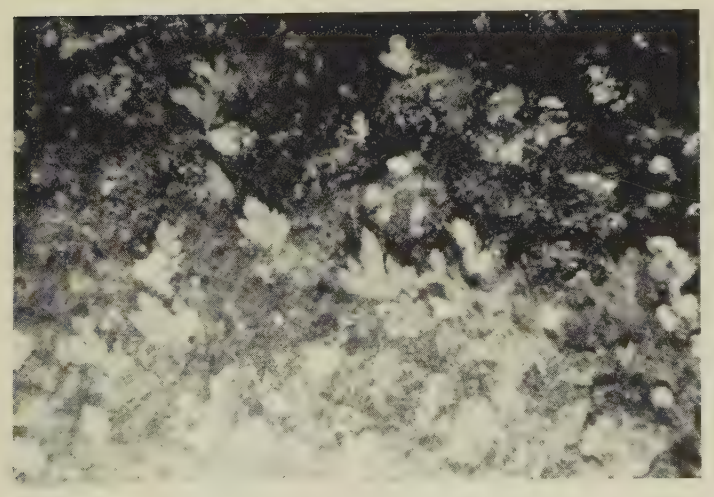

Plate 12

Photo. No.: Y 9,2
Dredge No.: Y 467
Depth: 76 m
Dredge sample:
rock–tf, sts
Marine life–sponge, sea-uschin, crab, Thuiaria

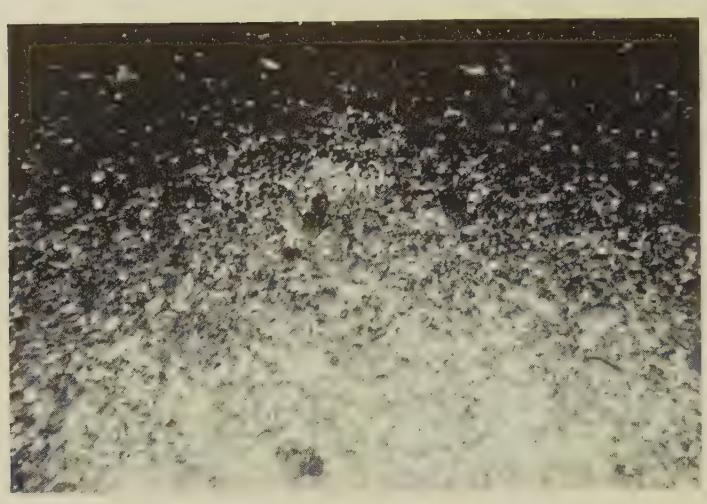

Plate 13

Photo. No.: Y 23, 8
Dredge No.: Y 347
Depth: 54 m
Dredge sample:
gravel–tf, ms, ad, qt, sts, gw, lp, clsl, sand–rough sand
Marine life–shells

Plate 14

Photo. No.: Y 35, 6
Dredge No.: Y 246
Depth: 56 m
Dredge sample:
gravel–slsh, sand–rough sand
Marine life–coral

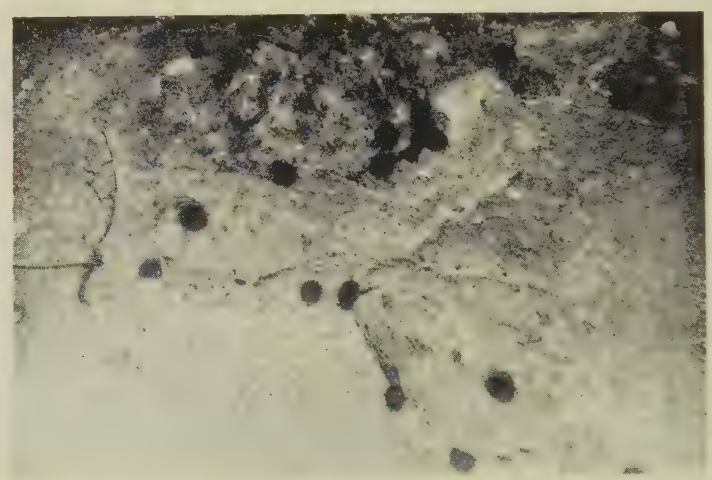

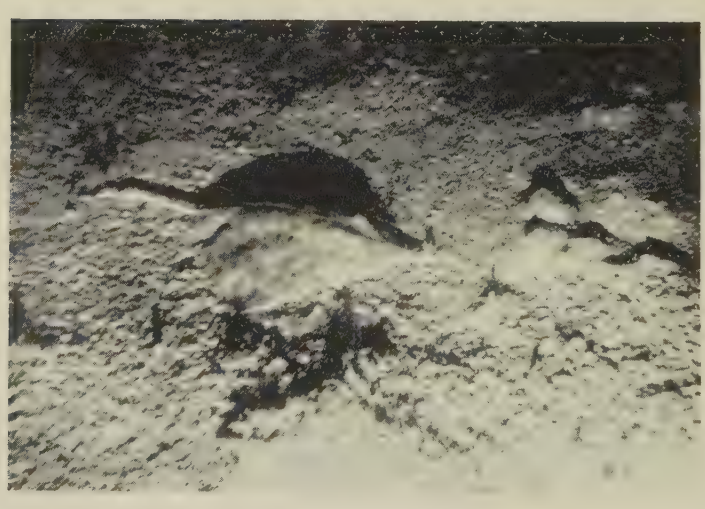

Plate 15

Photo. No.: Y 81, 6
Dredge No.: Y 135
Depth: 69 m
Dredge sample:
rock–slsh, ms
gravel–bst, slsh, qt, gr. hdsh, tf
Marine life–shells

Plate 16

Photo. No.: Y 31, 6
Dredge No.: Y 353
Depth: 59 m
Dredge sample:
gravel–hdsh, tf, sts, ss, ms, cg, ad, gw, slsh
sand–rough sand
Marine life–shells

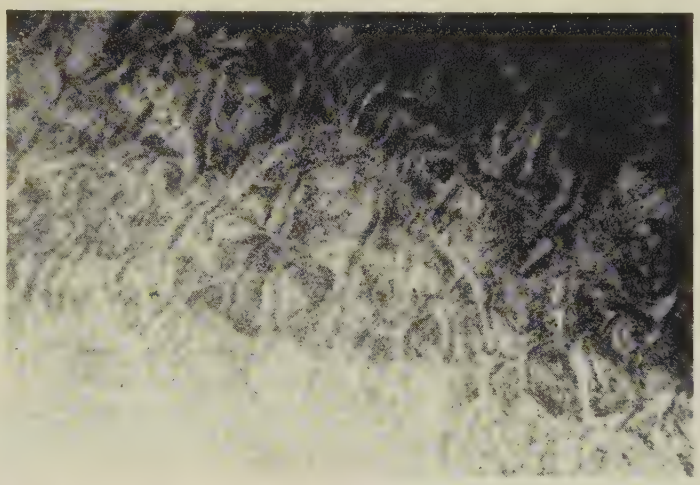

Plate 17

Photo. No.: Y 15, 8
Dredge No.: Y 334
Depth: 35 m
Dredge sample:
sand–sand
Marine life–shells

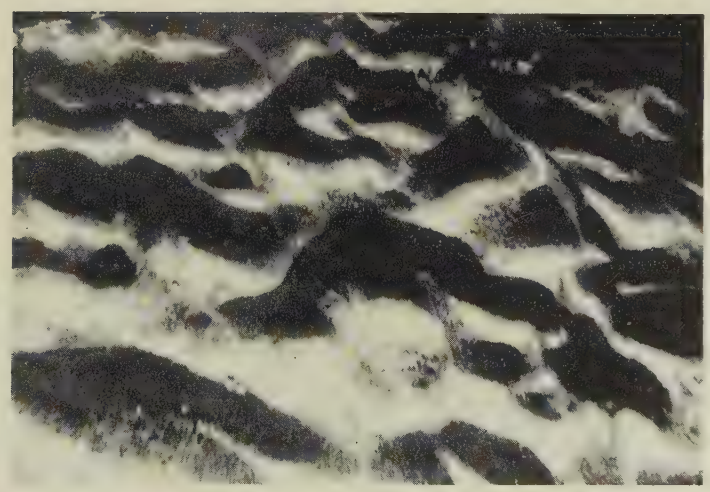

Plate 18

Photo. No.: Y 16, 3
Dredge No.: Y 290
Depth: 30 m
Dredge sample:
sand–rough sand
Marine life–shells

Records of Oceanographic Works
in Japan Vol, 3, No. 1,
March 1957.

# Maximum Permissible Concentration of $Sr^{90}$ in Food and its Environment

By

Yoshio HIYAMA

(Fisheries Institute, Faculty of Agriculture,
University of Tokyo)

(Received Aug. 15, 1956)

## 1. Introduction

Among the problems of hazard caused by nuclear fission products, either born by nuclear weapon or by atomic pile, the long-life nuclides, such as $Sr^{90}$, $Pu^{239}$ or $Cs^{137}$ is the matter of world wide concern as the future public hygene problem. Especially, $Sr^{90}$ is thought to be one of the most dangerous bone seeking element, and also abundant among the fission products. The maximum permissible concentration of this in water or food is decided by the International Commission of Radiological Protection (ICRP) as $8\times10^{-7}$ microcuire/cc (as taken 2.2 liter per day per person), and that in air to breathe is as $2\times10^{-10}$ microcurie/cc (1/10 for the public) because the contenous taking of this amount, by average man (70 kg in weight, 1 kg Ca and 7 g Sr in skeleton) would cause the concentration of 1 microcurie $Sr^{90}$ in total skeleton as which level is considered to produce the beta ray irradiation enough to cause the possible biological effect on bone marrow in some extent.

Therefore, already in some countries, chemical measure of this nuclide in some kind of food and environment is now going in various scales to know the present level of contamination in comparison with the maximum permissible level, especially on the food which is considered to be important Ca source, as Sr behaves near to Ca in chemical and biological procedure and Ca is necessary element for human metabolism.

However, as the maximum permissible amount in food is fairly small, the chemical analysis to decide this level requires huge amount of materials, scientific skill and expensive instruments, to know it in various kinds of food we are taking and growing various places.

Here, the author is going to mention his idea to enumerate the maximum permissible level of $Sr^{90}$ about food and its environment where it grows.

## 2. Ecology of strontium

(2-1) In nature strontium is rather commonly distributed through out earth surface, in minerals, in water and in various kind of organisms, though the

amount is fairly less than calcium, which is usually co-exist with it, and behaves close to it in chemical or biological procedures. And, the many of recent works by several chemists on strontium—calcium ratio on minerals, soil, water and organisms tell that this ratio differs greatly according to the kind of these materials. Taking a few example of this, in round figure in ratio of atom number, about minerals ASARI[1] found 1 : 10 level in Guano, Monazite, Xenotime, 1 : 100 level in many kinds, 1 : 1,000 level in some, and surely some are less than this. This variation makes that in soil so variable. About water area, oceanic water is known[2,3] to have 7 mg of strontium and 400 mg of calcium in a liter (atom number ratio 1 : 115) homogeneously, but in fresh-water areas it varies greatly according to locality. About fresh-water areas in Japan SUGAHARA[4] found the atom number ratios are 1 : 6—1,200, and in rain-water 1 : 2—8. For the Sr–Ca ratio in atom number of in total earth crust, Clark number was given as 1 : 3400. These elements exist mostly in various types of minerals, some in solution, and a few in various kinds of organisms.

(2–2) Almost of all the plants and animals living on land and in water contains more or less calcium and strontium in their body, concentrating these in particular tissue in higher organisms. These elements came originally from the environment where these grow eitheir directly through epidermal up-take or indirectly through their food organisms.

The Sr–Ca ratio in organisms generally varies remarkably according to their systematic position more than to that in the enviroment through the latter influence it in some degree. By THOMPSON and CHOW[5], this ratio was decided on huge number of marine organisms growing homogeneous specific concentration water conserning strontium and calcium, and found the ratio in number of atom varies from 1 : 100 level to 1 : 1,000 level in relation with the systematic position. ASARI[6,7] reports shells have it as 1 : 150—1,000, and fish bones have it as 1 : 50—1,000. About land animals and plants information on this is poor at present moment, but now analysis is going on many materials.

About human bone, the matter of concern by deposition of radio-active strontium, ASARI[8] reports Sr–Ca ratio in atom number 0.24 : 100, and the idea of average man by ICRP defines 0.7 : 100 it as weight ratio (0.35 : 100 in atom number) where 1 kg of Ca and 7 g of Sr exist in a total skeleton. This ratio is about 10 times of the Clark number, but near to some of the organisms.

In detail, this ratio would be different according to the tissue or the part of body of organisms, but not yet the detail is investigated.

These natural strontium and calcium exist in human bone came in from the environment mainly by taking various food and water, and a few part by respiration through inhalation of dust particles.

(2-3) So many physiological experiments were done about the up-take of strontium and calcium by numerous biologists on various kinds of organisms in various conditions especially since the tracer study by radio-isotopes started. Summarizing these works, it can be said that (1) strontium behaves near to calcium, and deposits in the same tissue, (2) though both strontium and calcium can be the substitute each other in physiology in a certain extent, the each has respectively some peculiar meaning in physiology of organism by the difference of chemical character, (3) the strontium-calcium ratio in a certain tissue of organism is quite indepedent from that in environment and food in normal physiology in nature usually, (4) but the strontium-calcium specific ratio in environmental medium, in the case of experimental culture where the volume of the medium is limitted, and where the concentration is abnormally different from it in nature, influences the up-take of these elements by organisms.

### 3. An idea of MPC of $Sr^{90}$ on earth surface

(3-1) In recent years, by the nuclear weapon tests, $Sr^{90}$ born by nuclear fissson procedure covers almost entire globe surface rather homogenously though some geographical variety was found, and also that in industrial waste does in certain limited area. This amount in unit area is now being measured by various countries, either by direct analysis of soil or water or by accumulation of periodical measure of fall-out. For the interpretation of this so often, the amount of $Sr^{90}$ is expressed in the ratio to the amount of calcium both in environments and in various organisms including human food, for example as that is called as Sun-shine unit.

The definition of Sunshine unit (1 : 1,000 of MPC) is based upon the idea that the strontium-calcium ratio is same all through in the environmental medium of food organisms, in human food and in human skeleton, defining this ratio as same as in human bone, which has 7 g of strontium and 1 kg of calcium in an average human skeleton as a standard, and to which one microcurie of $Sr^{90}$ is MPC.

However, as already mentioned in (2-1 and 2) Sr : Ca ratio differs according to the kind of environment and of organism by a factor of ten, hundred, thousand or more. Therefore this idea of the sunshine unit is inconvenient to be a right measure of future hazard from environment through food to human bone.

However, the ratio of $Sr^{90}$ to natural inactive strontium (mostly $Sr^{88}$, simply expressed as Sr here) is the one never change in usual biological and chemical procedure all through in environment, food and human skeleton. Therefore, if we can get this ratio in these materials we can get more exact method to know about MPC level on the earth surface.

Based upon the same figures already used for the Sunshine unit, 1 microcurie of $Sr^{90}$ (which weight is about $6\times10^{-9}$ g) in 7 g of natural strontium in a human standard skeleton has the $Sr^{90}$ : Sr ratio as $1:10^{9}$ approximately. My idea is that

the level of this ratio must be the maximum permissible ratio all through in human skeleton, in foods, and in environment. If 1/1,000 of MPC is necessary this ratio must be $1:10^{12}$. (may call it as Moon-light unit and its ratio as Moon-light ratio temporarily)

(3-2) It is easy to convert the Sunshine unit to Moonlight unit, if we could know the Sr : Ca ratio in that material, by the conversion factor, the ratio of Sr : Ca to 7 : 1,000 in weight (that of human bone). The both unit has same value in case of human bone, and the difference between the two would not differs so greatly in most of food, in which Sr : Ca ratio not differs greatly from that in human bone.

However, in the actual figures of Sunshine unit already obtained by food material or environmental medium, some are abnormally high or low, and it makes hard to see fair index between that of environment, food and human being. This large variation is commonly supposed to be caused by abnormal shortage or abundance of calcium in it. However, by my interpretation, it is supposed to be due to the variation of specific concentration of strontium in that material, which is, by usual chemical analysis included in calcium and the amount of it is usually millions times of that in fall out. This idea of Moonlight ratio can interprete more reasonablly not only these abnormality but also future human skeletonal concentration by contamination of food and environment.

(3-3) $Sr^{90}$ in fall-out in sky comes down on the earth surface mostly with rain in rainy country like Japan, and a few in fine dust. A part of these forms soluble radio-strontium either in water area or in soil which is available to be taken up by organisms where growing. So, to know about the Moonlight unit of either water or soil, we have to measure radiochemically both available Sr and $Sr^{90}$. However, if it is difficult to measure the available amount of Sr, as in case of some sort soil and vegetables in which foliage retention or absorption is remarkable, it is not necessary to measure it directly. If any of the organism growing there has a certain tissue in which quick and high concentration of Ca and Sr can be seen, by analysing that specific concentration of Sr chemically and specific activity of $Sr^{90}$ by radio-assay, we can get Moonlight ratio as same as in that environment in form of available to that organism. Materials now we are using are fish bone, shell in water area, deer horn, animal bone, land snail and others in land. To know about the average figure for a certain year, the animal must grown in a year. And, in the tissue where the rate of replacement (turn-over) is so slow, like bone of large sized mammal, the Moonlight ratio must be much lower than that in the environment or in the food. So, to select the material to know that in environment, it is better to get either short life plants and animals or fast growing tissue with complete physiological knowledge. In the

case of hervivorous animals either in land or water area, as they are taking fall-out $Sr^{90}$ adhered on the surface of plant plus that was up-taken, the ratio in their food must be higher than that in environment. But, after complete turn-over in bone which is a large reservoir of Ca and Sr, the same ratio they have in edible part like meat, milk or egg, which make the same ratio in human bone after the complete replacement of these taken place several years later.

(3-4) This idea of Moonlight ratio is based upon the assumption that the level of the specific concentration of $Sr^{90}$ on earth surface would be nearly constant during several years until human skeleton get complete replacement; in other words, equilibrium is established between human bone and environment. This would really happen by constant supply of it from stratosphere to compensate the reduction of activity by physical decay (about 28 years half-life) in the environment. (The biological decay in human bone is already considered in MPC value) This amount of supply can be checked by periodical measurement of fall-out on the earth-surface or in the stratosphere with fair knowledge of rate of falling.

(3-5) Practically, as the chemical separation of Sr from Ca is rather difficult and less accurate than to measure Ca (including Sr as a part), so the Sunshine is more easy to get. But, in the step of radio-assay to avoid the absorption by huge amount of co-existing Ca, it is better to separate Sr as purely as possible, and by that chance we can measure total strontium amount. Assuming 0.1 g of total strontium is in the material, single Moonlight unit (1/1.000 of MP ratio, or $1:10^{12}$ in Moonlight ratio) in it corresponds to $0.14\times10^{-10}$ curie or 30 dpm. To measure this level, if Sr : Ca ratio is 1 : 100, the amount of Ca in the material must be more than 10 g, and this amount of material is about the same as required to get sunshine unit. In radio-assay, co-existing $Y^{90}$ must be excluded in calculation, and to get more exact figure, $Sr^{89}$, co-existing in various percentage in case of young fission, must be eliminated by assaying $Y^{90}$ after separation, if it is necessary.

(3-6) The same idea can be appliable to other radio-isotops of long life, such as $Cs^{137}$ or else when all the necessary factor is known. And, in recent years, as accumulation of $Sr^{90}$ on surface of earth getting more year by year, we can determine the age (195?) by this ratio in certain organisms growing in the same area, as it is available to use $C^{14}:C^{12}$ ratio to measure long period.

**4. Relation with Food habit**

(4-1) As already mentioned, Sunshine and Moonlight ratio must differs according to the kind of food organism, and to the locality. And, the specific radioactivity of $Sr^{90}$ in human skeleton must be decided by taking various matters conteneously

during many years. Therefore, to measure the future hazard caused by certain level of contamination, the Moonlight units of various kinds of food must be put together by some reasonable method, though it is hard to include the up-take of $Sr^{90}$ through inhalation of air.

(4–2) For this purpose, we have to get the statistics on food habit regarding with calcium source, which apparently differs according to nation, and to person or age. In average (ICRP figure) a standard man is taking 1 g of calcium per day, including strontium in various ratio. (average for Japanese nation is 0.7 by statistics)

Table 1. Calcium in Foods of the Japanese Nation*

| | | Calcium (mg) | % |
|---|---|---|---|
| Cereals | Rice | 95 | 26.1 |
| | Barley | 15 | 4.1 |
| | Wheat | 13 | 3.6 |
| | Others | 1 | 0.3 |
| Nuts | | 4 | 1.1 |
| Potatoes | Sweet Potato | 4 | 1.1 |
| | Potato | 4 | 1.1 |
| | Others | 1 | 0.3 |
| Sugars | | 2 | 0.5 |
| Oils and fats | | 0 | 0.0 |
| Pulses | Soybean | 5 | 1.4 |
| | Miso | 28 | 7.7 |
| | Soybean products | 9 | 2.5 |
| | Otherss | 7 | 1.9 |
| Fishes | | 125 | 34.3 |
| Meat and Poultry | | 1 | 0.3 |
| Eggs | | 2 | 0.5 |
| Milk | | 13 | 3.6 |
| Milk products | | 3 | 0.8 |
| Vegetables | Green vegetable | 12 | 3.3 |
| | Others | 15 | 4.1 |
| Fruits | Oranges | 4 | 1.1 |
| | Others | 1 | 0.3 |
| Algae | | — | — |
| Total | | 364 | 100.0 |

* "Present Condition of Nutrition of the Japanese Nation" 1954. Ministry of Public Health and Welfare, JAPAN.

Table 1 shows the amount of Ca in various food taken daily in statistical average for Japanese nation, and which amount in a food, F$i$, is expressed as CaF$i$ in the following formula. If we could know, by chemical analysis, strontium calcium ratio in weight, SrCaF$i$, in it, and Moonlight ratio, $Sr^{90}$ : Sr, the amount

of $Sr^{90}$ taken daily through it can be expressed as

$$CaFi\,(mg)\times SrCaFi\times \text{Moonlight ratio.}$$

(4-3) MPC by ICRP for $Sr^{90}$ by daily ingestion of 2,200 cc is $8\times10^{-7}$ microcurie/cc. So, the total weight of it is $1.2\times10^{-8}$ mg, and the maximum amount for the public must be 1/10 of it. Then, for a certain nation, or for all the human being, the total amount of daily taking of $Sr^{90}$ can be

$$\sum CaFi\,(mg)\times SrCaFi\times \text{Moonlight ratio}$$

and this must be less than $1.2\times10^{-9}$ mg.

(4-4) By the same idea, the maximum permissible Moonlight ratio for a kind of food, F$i$, or for that environment, can be get by the following formula.

$$\text{Moonlight ratio (max.)}=1.2\times10^{-9}\,mg/CaFi\,(mg)\times SrCaFi$$

As it is hard to obtain these figures for all kinds of food and environment, simplifying Table 1, these figures were calculated for Japanese nation, for an example, as shown in Table 2.

Table 2.

| kind of food | CaF (mg) | SrCaF | Moonlight ratio (max.) |
|---|---|---|---|
| marine fish | 120 1/ | 1/100 | $1\times10^{-9}$ |
| freshwater fish | 5 1/ | 1/100 | $0.6\times10^{-7}$ |
| Rice and cereals | 150 | 1/1,000 2/ | $0.8\times10^{-8}$ 3/ |
| Vegetable, milk and others | 100 | 1/1,000 2/ | $1.2\times10^{-8}$ 3/ |

1/ By production statistics, the ratio between marine and fresh-water fish is about 100 : 1. Usually fish bone is about 1/4 of whole body and has Ca about 1/4 of its weight, while fish muscle has Ca about 0.03—0.05% of wet weight. So, if average man takes 100 g of fish muscle per day, Ca amount in it is less than 50 mg, and the remaining must come from small bone, by peculiar habit of Japanese nation to eat small fish altogether. As such small bony fish is more in freshwater fish than marine, the author used 120 : 5 instead of 100 : 1 to devide 125 mg into the two environment.

2/ Evaluation by Prof. YATAZAWA.

3/ Not including the foliage retention or absorption, which is less diluted by natural Sr in environment.

(4-5) Taking an example of $Sr^{90}$ concentration in sea-water as already enough factor is known about it, the Moonlight ratio (max.) thus calculated, $1:10^9$, means $10^{-9}$ curie/liter of $Sr^{90}$ in oceanic water.

(Revelle and others[9] calculated $6.8\times10^{-6}$ curie/liter as the concentration of $Sr^{90}$ in seawater after $10^{11}$ megawat/hour nuclear power production, when all the fission product from this is mixed in seawater.)

In freshwater and land soil, as natural strontium concentration available to organisms differs greatly according to the locality, only the way to monitor this level is to measure Moonlight ratio in the tissue something like, shell, horn, bone and others of fast growing animals.

## 5. Acknowledgement

The author wishes to express his thanks to Profs. Kenjiro KIMURA, Shingo MITSUI, Aritsune SAEGI of Tokyo University, and to Profs. Ken SUGAWARA, Michihiko YATAZAWA of Nagoya University for the kindness to help his idea and supplying the data for him.

## Literature cited

1) ASARI, TAMIYA. 1949. Jap. Jour. Chemistry Vol. 70, No. 7,8,9, 11–12. Vol. 71, No. 5.
2) CHOW, D. T. W. & THOMPSON, T. G. 1955: Anal. Chem., 27, 18.
3) SUGAWARA, KEN: in press.
4) SUGAWARA, KEN: in press.
5) CHOW, D. T. W.: 1955 Papers in marine biology and oceanography 20–39.
6) ASARI, TAMIYA: 1950. Jap. Jour. Chemistry Vol. 71, No. 1 and 2.
7) ASARI, TAMIYA: 1950. Ibid No. 4.
8) REVELLE and other: 1956. Peaceful Use of Atomic Energy, Vol. 13, pp. 371–380.

Records of Oceanographic Works
in Japan Vol. 3, No. 1,
March 1957.

# Up-take of Strontium by Marine Fish from the Environment

By

Yoshio HIYAMA, Ryushi ICHIKAWA

(Fisheries Institute, Faculty of Agriculture, University of Tokyo)
(Received Aug. 15, 1956)

## 1. Introduction

The rearing experiments to see up-take of strotium by fish from the environmental water investigated by SUEHIRO & others[1] and TOMIYAMA & others[2] have little explanation on the amount of strontium in the environment and that taken by fish. As already mentioned in my previous paper[3], the co-existence of the same nuclide in natural environment is an important factor to consider the amount of up-take of radio-isotope, especially so as to know about the level of contamination of food organisms growing in a contaminated environment.

Here, preparing various kinds of artificial environment, rearing some species of fish in it, two series of experiments were undertaken to know the absolute amount of up-take from environment, using the figures that already known by chemical analysis.

## 2. Rearing in different salinity

As it is known[4] [5] that the normal oceanic sea water has 7 mg of natural strontium per litre (calcium, about 400 mg) commonly, so this is supposed to effects the up-take of $Sr^{90}$ in rearing experiment. Thus, to check this, getting oceanic water from the point off MIURA peninsula (33‰ *cl*), diluting it by distilled water in three ratios; (A) 20 litre of sea water (no dilution), (B) 10 litre of sea water plus 10 litre of distilled water, (C) 5 litre of sea water plus 15 litre of distilled water; these three kinds of 20 litre rearing water were prepared in each thank (50 cm×70 cm×20 cm) lined by polyethylene film. "Mahaze" or Common goby, *Acanthogobius flavimanus*, a brackish water fish from Tokyo bay 15—17 inividuals of 15—20 g in weight for each tank, were kept alive in these waters since a few days before the experiments. Then $Sr^{90}$ was added to each tank so as to make the concentration of sea water as 1 $\mu$c/litre for all of three tank. These fishes were kept alive there without feeding during a week from Jul. 27th to Aug. 4th, 1956, (water temp. 24°C) and killed for anatomy and radio-assay as its result is shown in table 1. Table 1 tells (1) there is some individual variation on amount of up-take through external epithelium, (2) a

week rearing would be enough to replace strontium in muscle, but might not be in bone.

In these experiments strontium concentration in water, SrE, was (A) 7 mg/litre (B) 3.5 mg/litre (C) 1.8 mg/litre, and $Sr^{90}$ concentration in water, Sr*E, was 1 $\mu$c/litre = $6\times10^{-6}$ mg/litre for each of three tanks.

Table 1

$Sr^{90}$ concentration in fish tissues (Sr*F) of Common goby reared in 1$\mu$c/$l$ sea water.

| Environmental water | A 20 $l$ sea water | | B 10 $l$ sea water 10 $l$ dist. water | | C 5 $l$ sea water 15 $l$ dist. water | |
|---|---|---|---|---|---|---|
| | Muscle $10^{-5}$ $\mu$c/g | Bone $10^{-3}$ $\mu$c/g | Muscle $10^{-5}$ $\mu$c/g | Bone $10^{-5}$ $\mu$c/g | Muscle $10^{-5}$ $\mu$c/g | Bone $10^{-3}$ $\mu$c/g |
| 3 days | 2.8 | 0.47 | 2.5 | 0.48 | 5.2 | 1.3 |
| | 2.2 | 0.37 | 4.2 | 0.66 | 4.9 | 1.2 |
| | | | 3.3 | 0.65 | 4.5 | 1.4 |
| | | | 3.8 | 0.61 | 4.2 | 1.2 |
| | | | 2.9 | 0.80 | 5.5 | 1.4 |
| Average | 2.5 | 0.42 | 3.3 | 0.64 | 4.9 | 1.3 |
| 5 days | 2.5 | 0.38 | 3.9 | 2.35 | 7.1 | 1.5 |
| | 2.7 | 0.62 | 5.9 | 1.08 | 7.5 | 3.1 |
| | | | 3.7 | 1.01 | 6.6 | 2.1 |
| | | | 3.1 | 0.77 | 6.6 | 1.4 |
| | | | 2.9 | 0.91 | 5.7 | 1.7 |
| Average | 2.6 | 0.50 | 3.9 | 1.22 | 6.7 | 2.0 |
| 7 days | 2.1 | 0.40 | 5.0 | 1.21 | 11.7 | 3.2 |
| | 1.8 | 0.57 | 3.1 | 0.90 | 9.7 | 3.7 |
| | 2.4 | 0.59 | 2.1 | 1.02 | 7.4 | 1.8 |
| | | | 2.9 | 0.93 | 6.3 | 1.6 |
| | | | 2.0 | 0.83 | | |
| Average | 2.1 | 0.52 | 3.0 | 0.98 | 8.8 | 2.6 |
| Average (total) | 2.2 | 0.48 | 3.7 | 0.95 | 6.6 | 1.9 |

Getting $Sr^{90}$ concentration in muscle and bone of fish, Sr*F, by radio-assay as shown in table 1, if the hypothesis stated in my previous paper[6] is right, when the concentration of normal strontium in fish tissue, SrF, was calculated by the formula Sr*F/SrF = SrE*/SrE, the figures of SrF in fish tissue by all these three experiments must be the same. These figures of SrF obtained by this calculation, using average figure of Sr*F, are shown in table 2.

This table shows rather equal value of figure each for muscle and bone through all the experiment as it was expected to be so.

In the next step by using these average figure, if the replacement of strontium in tissue is supposed to be complete, we can calculate Sr : Ca ratio in these tissues, SrCaF, by the following data. About fish muscle the calcium content, CaF, is

Table 2

Calculated normal strontium concentration in fish tissue (SrF) of Common goby.

| Tissue / Environment | Muscle | Bone |
|---|---|---|
| A | $1.5\times10^{-4}$ mg/g | $3.4\times10^{-3}$ mg/g |
| B | $1.3\times10^{-4}$ mg/g | $3.3\times10^{-3}$ mg/g |
| C | $1.2\times10^{-4}$ mg/g | $3.3\times10^{-3}$ mg/g |

rather validly known by many workers as 0.0003—0.0005 of wet tissue[7) 8)]. So, strontium-calcium ratio, SrCaF, in muscle of experimented fish must be $1.3\times10^{-4}$ mg/3—$4\times10^{-1}$ mg = 1 : 2,300—3,700 (mean 3,300). This figure is the one never obtained by chemical analysis hitherto, though the validity of this would be discussed later. By the same way, as CaE of fish bone was measured 125 mg/g, SrCaF in experimented fish bone must be $3.3\times10$ mg : 125 mg = 1 : 36,000.

### 3. Difference between species and $Sr^{90}$ concentration

In the similar tanks, 50 litre of Oceanic water (33‰ *cl*) was kept to rear two kinds of marine fish, "Kusafugu," a puffer, *Fugu niphobles* (about 10 g body weight) and "Agohaze," a kind of marine goby, *Chasmichthys dolichognathus*

Table 3

Concentration of $Sr^{90}$ in tissues (Sr*F) after rearing.

| Fish | Puffer | | | | Goby | | | |
|---|---|---|---|---|---|---|---|---|
| $Sr^{90}$ concentration in sea water | 10 $\mu c/l$ | | 1 $\mu c/l$ | | 10 $\mu c/l$ | | 1 $\mu c/l$ | |
| Tissues / Reaving Period | Muscle | Bone | Muscle | Bone | Muscle | Bone | Muscle | Bone |
| | $10^{-5}$ $\mu c/g$ | $10^{-3}$ $\mu c/g$ | $10^{-5}$ $\mu c/g$ | $10^{-3}$ $\mu c/g$ | $10^{-5}$ $\mu c/g$ | $10^{-3}$ $\mu c/g$ | $10^{-5}$ $\mu c/g$ | $10^{-3}$ $\mu c/g$ |
| 2 days | 33.0<br>30.8<br>42.3 | 14.6<br>20.7<br>17.5 | 8.9<br>16.8<br>14.4<br>6.5 | 4.1<br>2.3<br>3.3<br>3.4 | 63.9<br>45.6 | 26.8<br>37.4 | 4.2<br>2.5 | 1.4<br>2.0 |
| Average | 35.4 | 17.6 | 11.7 | 3.3 | 54.8 | 32.1 | 3.4 | 1.7 |
| 4 days | 25.2 | 38.9 | 2.8<br>4.2 | 3.3<br>5.3 | 88.2<br>101.1 | 30.5<br>45.5 | 2.0<br>5.8 | 0.8<br>0.9 |
| Average | 25.2 | 38.9 | 3.5 | 4.3 | 94.7 | 38.0 | 3.9 | 0.9 |
| 6 days | 27.0<br>62.7 | 17.5<br>36.8 | 3.8<br>5.6 | 3.1<br>5.4 | | | | |
| Average | 44.9 | 27.2 | 4.9 | 4.3 | | | | |
| Total Average | 36.8 | 24.3 | 7.9 | 3.8 | 74.7 | 35.1 | 3.6 | 1.3 |

(about 5 g body weight). About 10 individuals of each were reared in each tank, during about a week, without feeding, to where $Sr^{90}$ was added to make its concentration of water up to 1 and 10 $\mu c$/litre respectively for each species. Tank was kept in back space of Aquarium at Misaki Marine Biological Station from July 15th to 21st, 1956 (where room temperature was 23 -25°C). The some were died during experiments but the some were killed for anatomy and the radio-assay as the results are shown in Table 3.

This shows (1) rather bigger variation between individuals than in case of the first experiments, (2) fish reared in 10 $\mu c$/litre tank took up about 10 times of that of fish reared in 1 $\mu c$/litre, as it was expected by the hypothesis above mentioned, but it is rather commonly less than 10 in puffer and more than that in goby, by unknown reason. (3) Comparing these figures in 1 $\mu c$/litre with A of the former experiment in table 1, puffer and marine goby took more $Sr^{90}$ as much as 3 to 7 times in both tissues. This might be comprehended more easily by the fact that rearing water was more (50 liter) in this experiment, while less (20 litre) in the foregoing experiment, than to comprehend it as caused by the difference of species. By these figure, also SrF was calculated by the same formula as above mentioned, and there are shown in table 4.

Table 4

Calculated normal strontium concentration in fish tissues (SrF)

| Fish | Puffer (14 individuals) | | | | Goby (10 individuals) | | | |
|---|---|---|---|---|---|---|---|---|
| Tissue | Muscle | | Bone | | Muscle | | Bone | |
| $Sr^{90}$ concentration in sea water | 10 $\mu c/l$ | 1 $\mu c/l$ | 10 $\mu c/l$ | 1 $\mu c/l$ | 10 $\mu c/l$ | 1 $\mu c/l$ | 10 $\mu c/l$ | 1 $\mu c/l$ |
| | ($10^{-4}$ mg/g) | | ($10^{-2}$ mg/g) | | ($10^{-4}$ mg/g) | | ($10^{-2}$ mg/g) | |
| Minimum | 1.7 | 2.9 | 1.0 | 1.6 | 3.2 | 1.4 | 1.9 | 0.6 |
| Maximum | 4.3 | 11.7 | 2.7 | 3.7 | 7.1 | 4.0 | 3.2 | 1.4 |
| Average | 2.6 | 7.8 | 1.7 | 2.6 | 5.2 | 2.5 | 2.4 | 0.9 |
| Average | 4.2 | | 2.2 | | 3.9 | | 1.6 | |

Table 4 shows rather bigger individual variation than table 2, and figure differs more than twice in some case between that of 10 $\mu c$/litre and 1 $\mu c$/litre. The reason for it is unknown for us. (possibly some body might feed some fish during in aquarium)

By using average figure of SrF for each tissue of each species, SrCaF was calculated as follows, by means already mentioned in the last chapter.

| | | |
|---|---|---|
| Puffer muscle | $4.2\times10^{-4}$ mg : 0.3—0.5 mg | 1 : 710—1,200 |
| ,, bone | $2.2\times10^{-2}$ mg ; 125 mg | 1 ; 5,500 |

| | | |
|---|---|---|
| Marine goby muscle | $3.9\times10^{-4}$ mg : 0.3—0.5 mg | 1 : 770—1,300 |
| ,, bone | $1.6\times10^{-2}$ mg : 250 mg | 1 : 7,800 |

These figures of these fishes are fairly larger than that obtained by common goby (muscle 1 : 2,300—3,700, bone 1 : 36,000). These ratio are quite different from Sr : Ca ratio (0.6 : 100) obtained by ASARI[9] about bone of mare goby "Donko" *Mogurnada obscura*, a most closely related fish among the many he studied. This difference can be comprehended that the replacement of these element in tissues was not perfect by less amount of water to rear the fish without feeding any calcium or strontium. For instance, total amount of strontium in whole fish in case of common goby can be calculated as 17 (individuals)×17 g (weight)×1/4 (bone in body)×1/8 (calcium in bone)×1/170 (SrCaF)=50 mg (where Ca is 8 g), while the water in tank A had 140 mg (Ca 8 g), tank B 70 mg (Ca 4 g) and C 35 mg (Ca 2 g). This amount of Ca and Sr in water is not enough to make entire replacement of Ca and Sr in fish body. On the other hand, in the latter case by puffer, strontium in total fishes to be replaced was 18 mg (10×10 g×1/4 ×1/8×1/170) while that in sea water was 350 mg (7 mg×50). So, the ratio replacement would be more in these than those experiment, that these figures may be more near to the nature.

**4. Rate of Replacement**

As it is clear in Table 1 and 3, apparently the bone was not saturated by the new coming strontium during a week long rearing experiment. So, we tired to enumerate the fraction amount of the new coming strontium to that in muscle and bone to know the rate of replacement or turn-over, by premising that SrCaF in muscle and bone must be the same.

By the chemical analysis ASARI[9] obtained SrCaF of bone of goby as 1 : 167, but Chiba (unpublished data) obtained as 1 : 500 for tuna bone. And the Calcium content in muscle and bone is known to be 0.0004 and 0.13 respectively by chemical analysis.

Thus, SrF in muscle can be calculated as $2.7\times10^{-6}$ (based on ASARI) or $8\times10^{-7}$ (based on CHIBA). On the other hand Table 4 shows SrF in muscle of puffer as 4.2 (1.7—11.7)$\times10^{-7}$, and that of marine goby as 3.9 (1.4—7.1)$\times10^{-7}$. If the replacement is complete, (many of the physiological experiments proof it) the figure by CHIBA is more close to that of figures especially to that of larger values. By the same idea, SrF in bone can be calculated as $7.8\times10^{-4}$ (based on ASARI) or $2.6\times10^{-4}$ (based on CHIBA). And, Table 4 shows SrF in bone of puffer as 2.2 (1.0—2.7)$\times10^{-5}$, and that of marine goby as 1.6 (0.9—3.2)$\times10^{-5}$. Even if this is compared with that obtained calculated based upon CHIBA'S ratio, still it is about 1/10 of the expected value.

By this reason, we can roughly measure that only 1/10 of total Sr or Ca was replaced in bone by the new coming atoms during a week long rearing experiment, while the muscle had complete turn-over.

The first experiment data shown in Table 2 were not used in this calculation on account of incomplete turn over as already stated above.

Here, it should be noted that all of the three species of fish we used in these experiments were young adult in some growing stage, and if the fishes of another growing stage was used, there would be a little difference from the figures we got.

By this sort of experiment, we can measure Sr concentration either in tissue or in environmental water in fairly low level as usual chemical analysis can not go further, just like a sort of bio-assay, And it would be also appliable to some of other nuclides. However, in this sort of radiological bio-assay, we must be carefull to use the large amount of water to keep fish enough to get complete replacement, because the usual fish in nature to compare with as physiological standard is living in water of infinitely large mass. And, also the the concentration of element considered must be near that in natural environment. Otherwise, the up-take of the element must differ from the usual physiology in nature. In these experiment, 1 $\mu c$/litre of $Sr^{90}$ in sea water has $Sr^{90}$ : Sr ratio as $1:10^6$, so the addition of $Sr^{90}$ to sea water has no measurable influence to the total concentration.

## 5. Summary

(1) $Sr^{90}$ concentration in fish tissue (Sr*F) reared in the water having $Sr^{90}$ as certain concentration (Sr*E) where already natural strontium existed in an concentration (SrE) proved to be decided by the following formula. Sr*F/SrF = Sr*E/SrF. This relation was so clear in the aquarium experiment of common goby in the laboratory, but had some slight deviation in case of puffer and marine goby in aquarium by unknown reason.

(2) By the figure of calcium content in fish tissue (CaF) known by chemical analysis, Sr : Ca ratio in these tissue (SrCaF) were calculated. The difference of this ratio between two experiments can be comprehended by the difference of ratio of replacement caused by the difference of total amount of strontium in environmental water compared with that in fish to be replaced. So, the figure of SrCaF in the second experiment is nearer to the real figure than that in the first experiment. And the bone requires more time and amount of trontiums in environment to have complete replacement, while the muscle would not do more than that in these experiment.

(3) Promising SrCaF in the musle is the same as in bone which was already got by chemical analysis, based upon the calculated figures of SrE in muscle and bone in the second experiment, the fraction of replacement of these elements to

the total amount in tissues from environment was calculated. As for muscle, replacement is thought to be complete, but as for bone it is supposed to be only 1/10 during a week long rearing experiment.

By this sort of biological experiment, we can measure the faint concentration of the element either in a certain tissue or in any environment in the lower level than usual chemical analysis can do. This sort of radiological bio-assay can be appliable to some other nuclides too, if the experiment is carefully done.

## Literature cited

1) SUEHIRO, Y. & others 1956: Transmission and metabolism of $Sr^{90}$ in aquatic animals. The research on the Effects and Influences of Nuclear Bomb Test Fxplosions. Vol. 1, pp. 1134–1142.
2) TOMIYAMA, T. & others 1956: Absorption of $Sr^{90}$ ($Y^{90}$) by carp. ibid.pp. 1181–1187.
3) HIYAMA, Y., ICHIKAWA, R., & YASUDA, F. 1956: Studies on the process of contamination of fish by fission products. ibid. pp. 1118–1133.
4) CHOW, T.J. & THOMPSON, T. G. 1955: Flame photometric determination of strontium in sea water. Anal. Chem., Vol. 27, pp. 18–21.
5) SUGAWARA, K. & KAWASAKI, N. 1956: unpublished.
6) HIYAMA, Y. 1956: Maximum Permissible concentration of $Sr^{90}$ in food and environment. Rec. Oceanogr. Works in Japan. Same issue.
7) OSHIMA, K. 1949: Chemistry of fishery animals (in Japanese) Asakura book Co. Tokyo.
8) OKUDA, Y. 1931: Fisheries Chemistry (in Japanese) Kobunsha Co. Tokyo.
9) ASARI, M. 1950: The geochemical distribution of strontium–VI. animal bones. Bull. Jap. Soc. Chem. Vol. 70, pp. 12–13.

Records of Oceanographic Works
in Japan Vol. 3, No. 1,
March 1957

# Mechanism of Utilization of Plankton by Some Fishes[1)]

Fujio YASUDA and Yoshio HIYAMA
(Fisheries Department, Faculty of Agriculture, The University of Tokyo)

## 1. Introduction

Discussing the productivity of water, such conditions as the concentration of nutrient salt, up-welling movement of water mass, the strength of light for synthesis, the density of plankton and so on, have been usually investigated. However, during the biotic process, the method of plankton utilization by fish is one of the keys to know the process of production. Here, the feeding mechanisms of some of the plankton feeders are investigated to see how the plankton is utilized by these to be the product of sea, either indirectly as the food of carnivorous fish or directly as the harvest. As the materials to be studied, the five important species as commercially fished in large amount at off shore area in Japan. There are "Saba", Mackerel, *Scomber japonicus Houttuyn*; "Aji", Horsh mackerel, *Trachurus japonicus* (*T & S*); "Samma", Mackerel pike or Skipper, *Cololabis saira* (*Brevoort*); "Iwashi", Sardine or Pilchard, *Sardinia melanosticta* (*T & S*); and "Katakuchi-iwashi", Anchovy, *Engraulis japonica* (*Houttuyn*); and the two minor species "Sappa", *Harengula zunasi* (*Bleeker*); "Urume-iwashi", Bigeyed-sardine or Round herring, *Etrumus micropus* (*T & S*) were selected.

## 2. Structure of gill and its filtering mechanism

It is well known that beside the gill filaments of respiratory function, the gill has gill rakers at inner side to serve as a sieve to collect plankton and bring

Table 1 Characteristics of Gills

| Character / Species | Gill rakers other than 1st gill arch | Gill sieves of 1st gill arch | No. of joint 1st gill arch | Arrangement of process | Size of fish the process developed BL. (cm) | The size of fish the gill rakers completely developed BL. (cm) | The number of gill raker completely developed BL. (cm) |
|---|---|---|---|---|---|---|---|
| Mackerell | Undeveloped | Developed | 1 | Asymmetry | 3 | 7- 9 | (12-14) + (26-29) |
| Horse mackerel | 〃 | 〃 | 1 | 〃 | 3 | 6- 9 | (14-15) + (37-40) |
| Mackerel pike | 〃 | 〃 | 1 | 〃 | 4 | 5-10 | ( 0 ) + (33-40) |
| Anchovy | Developed | Undeveloped | 2 | 〃 | 3 | 8- | (30-33) + (34-40) |
| Sardine | 〃 | 〃 | 2 | Nearly symmetry | 3 | 9- | (37-59) + (65-108) |
| Round herring | 〃 | 〃 | 2 | Asymmetry | 3 | * | * |
| "Sappa" | 〃 | 〃 | 2 | 〃 | 3 | * | * |

* Number of samples are too small to be noted here.

1) This is an abstract of the work for the Master's degree of Yasuda under Prof. Y. Hiyama.

them into the alimentary canal. The structure of the gill rakers, as well as gill sieve (Fig. 1–H) developed at the sides of the gill arch in some species, varies according to species and this is supposed to be one of the major factors determining the filtering function of the gills. Among the fishes here studied, the number of gill arches, number and length of gill rakers, the number and shape of processes

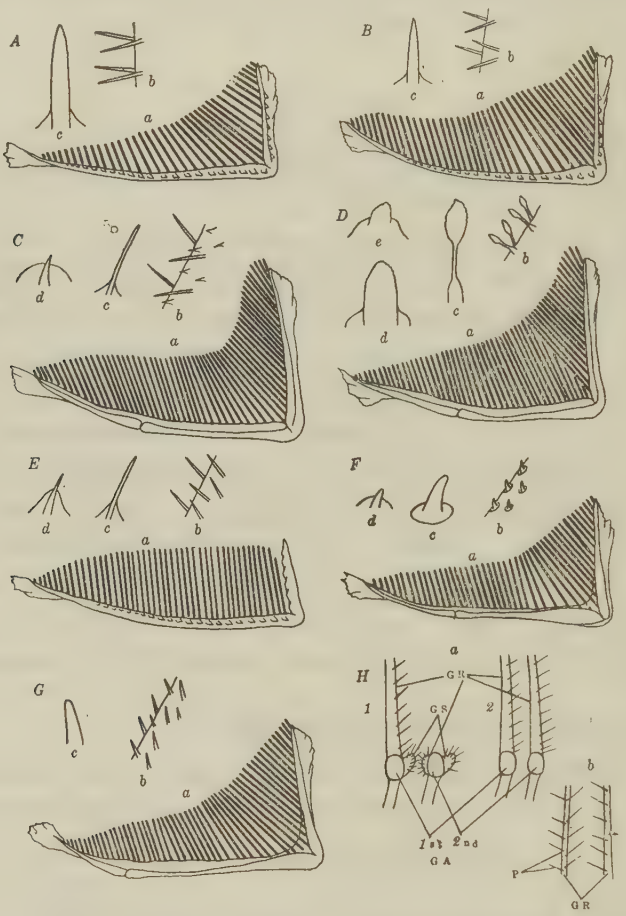


Fig. 1. Shown the gill structure of each species.

A—Mackerel. B—Horse mackerel. C—Anchovy. D—Sardine.
E—Mackerel pike. F—"Sappa". G—Round herring.
H—Structure of filtering system of the gill.
H-a—Structure of the gill (inside view of 1st gill arch, Plane figure).
1—Mackerel, Horse mackerel and Mackerel pike (Cross section).
2—Sardine species (Cross section).
H-b—Structure of the mesh (Arrangement of processes, Plane figure).
(GR—Gill raker. GS—Gill sieve. GA—Gill arch. P—Process.)
Magnitude
A (a–×1.2 c–×24) B (a–×1.2 c–×18) C (a–×3 c–×12 d–×18)
D (a–×4.2 c–×18 d–×42 e–×12) E (c–×12 d–×24)
F (a–×4.8 c–×18 d–×24) G (a–×4.8 c–×48)

in the gill rakers, presence or absence of gill rakers at the posterior gill arch, and that of gill sieve and other structure differ as shown in Fig. 1 and Table 1.

The mesh size of a plankton filtering system formed by the gill raker is determined by the interval of the gill rakers on the first gill arch and of the processes in it. The gill sieve and the gill rakers of the posterior gill arches serve as supplementary processes. This mesh becomes finer when the gill arch bends inward by the joint at the elbow of the arch and moreover that at the lower gill arch in some fishes, by crossing gill rakers on the upper and lower gill arches, as usually seen when the fish closes its mouth to swallow the food. In the aquarium observation the fish such as Sardine, Anchovy and others open their mouth and the gill openes as wide as possible when they feed planktons. In this state the gill rakers spread as wide as possible to make the filtering areas as broad as possible, and accordingly the mesh of it is coarser than that when the mouth and gill opening is closed. Thus, to express the mesh size of this plankton filtering system formed by gill rakers, the area surrounded by an interval of gill rakers and by an interval of processes in it is to be considered. However, as the former is fairly broader than the latter, the latter has more important meaning in the filtering function. (see Fig. 1-H)

Thus, the interval of the processes in gill raker of fish of these kinds were plotted in relation to the fish size (Fig. 2)

Comparing the structure and the mesh size formed by the gill rakers of these fishes with each other, it can be said that Mackerel and Horse mackerel have the most coarse structure while, Sardine and Anchovy have the finest structure, and that the Mackerel pike is between the two groups.

### 3. Size of food in stomach

By an examination of the stomach contents of 117 individuals of Mackerel, 75 individuals of Horse mackerel, 80 individuals of Mackerel pike, 80 individuals of Anchovy, 80 individuals of Sardine, 20 individuals of "Sappa", and 22 individuals of Round herring, it can be said generally that Mackerel and Horse mackerel take the plankton of larger size and of higher food order, while Sardine and Anchovy take the smaller ones, and the Mackerel pike is between the two groups, as shown in Table 2.

This fairly agrees with the structure of the filtering system of the gill, mentioned in the foregoing chapter. Among food organisms, Copepodes are taken commonly by all the species. However, that taken by Sardine, Anchovy and "Sappa" are very small sized.

By measuring the actual size of the various organisms found in the stomach of each size of fishes, except broken one*, and plotting the maximum and minimum

* Single individuals of plankton is measured in case that form colony.

Table 2 Stomach Contents.

| Stomach contents \ Species | Mackerel | Horse Mackerel | Mackerel pike | Ancohovy | Sardine | "Sappa" | Round herring |
|---|---|---|---|---|---|---|---|
| Fish adult | * | | | | | | |
| Fish yound | * | * | | | * | | * |
| Fish egg | * | * | | * | * | | |
| Cephalopoda | * | * | | | | | |
| Shelled-larva | | * | | * | * | | |
| Mysidacea | * | | | * | | * | |
| Euphausia | | | * | | | | |
| Shrimp | * | | | | | | |
| Megalopa | * | | | * | | | |
| Amphipoda | * | * | | * | | | |
| Ostracoda | | | * | * | * | * | |
| Copepoda | * | * | * | * | * | * | * |
| Phyllopoda | | * | | * | * | * | |
| Jelly-fish | * | | | | * | | |
| Sagitta | * | * | | * | * | | |
| Thaliacea | | | * | | | | |
| Phytoplankton | | | * | * | * | * | * |

* Indicates presence of food.

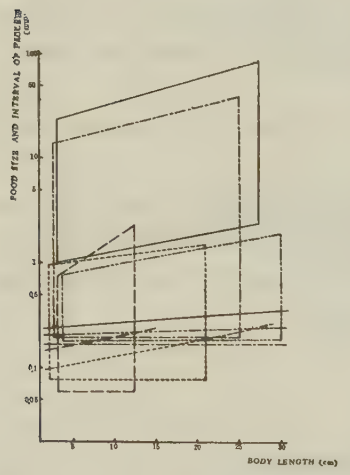


Fig. 2 Shown the maximum and minimum size of the food from the stomach contents, this is then compared with smallest arm of a mesh (interval of process).

——— Mackerel
— — — — Horse mackerel
— — — — — Mackerel pike
— — — Anchovy
— — — — — Sardine
Interval of process (Straight line).

sizes of the food in relation to fish size as shown in Fig. 2, we could obtain a pattern to express the size of food taken by these fishes of various sizes.

This graph tells us some facts. (1) Even though the size of the fish may be the same, since the mesh size of the filtering system of the gill differs according to species, the size of food taken also differs according to fish species. Mackerel and Horse mackerel take the larger organisms, while Sardine and Anchovy take smaller ones. (2) As the mesh size of the filtering system of the gill becomes larger by growth the larger size organisms are generally taken by larger sized fish. This tendency is notable in the case of Mackerel and Horse mackerel, but not in that of Mackerel pike and Sardines. Though the minimum (the bottom line of the square) is rather constant, the maximum (the upper line of the square) ascends prominently in the case of Anchovy.

Thus, it is clear that the mesh size in the filtering system of the gill decides the size of plankton to be taken especially that of the minimum size. But, probably due to the choking of the mesh by accumulated planktons or to the colony making charactors of some phytoplanktons, the smaller

organisms were found in the stomach than that of the mesh size in the filtering system, especially in Sardine and Anchovy.

### 4. Feeding experiments

The above mentioned findings are based on the hypothesis that the sea contains ample variation in the size of planktons which the fish takes as food. Thus, to check such a view several experiments were undertaken in the aquarium and laboratory of Misaki Biological Station.

As the first step, the aquarium experiment to feed Mackerel (12–13 cm long), Horse mackerel (10–15 cm long) and Anchovy (10–13 cm long) with brine shrimp eggs (*Artemia salina*, 0-18–0.22 mm diameter) was done, and examining the stomach we found that the Horse mackerel and Anchovy took the food but the Mackerel did not.

As the smaller organisms, purely cultured diatoms, *Thalassiosira sp* (0.03mm in length) was mixed into the sea water in various concentrations where these fishes were reared. However, since we hardly could find any cells in the stomach, we supposed that they passed through the filtering system of the gill.

As the food of large size as the brine shrimp shows no homogeneous distribution in the aquarium, artificial matter, an ion exchange resin (Amberlite IR-120, diameter 0.4–0.8 mm) was mixed in the water. But, as this particle has a specific gravity, a little larger than that of sea water, these fishes except Anchovy hardly took it when time passed.

Thus, through the filtering system of the gill in a fixed specimen of Mackerel (26 cm in length, 15 mm interval of gill raker, 0.3 mm interval of process), the ion exchange resin mixed in water was poured into the mouth at a speed approximetely near to the swimming speed of this fish. Though it differs according to its concentration in water, the resin of this size was caught by the filtering system of a little finer mesh.

The results of these three experiments are tabulated as follows.

Table 3 Summery of the Results of Experiments.

| Species \ Food | Diatom (0.03 mm in length) | Brine shrimp egg (0.15–0.22 mm in diam.) | Amberlite (0.4–0.8 mm in diam.) |
|---|---|---|---|
| Mackerel | – | – | +* |
| Horse mackerel | – | + | +* |
| Anchovy | – | + | + |

Foot note – means passed out and + means caught by filtering system of gill.
* means physical experiment.

This result is almost coincidental to that obtained by the stomach content examination, except for the case marked by *.

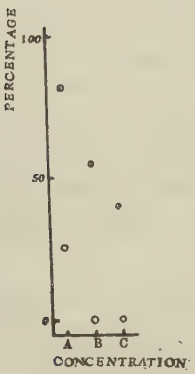


Fig. 3 Difference of food taking (the ratio of number of brine shrimp eggs taken by Horse mackerel to that in water) in different density and stomach condition.

○ full stomach
● empty stomach
A>B>C—concentration

living in the same area are contributing to bring the food material up to the carnivorous fish, to be harvested by man. Moreover, most of the larvae or young marine organisms of larger size are more or less doing the same. So, without knowing the size of the population of these fish unutilized by man, we cannot say about the total amount of plankton feeders in this area.

However, based upon the statistics available, if we see the total amount of these plankton feeders caught by fishing industry, as it is shown in Fig. 4, it is so interesting that the sum of catch of some species of plankton feeders

During the course of the feeding experiment we noticed a difference in the density of the organisms in water, and the amount of food in the stomach of experimented fish, effect the food taking so much, as shown Fig. 3.

## 5. Production of plankton feeding fish of the off shore region of Japan

Theses fishes we investigated are plankton feeders of the off shore area around Japan fished heavily by the industry. They have some similarity in food habit though it varies as mentioned above, and also have some similarity in habitat, though slightly differing with each group.

We know that many kinds of plankton feeders,

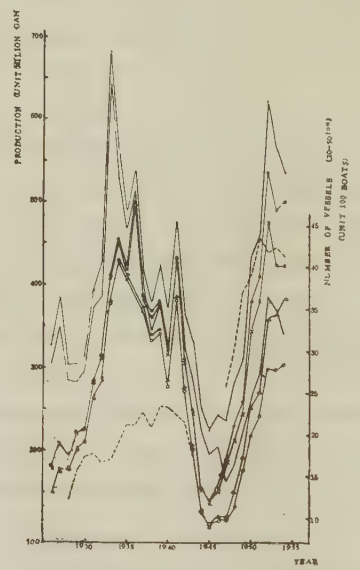


Fig. 4 Sum of Catch of various plankton feeders in coast of Japan

○ ○ Sardine species, Mackerel and Horse mackerel.
● ● Sardine species, Mackerel, Horse mackerel, Mackerel pike and Squid.
△ △ Sardine species, Mackerel, Horse mackerel and Mackrel pike.
× × Sardine species, Mackerel, Horse mackerel and Squid.
Sardine species, Mackerel, Horse mackerel and Herring.
– – – Sardine species, Mackerel, Horse mackerel, Mackerel pike, Herring and Squid.
– – – – Number of vessels (20–50 ton.)

is nearly equal between that in the pre-war time and post-war time, leaving aside the war time decrease of fishing effort, though the latter shows a great decrease in density (catch per unit fishing effort which is expressed as number of boats.) due to the more extensive fishing area and more efficient gears. The disappearance of Sardine is apparently compensated by the increased catch of the Skipper and Squid (if this is an animal to be discussed here).

At the present moment we don't know that this might be a phenomenon due to ecology as these fishes are competitors of each other and plankton production has been constant during this period, or to be understood as an economical problem as the one substitutes the other as the object of fishing industry or as the necessary animal protein resource for this nation.

To know about this we must investigate further about other species which does not appear in statistics as no fishing industry has any interest.

Here, to increase the productivity of the sea the authors want to point out the necessity of co-existence of various plankton feeders, as the size of planktons, in other words the species of it, taken by fish differs according to fish species. For example, Anchovy can be a substitute for the Sardine, but cannot be for the Mackerel or Horse mackerel, and vise versa, as cleared by this investigation.

## References

1) T. Hanaoka. (1954): A consideration on fisheries resources as a community of organisms iu the sea. *Contributions of Naikai fisheries research laboratory* No. 41.
2) J. Nakai. (1938): Comparative study of the gill structure and food of Sardine. (in Japanese) *Journal of fisheries* Vol. **33**, No. 12.
3) Y. Suyehiro. (1942): A study on the digestive system and feeding habits of fish. *Japanese Journal of Zoology.* Vol. **10**, No. 1.
4) Progress Reports (1952–1953): California Cooperative Oceanic Fisheries Investigation.
5) Agriculture, Forestry and Fisheries Statistics Bulletin.

Records of Oceanographic Works
in Japan Vol. 3, No. 1,
March 1957.

# Optical Properties of the Water in the Kuroshio Current (II)

By

Tadayoshi SASAKI*, Noboru OKAMI**, Seiichi WATANABE**,
and Gohachiro ŌSHIBA**

(*Tokyo University of Fisheries and Scientific Research Institute,
**Scientific Research Institute, Tokyo)

## 1. Introduction

Optical properties of the water in the vicinity of the east coast of the Izu peninsula have been investigated by a high sensitive underwater photometer, February 1–8, 1955.(1)

In the present, the extinction coefficients of the water for violet, blue, green, yellow and red lights were measured on board immediately after the water had been taken up on the ship.

Measurements were made at 15 stations in the region of the Kuroshio Current for 120 samples collected from various depths down to 874 m, February 23–26, 1956.

The extinction coefficient can be used as the turbidity which indicate the motion of the water mass. Similar investigations have been carried out by many authors.(4,6,7,8) In the present, the observed extinction coefficients for violet light was regarded as turbidity and the relation between its horizontal and vertical distributions and the motion of the water mass was studied.

## 2. Apparatus and Methods

An outline of the apparatus used is shown in Fig. 1, *S* the light source, *L* the condenser lens, *E* the diaphragm having a round hole of 0.8 cm in diameter, *F* the color filter, and *H* the glass cell of 2.6 cm in diameter having two plane parallel glass plate attached to its ends. The length of the light pass in the cell

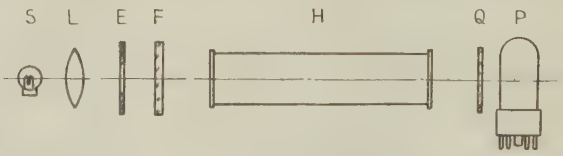


S: Lamp (6 V. 5A)
L: Condenser lens
E: Diaphragm
F: Color filter
H: Absorption cell (15 cm length)
Q: Diffuser
P: Photomultiplier (R.C.A. 931–A)

Fig. 1 Diagram of apparatus for measuring extinction coefficient.

Table 1 Summary of observations at Om depth

Extinction coefficient ($cm^{-1}$)

| Station number | 1 | 6 | 7 | 9 | 13 | 14 | 15 |
|---|---|---|---|---|---|---|---|
| Latitude: N | 33°-40.8′ | 34°-15.5′ | 33°-40.8′ | 33°-35.0′ | 34°-13.0′ | 34°-40.0′ | 35°-00.4′ |
| Longitude: E | 134°-53.9′ | 137°-05.4′ | 137°-07.8′ | 137°-38.0′ | 138°-35.0′ | 139°-11.4′ | 139°-36.7′ |
| Date: 1956 | Feb. 23 | Feb. 24 | Feb. 24 (1000m Depth) | Feb. 24 | Feb. 26 | Feb. 26 | Feb. 26 |
| (V) 4450Å | $149\times10^{-4}$ | $64.1\times10^{-4}$ | $1.14\times10^{-4}$ | $30.8\times10^{-4}$ | $50.8\times10^{-4}$ | $24.8\times10^{-4}$ | $63.4\times10^{-4}$ |
| (B) 4700 | 135 | 57.6 | | 33.3 | 52.0 | 28.5 | 58.2 |
| (G) 5000 | 124 | 71.3 | | 28.5 | 62.0 | 24.8 | 50.7 |
| (G′) 5250 | 115 | 57.2 | | 28.5 | 49.2 | 22.7 | 49.2 |
| (Y) 5760 | 118 | 57.2 | | 24.8 | 49.2 | 24.8 | 51.6 |
| (R′) 6200 | 121 | 69.8 | | 42.0 | 64.7 | 37.5 | 63.4 |
| (R) 6400 | 143 | 78.2 | 18.6 | 55.2 | 70.5 | 39.9 | 65.8 |

being 15 cm. 75cc of water is needed to fill the cell. Inner wall of the cell is blackend to prevent the stray light.

The intensity of the light passed through the cell is measured by a photo multiplier (RCA 931-A) using a circuit shown in Fig. 2. The photo-current increased linearly with the light intensity in the region of the measurements.

Seven kinds of extinction coefficients were measured by using seven color filters. Fig. 3 shows the spectral response curves obtained with the phototube; the maximums of the curves are found at the wavelengths of 4450, 4700, 5000, 5250, 5760, 6200 and 6400Å.

The apparatus shown in Fig. 2 is placed in a light-proof box.

An extinction coefficient $\tau$ obtained by this apparatus for

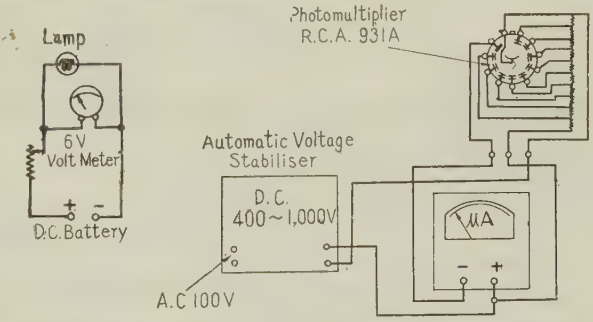


Fig. 2 Schematic circuit diagram for measuring photo-current.

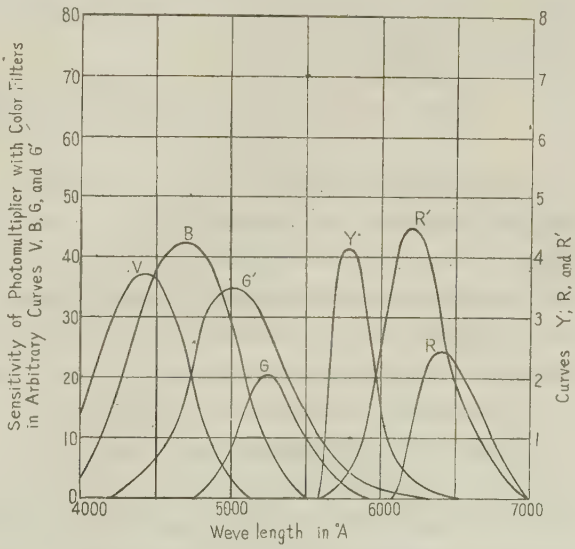


V. B. G. Y. R.: Kaken monochromatic filter
G′. R′: Matsuda color filter.

Fig. 3 Spectro-sensitivity cuves of photomultiplier with color filters.

a specified wave-length is expressed in the following equations.

$$I = I_0 T^2 \exp(-\tau d), \qquad (1)$$

where $I$ and $I_0$ are the light intensities at the two points before and behind the cell, $d$ the light pass in the sample and $T$ is a coefficient concerning to the reflexion loss at the ends of the cell;

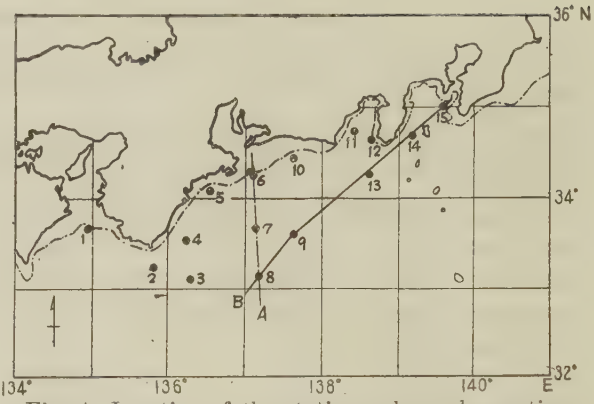


Fig. 4 Location of the stations where observation were made.

$$T = \left\{1 - \frac{(n_1-1)^2}{(n_1+1)^2}\right\}\left\{1 - \frac{(n_1-n_2)^2}{(n_1+n_2)^2}\right\}, \qquad (2)$$

where $n_1$ and $n_2$ are the refractive indexes of the glass and the water. From equation (1)

$$\tau = \frac{2\cdot 3}{d} \times \left\{\log_{10}\left(\frac{I_0}{I}\right) + 2\log_{10} T\right\} \qquad (3)$$

As a linear relation exist between the light intensity and the photo-current,

$$I_0/I = I_{i0}/I_i$$

where $I_i$ and $I_{i0}$ are the measured photo-currents with and without the cell. Then from the equation (3)

$$\tau = \frac{2\cdot 3}{d} \times \left\{\log_{10}\left(\frac{I_{i0}}{I_i}\right) + 2\log_{10} T\right\}. \qquad (4)$$

The extinction coefficients of the samples are determined by the equations (2) and (4) using the observed values of $I_{i_0}$ and $I_i$. In the present calculation the values of $n_1$ and $n_2$ are assumed as 1.50 and 1.33.

For the sake of obtainning a constant light intensity, the voltage (6V) of the lamp terminal was made constant by regulating resistance in the lamp circuit. Voltage of the battery was 24 volt. Three measurements were made for each color filter and the mean value of them was adopted.

At Om depth the water was taken up by a bucket, at more than Om depth a Nansen type water sampler attached to a reversing thermometer was used. In the latter case a part of the sample water was used for the measurements of salinity, dissolved oxygen and phosphate, and the remainning part (300 cc) was used for the optical measurement. Since the water needed for the measurement is 75 cc, 300 cc of the water is sufficient for the washing of the cell.

Fig. 4 shows the observation stations. Observations were made for the waters sampled at the depths of 0, 25, 50, 100, 150, 200, 400, 600, 800, and 1000 m. The time needed for the observations at one station was about 1 hr.

### 3. Observation and Discussion

Extinction coefficients of the surface water at 7 stations observed for every wave-length are listed in Table 1. The same data are plotted in Fig. 5. In the figure, all the curves have minimum values at a wave-length of 5400 Å.

For every wave-length, the maximum extinction coefficient was observed at the Station 1, in the entrance of Kii-Channel. From the fact that the extinction coefficient increases with decreasing wave-length, a large amount of suspended matter is thought to be floating in this region.

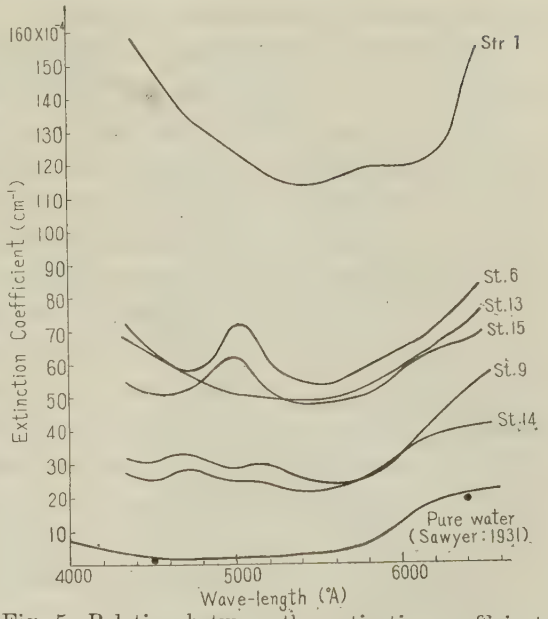


Fig. 5 Relation between the extinction coefficient of the surface water obtained at the typica stations and wave-length. 1

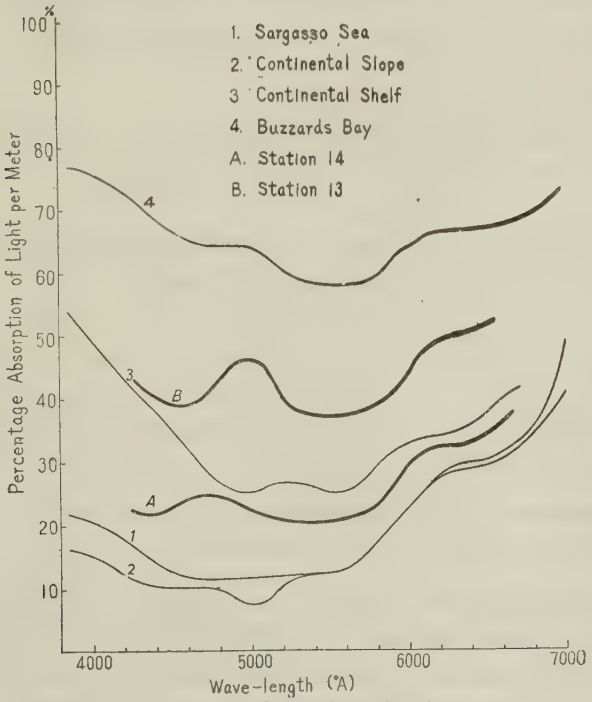


Fig. 6 Percentage absorption of light per meter.
1, 2, 3, 4: Obtained by Clarke (1938) for the sea waters collected from various parts of north Atlantic Ocean.
A, B: Obtained in the present observation.

Minimum extinction coefficient was observed at the Station 14, the middle part between the Izu peninsula and Oshima. This result agrees with the observation made by underwater photometer last February[1] and indicates a branch of the Kuroshio Current passing through this area to Sagami Bay.

Extinction coefficient determined at the Station 14 may be considered as a characteristic

of the branch of the Kuroshio Current.

The water in the vicinity of the Stations 6, 13, and 15 is supposed to be a mixture of the coastal water and the Kuroshio Current.

The water at the Station 6 was clearer than that at the Station 13, but the relation between the extinction coefficient and the wave-length is quite similar for the two Stations, i. e., the coefficients have large values at the wave-length of 5000 Å. Comparatively large amount of suspended matters having high extinction coefficient at this wave-length will be the cause of this phenomenon.

Black circles in Fig. 5 show the extinction coefficient of the water at the Station 7 at the depth of 874m. Observed extinction coefficient being $1.14\times10^{-4}$ and $18.6\times10^{-4}cm^{-1}$ for violet and red lights. These values are nearly equal to those by Sawayer[2] for a redistilled water. G. L. Clarke has found that the order of magnitude of the extinction coefficient of the sea water free from suspended matter is as same as that of the redistilled water. Result of the present observation suggest that at the depth of about 1000 m in the open sea the dead bodies of the planktons is dissolved to make a water having no suspended matter.

In 1938, G. L. Clarke has made a same optical measurement in his laboratory for the waters which had been collected from the various parts in the north Atlantic Ocean.[3] In Fig. 6 the curves 1, 2, 3, and 4 are the percentage absorp-

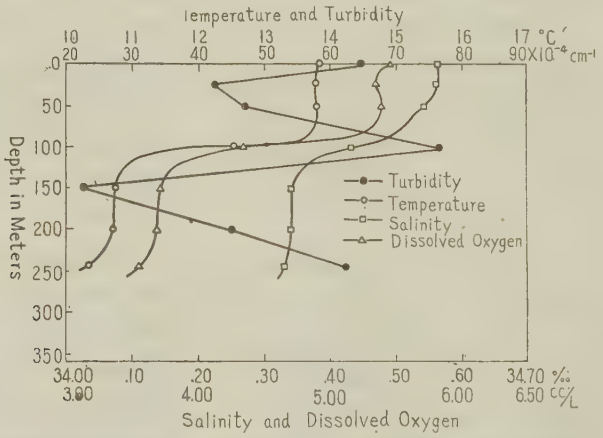


Fig. 7 Vertical distributions of turbidity, temperature. Salinity and dissolved oxygen at the Station 6.

tion of light per meter measured by Clarke for the waters brought from Sargasso Sea, Continental Slope, Continental Shelf, and Buzzards Bay respectively. Curves A and B are the plots of the results obtained by the method described before at the Stations 13 and 14 in the Kuroshio Current. From the figure is noticed that through the water in the Kuroshio Current has high transparency, it is less clearer than the water in Sargasso Sea.

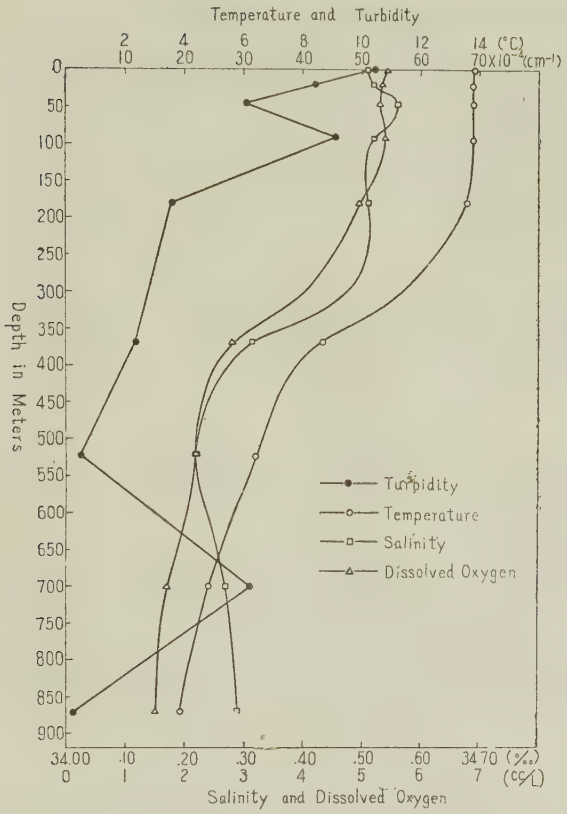


Fig. 8 Vertical distributions of turbidity, temperature, salinity and dissolved oxygen at the Station 7.

Fig. 7 shows the vertical distribution of the turbidity for violet light, salinity, temperature, and dissolved oxygen at the Station 6 (Daiō-Zaki 278 S, 9.3 miles). As shown in the figure, the water becomes clear with increasing depth down to the middle layer. In the case when the surface layer has high turbidity, a large amount of the dissolved oxygen is always found in the same layer. This phenomenon was observed in many other places and indicate the existence of a close relation between the turbidity and the plankton. Refering the spring layer appeared at the depth of about 100 m, the cause of the maximum turbidity observed at the same depth seems to be an accumulation of the suspended matter[5]. Turbidity of the water in the bottom layer will be discussed later.

Fig. 8 shows a vertical distribution of turbidity, salinity, temperature and dissolved oxygen at the Station 7 situated 35 miles off the Station 6. In the figure the maximum turbidity is seen at the surface and the turbidity at the depth of about 100 m in this region is higher than that observed at other depths. There is no spring layer at the same depth but the amount of the dissolved oxygen is large in this layer. The water down from this layer to the depth of

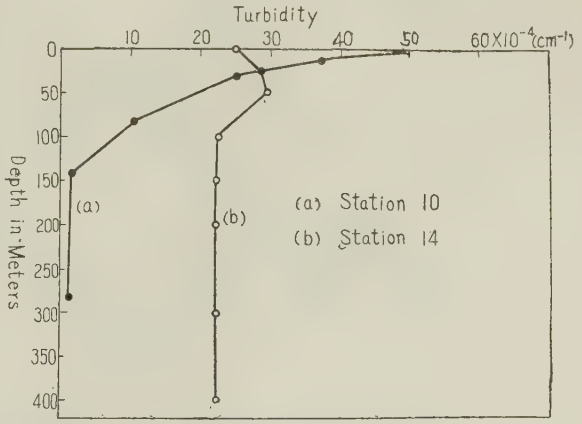


Fig. 9 Vertical distributions of turbidity at the Stations 10 and 14.

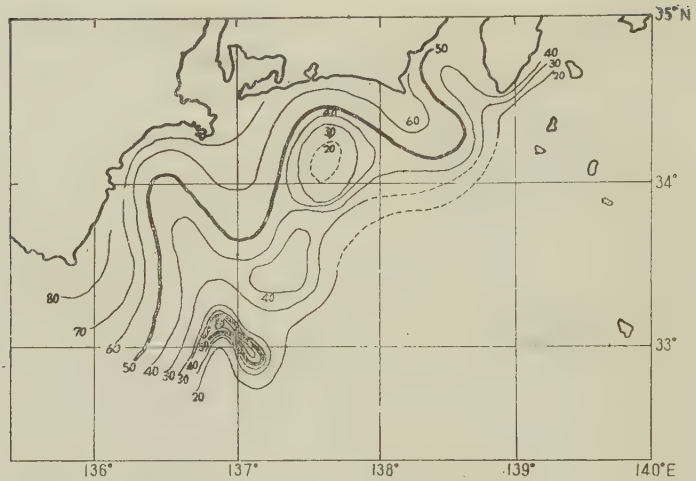


Fig. 10 Horizontal distribution of turbidity in the Om layer.

500m becomes clear with increasing depth.

Vertical distribution of the turbidity at the Station 10 is shown in Fig. 9 (a). The turbidity decrerases with increasing depth. It is worthy of notice that the turbidity of the water at the depth of about 150m was as small as that of the pure water or the water collected at the Station 7 in the depth of 874m. Similar distribution curves were obtained for the Stations 11 and 12 at the entrance of Suruga Bay.

Fig. 9 (b) shows a turbidity distribution at the Station 14 (west of Ōshima at the entrance of Suruga Bay). As shown in the figure the turbidity remains almost constant down to the depth of 400m indicating the existence of the same water mass in the region.

Fig. 10 shows the horizontal distribution of the turbidity for the surface

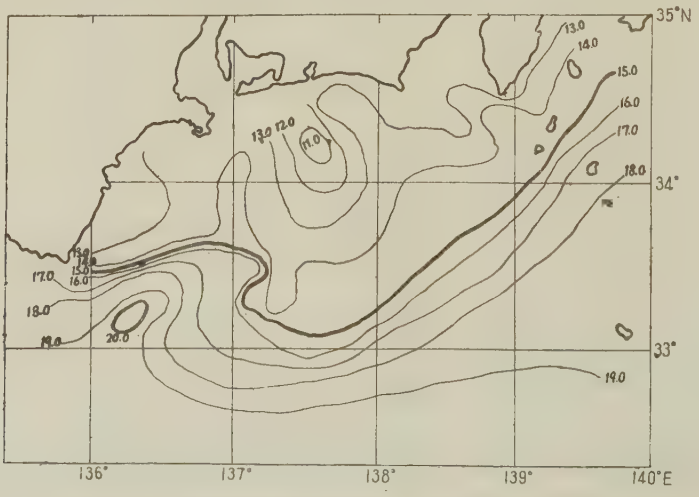


Fig. 11 Horizontal distribution of water temperature in the Om layer.

layer. From this complicated isoturbidity lines, two regions can be distinguished, i. e., the clear and turbid regions having their centers at N: 34°10′, E: 137°40′ and N: 33°30′, E: 137°25′ respectively. Round the off side of these regions a line corresponding to the minimum turbidity runs to the N. E. direction.

Figs. 11 and 12 show the horizontal distributions of the temperature and the salinity. Low salinity regions having its center at N: 33°30′, E: 137°30′ is seen in the figure at the place corresponding to the turbid region just mentioned above. This region, though it does not appear in the figure of the temperature distribution, probably correspond to the so-called "the cold water mass off the Enshu-Nada." This turbidity distribution clearly tells an existence of the Kuroshio Current which flows around the offside of this cold water region.

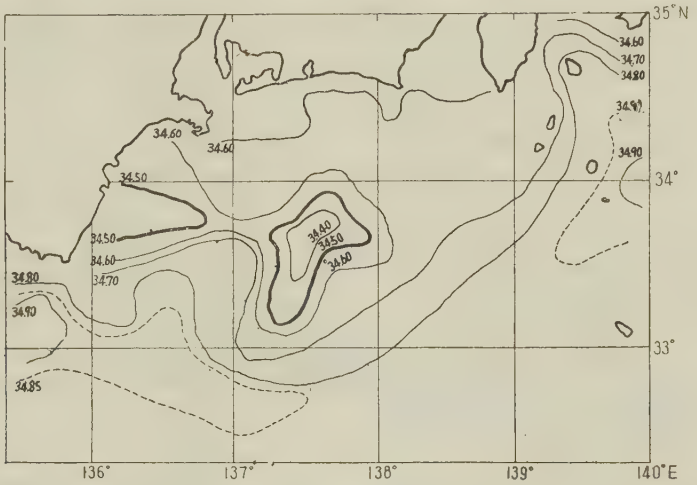


Fig. 12 Horizontal distribution of salinity in the Om layer.

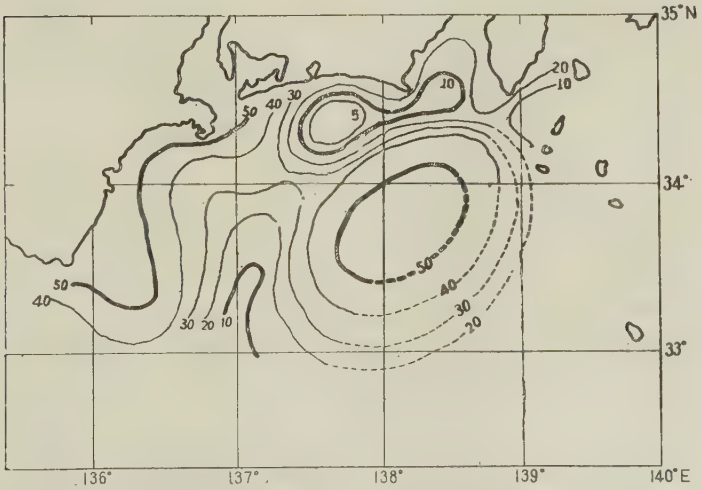


Fig. 13 Horizontal distribution of turbidity in the 200m layer.

A strip of turbid region seen between the cold water mass and the maximum transparency line is supposed to be the school of suspended matter accumulated at the borderline between the Kuroshio Current and the cold water mass.

The horizontal distribution of the turbidity, temperature, and salinity at the depth of 200m shown in Figs. 13, 14 and 15 indicate a low temperature, low salinity, and high turbidity region having its center at N : 33°40′ and E : 137°00′. In this turbidity distribution a low turbidity region having different character is seen off the "Enshu-Nada."

In the layer of 200m depth, there is a close relation between the turbidity distribution and the salinity and temperature distributions, while in the surface layer they are almost independent in shape. From this observation it may be

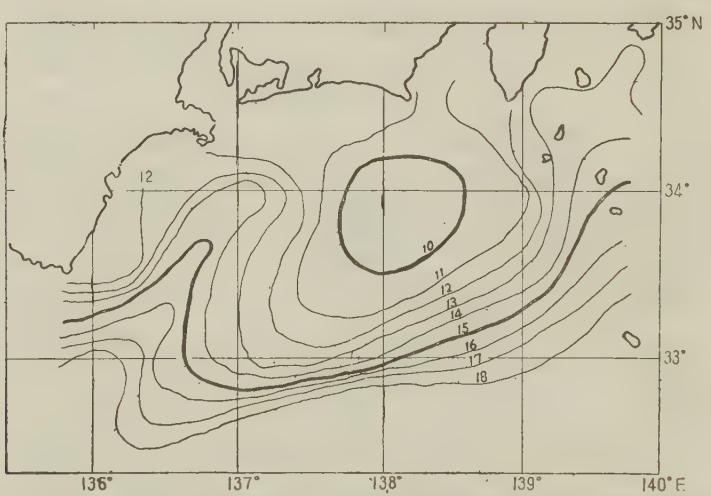


Fig. 14 Horizontal distribution of water temperature in the 200m layer.

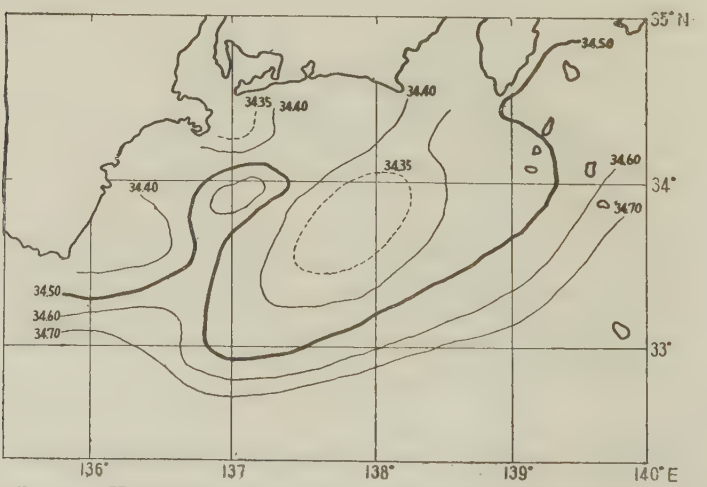


Fig. 15 Horizontal distribution of salinity in the 200m layer.

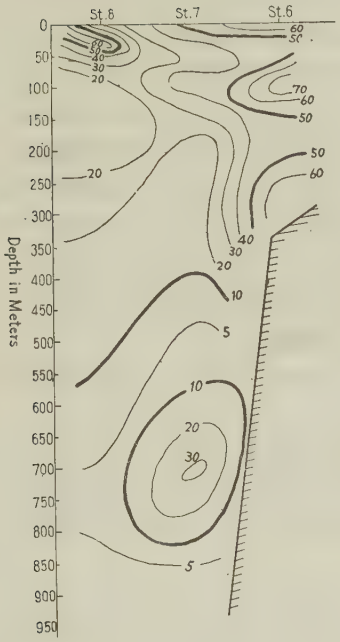


Fig. 16 Vertical distribution of turbility at the section A.

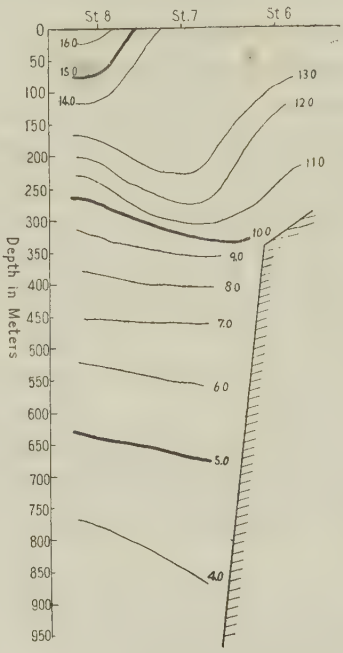


Fig. 17 Vertical distribution of water temperature at the section A.

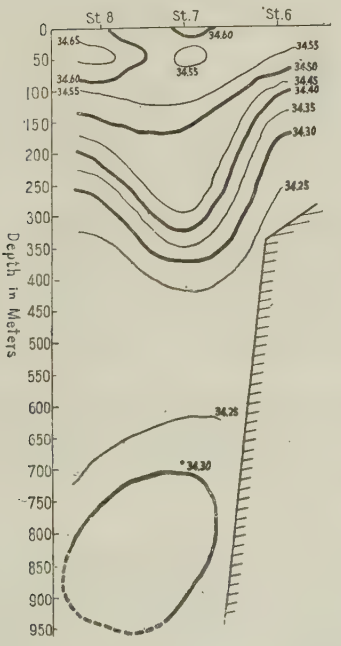


Fig. 18 Vertical distribution of salinity at the section A.

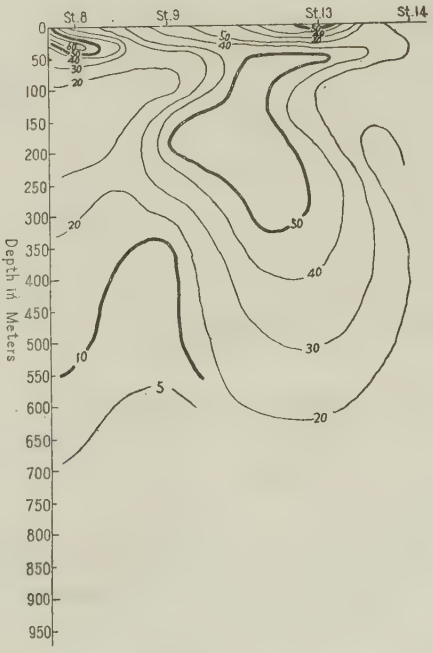


Fig. 19 Vertical distribution of turbidity at the section B.

supposed that in the surface layer the turbidity distribution is disturbed by the coastal water, while in the deep layer the only factor affecting the turbidity is the suspended matter which is rather simple in its distribution.

Figs. 16, 17, and 18 show the distributions of turbidity, temperature and salinity in a vertical plane including the A line which links the Stations 6, 7 and 8. These figures may be explained as follows; the high turbidity region appeared in the bottom layer of the Station 6 may be due to the bottom deposit which is disturbed by the local current in the region. The high turbidity region in the middle layer is supposed to be composed of the suspended matter which is accumulated above the spring layer mentioned before.

Fig. 19 shows the turbidity distribution in a vertical plane including the B line which links the Stations 8, 9, 13, and 14. It is seen from the figure that the high turbidity region appeared between the Stations 9 and 13 correspond to the cold water mass and it extends down to a depth of 300m. Figs. 16 and 19 also show the middle layer of the clear Kuroshio Current flowing around this cold water mass.

## 4. Summary

(1) Extinction coefficients of 120 sample waters collected from 15 stations in the Kuroshio Current region were measured for violet, blue, green, yellow, and red lights. Sampling of the water was made by a bucket in the surface layer and Nansen bottle attached to a reversing thermometer was used in the deep layer. A part of the sample water was used for the measurements of salinity, dissolved oxygen and phosphate and the remaining part (300cc) was used for the optical measurement. All the measurements were made in the laboratory on the "Umitaka-Maru", the training ship, immediately after the water was collected.

(2) At every station, the extinction coefficient of the surface water has a minimum value at the wave-length of about 5400Å. The water in the Kii-Channel shown the maximum turbidity and the most transparent water was found in the entrance of Sagami-Bay at the middle part between the Izu peninsula and Ōshima.

(3) The order of magnitude of the extinction coefficient of the water collected at 874 m depth in the region 45 miles south of the Daiō-Zaki was as small as that of the redistilled water. For the measurement of such a small extinction coefficient, violet and red lights were used.

(4) Comparing the extinction coefficient measured for the Kuroshio Current with that observed by Clarke for the water in the north Atlantic Ocean in 1939, it was found that though the water in the Kuroshio Current has high transparency, it is less clearer than the water in Sargasso Sea.

(5) Horizontal and vertical distributions of the turbidity were determined

from the data of the extinction coefficient measured for violet light, and these distributions are compared with the distributions of temperature, salinity, and dissolved oxygen. Relation between the turbidity and the water mass was also studied. In the surface layer high turbidity was observed in the region where a large amount of dissolved oxygen was detected. Vertical and horizontal distributions of the extinction coefficient tell the existence of the clear Kuroshio Current flowing around "the cold water mass off the Enshu-Nada" which has rather high turbidity. At every station, in general, the water become clear with increasing depth, but in some places the water was rather turbid in their bottom layers. These turbid layers may be due to the bottom deposits disturbed by the local currents.

**Acknowledgement**

The present study was carried out as a part of the oceanographic and biological investigation on the Kuroshio Current made by the commitee of UNESCO in Japan.

The authors wish to express their hearty thanks to Prof. Dr. M. Uda for his kind help and presentation of valuable data on the oceanographic observation. They are also indebted to Prof. T. Kumagori, the captain of the training ship "Umitaka-Maru" of Tokyo University of Fisheries, Messrs. M. Ishino and H. Ōtsubo of Tokyo University of Fisheries for their collaboration with them throughout the course of this investigation.

**Referencrs**

(1) T. Sasaki, N. Okami, S. Watanabe and G. Ōshiba, Records Oceanogr. Works. Japan **2** (1) (1955).
(2) W. R. Sawyer: Contr. Canad. Biol. Fish., V.S. **9** (8) D. 1, (1931).
(3) G. L. Clarke, and H. R. James: J. O. S. A., **29** (2) (1939).
(4) K. Hishida, J. Oceanogr. Soc. Japan, **9** (3~4) (1954).
(5) H. Pettersson: Rap. Proc-Verb. Reun., **101** (2) (1936).
(6) V. J. Joseph: Deut. Hydro. Zeit., **2** (5) (1949).
(7) M. Fukuda, N. Inoue, and S. Nishizawa: Bull. Fac. Fish., Hokkaido Univ., **5** (1) (1954).
(8) N. G. Jerlov: Rep. Swed. Deep-Sea. Exp. (Phys. and Chem. 3) (1953).

PRINTED BY
KASAI PUBLISHING & PRINTING CO.
(PAN-PACIFIC PRESS)